

MANUFACTURING AND STRUCTURAL ANALYSIS OF A LIGHTWEIGHT
SANDWICH COMPOSITE UAV WING

A THESIS SUBMITTED TO
THE GRADUATE SCHOOL OF NATURAL AND APPLIED SCIENCES
OF
MIDDLE EAST TECHNICAL UNIVERSITY

BY

TAHİR TURGUT

IN PARTIAL FULFILLMENT OF THE REQUIREMENTS

FOR

THE DEGREE OF MASTER OF SCIENCE

IN

AEROSPACE ENGINEERING

SEPTEMBER 2007

Approval of the thesis:

**MANUFACTURING AND STRUCTURAL ANALYSIS OF A
LIGHTWEIGHT SANDWICH COMPOSITE UAV WING**

submitted by **TAHİR TURGUT** in partial fulfillment of the requirements for
the degree of **Master of Science in Aerospace Engineering Department,**
Middle East Technical University by,

Prof. Dr. Canan Özgen
Dean, Graduate School of **Natural and Applied Sciences**

Prof. Dr. İsmail H. Tuncer
Head of Department, **Aerospace Engineering**

Assoc. Prof. Dr. Altan Kayran
Supervisor, **Aerospace Engineering Dept., METU**

Examining Committee Members:

Prof. Dr. Nafiz Alemdaroğlu
Aerospace Engineering Dept., METU

Assoc. Prof. Dr. Altan Kayran
Aerospace Engineering Dept., METU

Asst. Prof. Dr. Merve Erdal
Mechanical Engineering Dept., METU

Dr. Volkan Nalbantoğlu
Aerospace Engineering Dept., METU

Dr. Güçlü Seber
Aerospace Engineering Dept., METU

Date: _____

I hereby declare that all information in this document has been obtained and presented in accordance with academic rules and ethical conduct. I also declare that, as required by these rules and conduct, I have fully cited and referenced all material and results that are not original to this work.

Name, Last Name: Tahir Turgut

Signature :

ABSTRACT

MANUFACTURING AND STRUCTURAL ANALYSIS OF A LIGHTWEIGHT SANDWICH COMPOSITE UAV WING

Turgut, Tahir

M.S., Department of Aerospace Engineering

Supervisor: Assoc. Prof. Dr. Altan Kayran

September 2007, 104 pages

This thesis work deals with manufacturing a lightweight composite unmanned aerial vehicle (UAV) wing, material characterization of the composites used in the UAV wing, and preliminary structural analysis of the UAV wing.

Manufacturing is performed at the composite laboratory founded in the Department of Aerospace Engineering, and with hand lay-up and vacuum bagging method at room temperature the wing is produced. This study encloses the detailed manufacturing process of the UAV wing from the mold manufacturing up to the final wing configuration supported with sketches and pictures.

Structural analysis of the composite wing performed in this study is based on the material properties determined by coupon tests and micromechanics approaches. Contrary to the metallic materials, the actual material properties of composites are generally not available in the material handbooks, because the elastic properties of composite materials are dependent on the manufacturing process. In this study, the mechanical properties, i.e. Young's Modulus, are

determined utilizing three different methods. Firstly, longitudinal tensile testing of the coupon specimens is performed to obtain the elastic properties. Secondly, mechanics of materials approach is used to determine the elastic properties. Additionally, an approximate method, that can be used in a preliminary study, is employed. The elastic properties determined by the tests and other approaches are compared to each other.

One of the aims of this study is to establish an equivalent material model based on test and micromechanics approach, and use the equivalent model in the structural analysis by finite element method. To achieve this, composite structure of the wing is modeled in detail with full composite material descriptions of the surfaces of the wing structure, and comparisons are made with the results obtained by utilizing equivalent elastic constants. The analyses revealed that all three approaches have consistent, and close results; especially in terms of deflections and natural frequencies. Stress values obtained are also comparable as well.

For a case study on level flight conditions, spanwise wing loading distribution is obtained using a program of ESDU, and the wing is analyzed with the distributed loading. Reasonable results are obtained, and the results compared with the tip loading case.

Another issue dealt in this study is analyzing the front spar of the wing separately. The analysis of the front spar is performed using transformed section method and finite element analysis. In the results, it is found that both methods calculates the deflections very close to each other. Close stress results are found when solid elements are used in the finite element analysis, whereas, the results were deviating when shell elements are used in the analysis.

Keywords: Composites, material characterization, UAV, vacuum bagging, manufacturing, structural analysis

ÖZ

SANDVIÇ KOMPOZİT MALZEMEDEN YAPILMIŞ HAFİF BİR İHA KANADININ ÜRETİMİ VE YAPISAL ANALİZİ

Turgut, Tahir

Yüksek Lisans, Havacılık ve Uzay Mühendisliği Bölümü

Tez Yöneticisi: Assoc. Prof. Dr. Altan Kayran

Eylül 2007, 104 sayfa

Bu tez çalışması, kompozit malzemeden yapılmış hafif bir insansız hava aracı (İHA) kanadının üretimi, bu kanatta kullanılan malzemelerin nitelendirilmesi ve kanadın yapısal analizi ile ilgilenebilir.

Kanat üretimi Havacılık ve Uzay Mühendisliği bölümünde kurulan kompozit laboratuvarında, elle serme ve vakum çantalama yöntemiyle oda sıcaklığında kür edilerek gerçekleştirilmiştir. Bu çalışma, İHA kanadının kalıp üretiminden nihai kanat yapılanmasına kadar olan, taslak çizimler ve fotoğraflarla desteklenmiş detaylı üretim sürecini kapsar.

Bu çalışmada yapılan yapısal analizler, kupon testleri ve mikromekanik yaklaşımlarla elde edilen malzeme özelliklerine dayandırılmıştır. Metalik malzemelerin aksine, kompozit malzemelerin mekanik özellikleri üretim yöntemine bağlı olduklarından, genellikle malzeme el kitaplarında yer almaz. Bu çalışmada, malzeme özellikleri (elastisite modülü) üç ayrı yöntem kullanılarak

tain edilmiştir. İlk olarak, kupon numunelerin boylamsal ekseninde çekme testleri yapılarak elastik özellikler saptanmıştır. Malzeme özelliklerini belirlemede kullanılan ikinci yöntem malzeme mekaniği yaklaşımıdır. Üçüncü yöntem olarak bir ön çalışmada kullanılacak tahmini bir yaklaşım kullanılmıştır. Farklı yöntemlerle elde edilen malzeme özellikleri birbirleriyle karşılaştırılmıştır.

Bu çalışmanın temel amaçlarından biri çekme testi sonuçları ve mikromekanik yaklaşımı temel olarak eşdeğer malzeme modeli ortaya çıkarmaktır. Bunu sağlayabilmek için, kanat yapısı elde edilen farklı malzeme özellikleriyle modellenmiş ve sonlu eleman analizleri karşılaştırılmıştır. Analizlerin sonucunda üç farklı yaklaşımda da tutarlı ve birbirine yakın sonuçlar elde edilmiştir. Özellikle deplasman ve doğal frekans değerleri birbirine çok yakın bulunmuştur. Gerilme değerlerinde birbiriyle kıyaslanabilir sonuçlar elde edilmiştir.

Yatay uçuş durumunu incelemek için ESDU'nun kanat açıklığı boyunca yük dağılımı hesaplayan programıyla yükler hesaplanmış ve kanat bu yüklerle analiz edilmiştir. Makul sonuçlar elde edilmiş ve bu sonuçlar kanat ucu yüklemesi sonuçlarıyla karşılaştırılmıştır.

Bu çalışmada ele alınan diğer bir konu da kanadın ön kirişinin ayrı olarak analizidir. Ön kiriş analizi, kesit dönüştürme yöntemi ve sonlu elemanlar analizi kullanılarak gerçekleştirilmiştir. Analiz sonucunda iki yöntemin de deplasmanları birbirine çok yakın olarak saptadığı tespit edilmiştir. Sonlu eleman analizinde, modellemede katı elemanlar kullanıldığında gerilme sonuçlarının da birbirine yakın çıktığı, kabuk elemanlar kullanıldığında ise gerilme sonuçlarının farklı olduğu gözlemlenmiştir.

Anahtar Kelimeler: Kompozitler, malzeme nitelendirilmesi, İHA, vakum çantalama, üretim, yapısal analiz

to my family ...

ACKNOWLEDGMENTS

I would like to express my sincere gratitude to Assoc.Prof.Dr. Altan Kayran for his valuable efforts in every step of this thesis. His encouragement, support and patience always guided me throughout this period.

I would like to thank Prof.Dr. Nafiz Alemdarođlu, supervisor of the UAV project, for financial and facility support. I also thank our technician Murat Ceylan for helping me in the specimen manufacturing, and Cenk Iřık and Alpay Oral for their assistance during the tensile testing of the specimens.

I appreciate the useful discussions we had with Sercan Soysal, Volkan Kargın and Fatih Karadal during this thesis.

I would like to thank my dearest friends Evrim Dizemen, Buřra Akay, Mustafa Kaya, Özgür Demir and Gökhan Ahmet who have always boosted me with their positive energy and moral support in this challenging study.

Special thanks to other residents of SOTE, Emrah Konokman and Ođuzhan Ayısıt, for providing me such a warm and sincere home environment. It is a great pleasure to see that an academic study can be succeeded even in SOTE.

I also thank Alper Ezertař, Deniz Yılmaz and Onur Tarmcı for their most noteworthy support.

Finally, I would like to thank my family who supported me throughout my life for their trust, understanding and patience.

TABLE OF CONTENTS

ABSTRACT	iv
ÖZ	vi
DEDICATON	viii
ACKNOWLEDGMENTS	ix
TABLE OF CONTENTS	x
LIST OF TABLES	xiii
LIST OF FIGURES	xv
LIST OF SYMBOLS	xix
CHAPTERS	
1 INTRODUCTION	1
1.1 An Introduction to Composite Materials	1
1.2 An Introduction to Unmanned Aerial Vehicles	8
1.3 Mini UAV System Built In Aerospace Engineering Department	11
1.4 Aim and Scope of the Thesis	12
2 MANUFACTURING OF THE UAV WING	14
2.1 Vacuum Bagging Method	14
2.1.1 Manufacturing a Composite Plate with Vacuum Bagging Method	17
2.2 Manufacturing of the Skin Molds of the Mini UAV Wing	23
2.2.1 Manufacturing Process of Male Models of the Wing	23
2.2.2 Manufacturing Process of the Upper and Lower Wing Skin Fe- male Molds Using the Male Wing Model	34

2.3	Manufacturing the UAV Wing	46
2.3.1	Manufacturing the Components of the Wing	46
2.3.2	Assembling the Inner Components of the Wing	49
2.3.2.1	Assembly of the main wing inner structure	49
2.3.2.2	Assembly of the outer wings inner structures	52
2.3.2.3	Setting up the connection parts between the main and outer wings	53
2.3.3	Assembling the Wing	56
3	CHARACTERIZATION OF THE MATERIALS USED IN THE UAV	58
3.1	Determination of Tensile Properties of Woven Fabric Lamina	59
3.1.1	ASTM Standard and Test Procedure	61
3.1.2	Tensile Tests Performed and Results	64
3.1.2.1	Results of Case I	66
3.1.2.2	Results of Case II	67
3.1.2.3	Results of Case III	68
3.1.3	Discussion of the Results	68
4	FINITE ELEMENT MODEL AND ANALYSIS	72
4.1	Finite Element Model	72
4.2	Determination of Elastic Modulus	74
4.2.1	Mechanics of Materials Approach	74
4.2.2	Mechanical Testing of Composites	76
4.2.3	An Approximate Method for Obtaining Elastic Properties	76
4.3	Analysis of the Wing	78
4.3.1	Results of Case I	82
4.3.2	Results of Case II	86
4.3.3	Results of Case III	88
4.3.4	Discussion of Results	90
4.4	Case Study: Spanwise distributed wing loading	91
4.5	Analysis of Front Spar	94
4.5.1	Analysis with Transformed Section Method	95

4.5.2	Analysis with Finite Element Method	96
5	DISCUSSION AND CONCLUSION	99
	REFERENCES	103
	APPENDICES	
A	SPECIMEN DATA AND TENSILE TEST RESULTS	105

LIST OF TABLES

TABLES

Table 1.1	Composite components in aircraft applications for various types of aircraft [6].	6
Table 1.2	Classification of UAVs defined by UVS International	10
Table 1.3	Specifications of Güventürk	11
Table 2.1	Properties of the materials used in the wing skin.	47
Table 2.2	Properties of the materials used in the front spar.	48
Table 2.3	Properties of the materials used in the ribs and rear spar.	49
Table 3.1	Specifications of the woven fabrics used in the mini UAV.	60
Table 3.2	Mechanical properties of the fibers composing the fabrics.	60
Table 3.3	Tensile specimen geometry recommendations.	62
Table 3.4	Average specimen geometry and mass data	64
Table 3.5	Test results of the specimens cured at room temperature.	67
Table 3.6	Test results of Case II.	67
Table 3.7	Percent changes of the mechanical properties when post-curing at 100°C for 4 hours is applied.	67
Table 3.8	Test results of Case III.	68
Table 3.9	Percent changes of the mechanical properties when post-curing at 80°C for 8 hours is applied.	68
Table 4.1	Mechanical properties of the fibers and matrix material used in the UAV. . . .	75
Table 4.2	Unidirectional Elastic properties of the composites used in the UAV based on micromechanics of composites.	75
Table 4.3	Average elastic moduli of the specimens obtained from tensile testing.	76
Table 4.4	Elastic moduli of the composites obtained from an approximate method. . . .	77
Table 4.5	Material properties to be used in the finite element analysis.	78
Table 4.6	Comparison of distributed elliptic loading and tip loading cases.	81
Table 4.7	Results of linear static and modal analyses of Case I.	82
Table 4.8	Results of linear static and modal analyses of Case II.	86

Table 4.9 Results of linear static and modal analyses of Case III.	88
Table 4.10 Results of stall case analysis using different material definitions.	92
Table 4.11 Comparison of results obtained from the front spar analysis.	96
Table 4.12 Comparison of results of the test case.	98
Table A.1 Average properties of specimens used in Tensile Test # 1, and test results. . .	105
Table A.2 Average properties of specimens used in Tensile Test # 2, and test results. . .	106
Table A.2 Average properties of specimens used in Tensile Test # 2, and test results (continued).	107
Table A.3 Average properties of specimens used in Tensile Test # 3, and test results. . .	108
Table A.4 Average properties of specimens used in Tensile Test # 4, and test results. . .	109
Table A.4 Average properties of specimens used in Tensile Test # 4, and test results (continued).	110

LIST OF FIGURES

FIGURES

Figure 1.1	Typical composite structures used in a commercial aircraft [7].	6
Figure 1.2	Typical composite structures used in a military aircraft [7].	7
Figure 1.3	Composite components used in an engine application [7].	7
Figure 1.4	Composite components used in a satellite application [7].	8
Figure 1.5	Examples for the UAV types: (a) Micro, (b) Mini, (c) Medium Range, (d) Medium Altitude Long Endurance, (e) High Altitude Long Endurance	10
Figure 1.6	Mini UAV system, Güventürk in operation.	12
Figure 2.1	Schematic drawing of vacuum bagging process.	16
Figure 2.2	Manufacturing steps of a composite plate with vacuum bagging method. . . .	21
Figure 2.2	Manufacturing steps of a composite plate with vacuum bagging method (con- tinued).	22
Figure 2.3	3-D model of the wing.	23
Figure 2.4	Numerically controlled foam cutting machine.	24
Figure 2.5	Schematic set-up of the foam cutting machine.	24
Figure 2.6	Male and female wing molds prepared from the foam material.	25
Figure 2.7	Adjustment of the dihedral angle in the male-female foam mold assembly. . .	26
Figure 2.8	Final dihedral angle formed.	26
Figure 2.9	Positioning of the outer wing with respect to the center wing.	27
Figure 2.10	Side view of the mold assembly after the upper female foam mold is removed.	27
Figure 2.11	Application of composite layers on one side of the male foam mold.	27
Figure 2.12	Male wing mold removed from the mold assembly.	28
Figure 2.13	Adjustment of the male wing mold in the upper female foam mold.	29
Figure 2.14	Application of composite layers on the foam side of the male mold.	30
Figure 2.15	Preparation of wing tip profiles.	31
Figure 2.16	Application of leading edge composite fabric.	31
Figure 2.17	Final painting operation of the male wing model.	32
Figure 2.18	Final surface finishing operation of the surface of the male wing model. . . .	32

Figure 2.19 Picture of the male wing model after final operations.	33
Figure 2.20 Positioning of the male wing model on the tool table.	34
Figure 2.21 Section of the center wing/reference block assembly.	35
Figure 2.22 Top view of the wing model and reference blocks.	35
Figure 2.23 Front view of the wing mold and reference blocks.	36
Figure 2.24 Section of the outer wing/reference block assembly; tip section.	36
Figure 2.25 Sealed edges of the wing/reference block assembly.	37
Figure 2.26 Application of polyester resin layers over the wing mold and reference blocks.	37
Figure 2.27 Application of fabric layers to form the thickness of the female mold; side tip view.	39
Figure 2.28 Wall thickness of the female mold; side tip view.	39
Figure 2.29 Schematic view of the back-up structure of the female mold.	40
Figure 2.30 Connection of the back-up structure to the female mold by chopped fiber/polyester resin combination.	40
Figure 2.31 Front view of the mold assembly after it is turned upside down.	41
Figure 2.32 Schematic top view of the mold assembly showing the flange of the female mold and the male wing.	42
Figure 2.33 Front view of the mold assembly after the built-up of the wall of the female mold.	43
Figure 2.34 Back-up structure built on the new female mold surface.	43
Figure 2.35 Position of the holes of the guide pins.	44
Figure 2.36 Detail view of the guide pin connection.	44
Figure 2.37 Side view of the male model and female mold with its back-up structure.	45
Figure 2.38 Upper and lower wing skin female molds, and the back-up structure.	46
Figure 2.39 Configuration of the wing skin.	47
Figure 2.40 Configuration of the front spar.	48
Figure 2.41 Configuration of the rear spar.	48
Figure 2.42 Inner configuration of the main wing (top view)	50
Figure 2.43 Cutting process of the lower skin in the female mold (top view)	50
Figure 2.44 Positioning the ribs in the upper skin of the main wing (top view)	51
Figure 2.45 Placing strips of e-glass to the sides of the spars (side view)	51
Figure 2.46 Placing strips of e-glass to the sides of ribs, skin and spars (top view)	52
Figure 2.47 Inner configuration of the outer wings (top view)	52
Figure 2.48 Styrofoam removal process (top view)	53
Figure 2.49 Positioning the tube assembly in the front spar (top view)	54
Figure 2.50 Positioning the tube assembly next to the rear spar (top view)	54
Figure 2.51 Fastener mechanism at the wing connection (isometric view)	55

Figure 2.52 Female molds clamped during wing assembly.	57
Figure 2.53 Pictures of main and outer wing after post-manufacturing.	57
Figure 3.1 Tension test specimen geometry.	62
Figure 3.2 Zwick/Roell Z010 Universal Static Testing Machine.	63
Figure 3.3 Stress-strain curves for a set of composite specimens.	66
Figure 3.4 Samples of fractured specimens (namely, kevlar, e-glass, and carbon from top to bottom).	66
Figure 4.1 Finite element model of the wing.	72
Figure 4.2 Detailed views of outer and main wing.	73
Figure 4.3 Schematic drawings of the configurations of components of the UAV.	73
Figure 4.4 Axis system used.	74
Figure 4.5 A general and a detail view of woven architecture.	79
Figure 4.6 Two different approaches for modeling woven lamina used in this study.	79
Figure 4.7 Stacking sequence used in Case I.	80
Figure 4.8 Stacking sequence used in Cases II and III.	80
Figure 4.9 Loading and the boundary condition defined in the wing model.	81
Figure 4.10 Stress and displacement contours of the wing (material orientation: $[0^\circ/90^\circ]$).	83
Figure 4.11 Detailed views of stress contours at Layer 1 and Layer 2 of the wing (material orientation: $[0^\circ/90^\circ]$).	83
Figure 4.12 Stress and displacement contours at the front spar (material orientation: $[0^\circ/90^\circ]$).	84
Figure 4.13 Detailed views of stress contours at Layer 1 and Layer 2 at the front spar (material orientation: $[0^\circ/90^\circ]$).	84
Figure 4.14 First three mode shapes of the wing structure (material orientation: $[0^\circ/90^\circ]$).	84
Figure 4.15 Stress and displacement contours of the wing (material orientation: $[90^\circ/0^\circ]$).	85
Figure 4.16 Detailed views of stress contours at Layer 1 and Layer 2 of the wing (material orientation: $[90^\circ/0^\circ]$).	85
Figure 4.17 Stress and displacement contours at the front spar (material orientation: $[90^\circ/0^\circ]$).	85
Figure 4.18 Detailed views of stress contours at Layer 1 and Layer 2 at the front spar (material orientation: $[90^\circ/0^\circ]$).	86
Figure 4.19 First three mode shapes of the wing structure (material orientation: $[90^\circ/0^\circ]$).	86
Figure 4.20 Isometric and detail views of stress contour of the wing.	87
Figure 4.21 Displacement contours of the wing and the front spar.	87
Figure 4.22 Isometric and detail views of stress contour of the front spar.	88
Figure 4.23 First three mode shapes of the wing structure.	88

Figure 4.24 Isometric and detail views of stress contour of the wing.	89
Figure 4.25 Displacement contours of the wing and the front spar.	89
Figure 4.26 Isometric and detail views of stress contour of the front spar.	90
Figure 4.27 First three mode shapes of the wing structure.	90
Figure 4.28 Spanwise wing loadings for 4 different level flight conditions.	91
Figure 4.29 Close-up view of distributed force and moment applied on a section over the front spar.	92
Figure 4.30 Isometric and detail views of stress contour of the wing.	93
Figure 4.31 Displacement contours of the wing and the front spar.	94
Figure 4.32 Isometric and detail views of stress contour of the front spar.	94
Figure 4.33 Method of transformed section.	95
Figure 4.34 Stress contours at carbon and styrofoam layers of the front spar.	96
Figure 4.35 Displacement contour of the front spar.	97
Figure 4.36 Geometry and mesh structure of the test case	98

LIST OF SYMBOLS

ROMAN SYMBOLS

E_i	Young's modulus in i direction
G_{ij}	Shear modulus in ij plane
V	Volume fraction
g	Gravitational acceleration

GREEK SYMBOLS

σ	Normal stress
δ	Displacement
ν_{ij}	Poisson's ratio in ij plane
ρ	Density
η	Efficiency factor

SUBSCRIPTS

f	Fiber properties
m	Matrix properties
i	1, 2
j	1, 2, 3

CHAPTER 1

INTRODUCTION

1.1 An Introduction to Composite Materials

Composites are, by definition, materials consisting of two or more materials which together produce beneficial properties that cannot be attained with any of the constituents alone. One of the most common examples, fiber-reinforced composite materials consist of high strength and high modulus fibers in a matrix material. Reinforced steel bars embedded in concrete provide an example of fiber-reinforced composites [1]. In these composites, the function of the fibers is carrying the load exerted on the composite structure, and providing stiffness, strength, thermal stability and other structural properties. Matrix material carries out several functions in a composite structure, some which are binding the fibers together and transferring the load to the fibers, and providing protection to reinforcing fibers against chemical attack, mechanical damage and other environmental effects like moisture, humidity, etc [2].

Composites have unique advantages over monolithic materials, such as high strength, high stiffness, long fatigue life, low density, and adaptability to the intended function of the structure. They offer further improvements in corrosion resistance, wear resistance, appearance, temperature-dependent behavior, thermal stability, thermal insulation, thermal conductivity, and acoustic insulation. The basis that makes the composites to have superior structural per-

formance stands on their high specific strength (strength to density ratio) and high specific stiffness (modulus to density ratio) and the anisotropic and heterogeneous character of the material. The anisotropic and heterogeneous character also provides freedom to design a structure with optimum configuration for serving a specific function [3].

Composites can be classified on the basis of the form of their structural components: *fibrous composites*, which consist of fibers of one material in a matrix material of another; *particulate composites*, which are composed of macrosized particles of one material in a matrix of another; and *laminated composites*, which are made of layers of different materials, including composites of the first two types [1].

Fibrous composites exist in two types: discontinuous or short-fiber composites, and continuous fiber composites. Discontinuous or short-fiber composites contain short fibers or whiskers as the reinforcing member. These short fibers, which can be fairly long compared with the diameter, can be either all oriented along one direction or randomly oriented within the composite structure. Continuous fiber composites are reinforced by long continuous fibers and are the most efficient from the point of view of stiffness and strength. The continuous fibers can be parallel (unidirectional continuous fiber composite), can be oriented at right angles to each other (cross ply or woven fabric continuous fiber composite), or can be oriented along several directions (multidirectional continuous fiber composite) depending on the design of the structure [3].

Particulate composites consist of particles of various sizes and shapes randomly dispersed within the matrix. Particulate composites may consist of nonmetallic particles in a nonmetallic matrix; metallic particles in nonmetallic matrices; metallic particles in metallic matrices; and nonmetallic particles in metallic matrices [3].

Laminated composites consist of layers of at least two different materials that are bonded together. Lamination is used to combine the best aspects of the constituent layers in order to

achieve a more useful material. The properties that can be emphasized by lamination are strength, stiffness, low weight, corrosion resistance wear resistance, thermal and acoustical insulation, etc [4].

Composites have been customarily designed and manufactured for applications in which high performance and light weight are needed. They offer several advantages over traditional engineering materials [2].

From the structural mechanics point of view; composite materials have high specific stiffness, and high specific strength. Due to this property, composite parts are lighter than their counterparts. This leads to achieve higher performance in vehicles with better fuel efficiency. Moreover, the fatigue strength is much higher for composite materials. Steel and aluminum alloys exhibit good fatigue strength up to about 50% of their static strength, whereas, unidirectional carbon/epoxy composites have good fatigue strength up to almost 90% of their static strength. In addition to these, composites offer good impact properties. Glass and Kevlar composites, for example, provide higher impact strength than steel and aluminum.

From the manufacturing point of view; composite materials offer increased amounts of design flexibility. For example, the coefficient of thermal expansion of composite structures is much lower than for metals. This provides good dimensional stability in composite structures. Hence, net-shape or near-net-shape parts can be produced with composite materials. This feature eliminates several machining operations and thus reduces process cycle time and cost. Composite materials provide capabilities for part integration as well. Several metallic components can be replaced by a single composite component. Fabrication of complex parts with certain appearance, and special contours, which are sometimes not possible with metals, is possible using composite materials; even without welding or riveting the separate pieces. This increases reliability and reduces production times. It offers greater manufacturing feasibility. These improvements help minimize the number of parts in a product and thus reduce assembly

and joining time. By eliminating joints, high-strength structural parts can be manufactured at lower cost. Cost benefit comes by reducing the assembly time and cost. Furthermore, in composite processing, tooling requires lower pressure and temperature when compared to metal processing. This results in a lower tooling cost. This offers greater flexibility for design changes in this competitive market where product lifetime is continuously reducing.

From the usage point of view; composite materials offer high corrosion resistance. Iron and aluminum corrode in the presence of water and air and require special coatings and alloying. Because the outer surface of composites is formed by plastics, corrosion and chemical resistance are very good. Also, noise, vibration, and harshness characteristics are better for composite materials than metals. Composite materials dampen vibrations an order of magnitude better than metals. Additionally, glass-reinforced and aramid-reinforced phenolic composites meet FAA and JAR requirements for low smoke and toxicity. This feature is required for aircraft interior panels, stowbins, and galley walls. Along with these, composite structures provide in-service monitoring or online process monitoring with the help of embedded sensors. This feature, which is known as ‘smart structure monitoring’, is used to monitor fatigue damage in aircraft structures.

Although composite materials offer many benefits, they have some disadvantages that limit the usage areas and prevent becoming widespread in industry [2].

From the design and manufacturing point of view; classical ways of designing products with metals depend on the use of machinery and metals handbooks, and design and data handbooks. Large design databases are available for metals. Designing parts with composites lacks such books because of the lack of a database. Moreover, the materials cost for composite materials is very high compared to that of steel and aluminum. It is almost 5 to 20 times more than aluminum and steel on a weight basis. Even though, recent advances in manufacturing methods like pultrusion, resin transfer molding, structural reaction injection molding, compression

molding of sheet molding compound, and filament winding have been automated for higher production rates, the lack of high-volume production methods limits the widespread use of composite materials.

From the usage point of view; the temperature resistance of composite parts depends on the temperature resistance of the matrix materials. Because a large proportion of composites uses polymer-based matrices, temperature resistance is limited by the plastics' properties. Average composites work in the temperature range -40 to $+100^{\circ}\text{C}$. The upper temperature limit can range between $+150$ and $+200^{\circ}\text{C}$ for high-temperature plastics such as epoxies. Additionally, solvent resistance, chemical resistance, and environmental stress cracking of composites depend on the properties of polymers. Some polymers have low resistance to solvents and environmental stress cracking. Also, composites absorb moisture, which affects the properties and dimensional stability of the composites.

Offering several advantages, composites have drawn the attention of many industries. The aerospace industry was among the first to realize the benefits of composite materials. In aerospace, the demands upon materials are usually greater than in other applications. The four most important requirements are light weight, high strength, high stiffness, and good fatigue resistance. Composites, particularly the high performance types, are the only existing materials efficiently meeting these requirements.[5]

The use of composites in aircraft is increasing rapidly, especially in military aircraft, where the pay-off is the greatest. In commercial aircraft, the acceptance of composites as primary structures have been slower, but is now increasing rapidly. The composite components used in the aircraft are mainly, horizontal and vertical stabilizers, wing skins, fin boxes, flaps, and various other structural components as shown in Table 1.1. In spacecraft, where the weight is of the greatest importance, the composites are accepted as primary materials [5]. Figures 1.1 and 1.2 shows the typical composite structures used in commercial and military aircrafts.

Composite components used in engine and satellite applications are shown in Figures 1.3 and 1.4.

Table 1.1: Composite components in aircraft applications for various types of aircraft [6].

Aircraft	Composite components
F-14	Doors, horizontal tail, fairings
F-15	Rudder, vertical tail, horizontal tail, speed brake
F-16	Vertical tail, horizontal tail
F-18	Doors, vertical tail, horizontal tail, wing box, speed brake, fairings
B-1	Doors, vertical tail, horizontal tail, flap, slats, inlet
AV-8B	Doors, rudder, vertical tail, horizontal tail, aileron, flap, wing box, body, fairings
757	Doors, rudder, elevator, aileron, spoiler, flap, fairings
767	Doors, rudder, elevator, aileron, spoiler, fairings

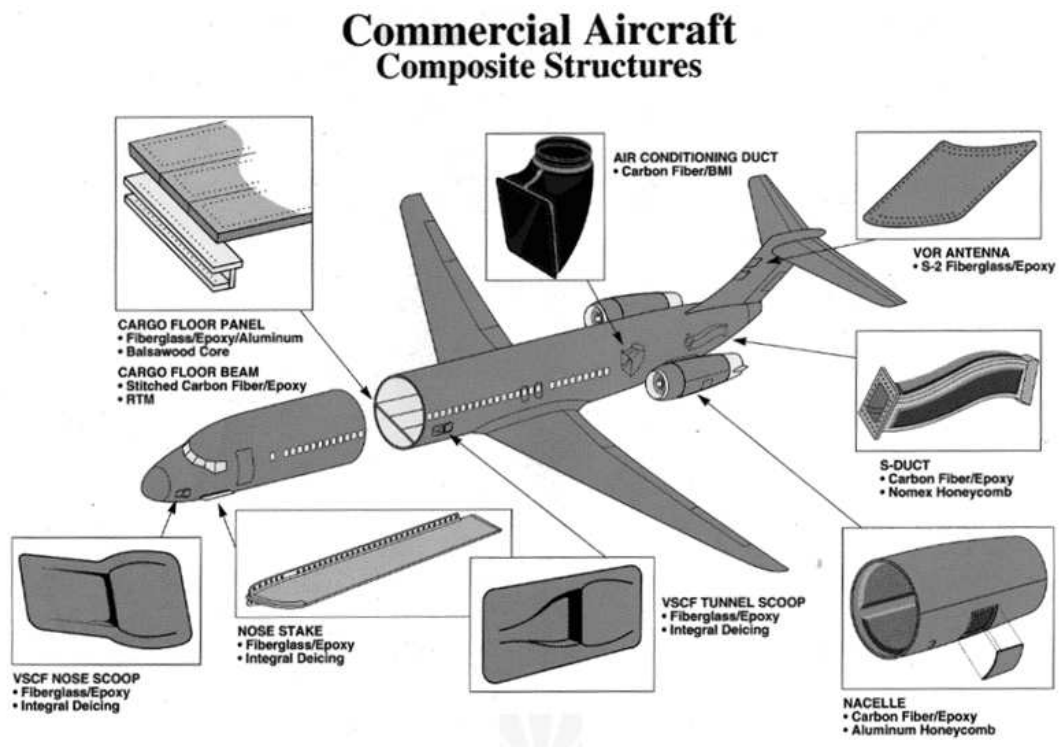


Figure 1.1: Typical composite structures used in a commercial aircraft [7].

Military Aircraft Composite Structures

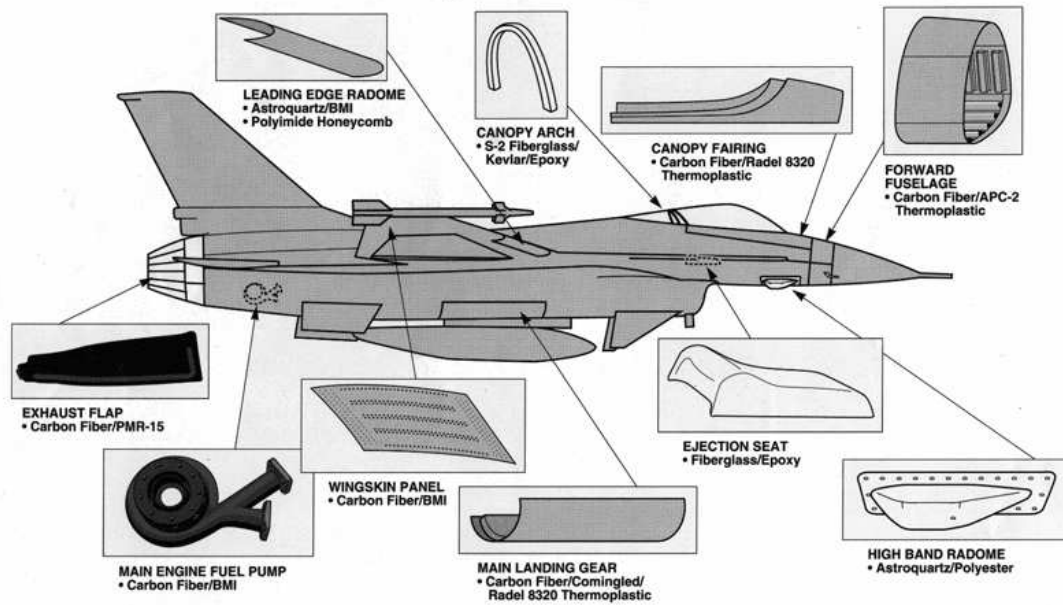


Figure 1.2: Typical composite structures used in a military aircraft [7].

Engine Components

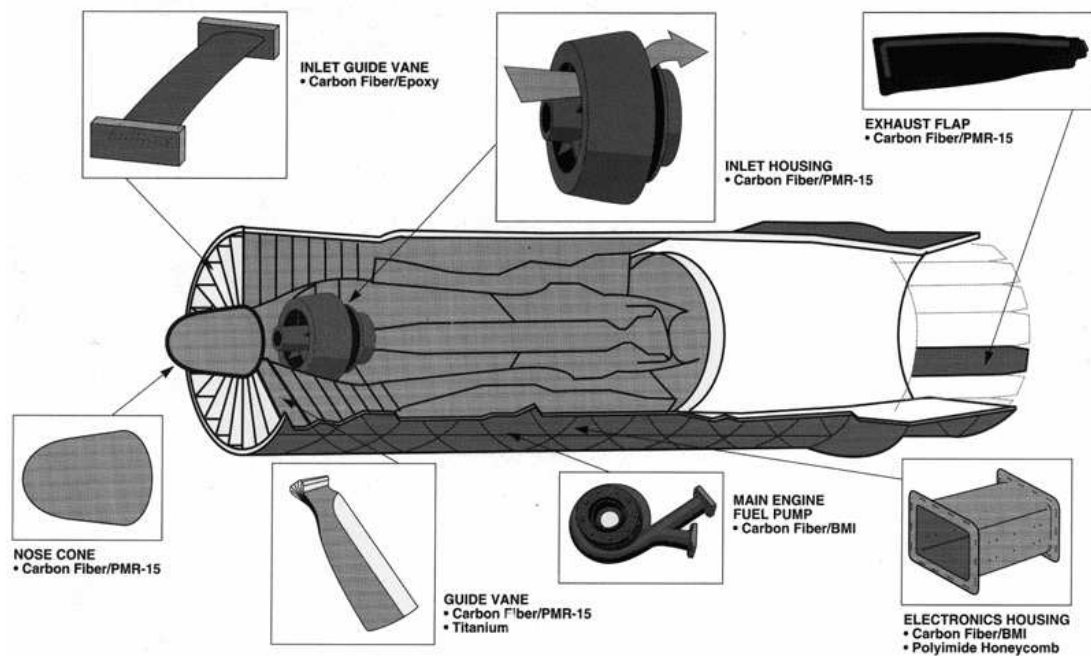


Figure 1.3: Composite components used in an engine application [7].

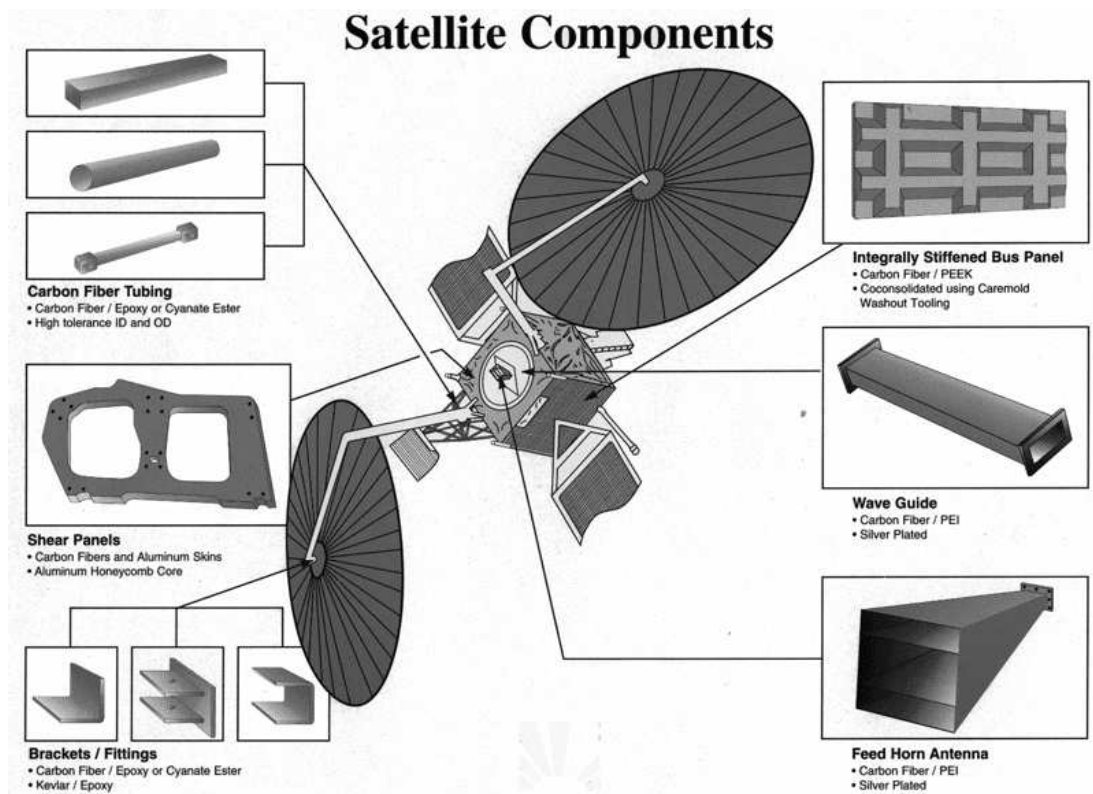


Figure 1.4: Composite components used in a satellite application [7].

1.2 An Introduction to Unmanned Aerial Vehicles

An unmanned aerial vehicle (UAV) is defined as a type of powered aircraft that does not carry a human pilot, uses aerodynamic forces to provide lift, can fly autonomously or be remotely controlled, can be expendable or recoverable, and can carry a lethal or non-lethal payload [8]. In the recent decades, the use of UAVs is increased rapidly both in the military and civil aviation applications. Being more cost effective than manned systems, and being a multi-purpose versatile aircraft are some of the main aspects that can be addressed to the reasons of the increase in the popularity of the use of the UAVs.

The developments in the materials technology made it easy to access and purchase composite materials. Recently, with the advances in the composite manufacturing technology very complex shaped parts can be built effortlessly within a few days. Since, most of the UAVs are

built from composite materials, it became possible to manufacture a UAV in a laboratory or a workshop by 4 or 5 people within a few week. Moreover, the maintenance and repair processes of the UAVs can be performed very quickly and easily, since they are assembled from small, cheap and easy to manufacture composite parts.

Inasmuch as no pilot is inhabited, limitations from the human abilities are disregarded in the design which leads to aircrafts with increased maneuverability, reduced size and weight, and improved control characteristics with the help of autopilot systems. The UAVs can perform dull, dirty and dangerous missions that would be very risky for a pilot to endure like battlefields, enemy territories, atrocious weather and environments with noxious gases or smokes.

The UAVs differ from the size of a small bird to a commercial airplane with many different mission profiles. Airbourne intelligence, surveillance and reconnaissance, close air support, air combat and ground strike, and homeland security are some of the military associated usage areas. In addition to the military usage, search and rescue, disaster and public infrastructure monitoring, meteorological data acquisition, precision farming, remote aerial mapping, habitat inspection can be given as examples of civilian usage areas of the UAVs.

There are many ways to classify the UAVs. A general classification defined by the Unmanned Vehicle Systems (UVS) International is shown in Table 1.2 [9]. Since the UAVs are designed considering a defined mission profile, their sizes and other performance parameters like range, endurance and flight altitude are indicators of their usage areas. For example, owing to their small size and low take-off weight micro and mini UAVs are generally used in airbourne intelligence, surveillance and reconnaissance missions in the close range by carrying cameras or other types of small electronic equipment as a payload. Medium range UAVs are generally designed to have a more flexible choice of payloads, and are capable of performing more complicated missions in addition to airbourne intelligence, surveillance and reconnaissance missions. With the impressive performance parameters, medium and high altitude long endurance type UAVs

can surmount any kind of mission successfully in almost any flight condition. Sample photos of the example UAVs given in Table 1.2 can be seen in Figure 1.5.

Table 1.2: Classification of UAVs defined by UVS International

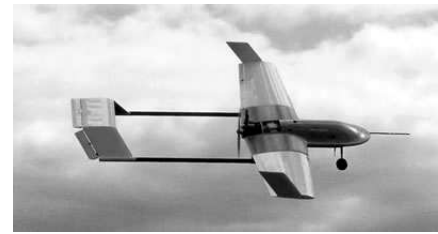
UAV Category	Range [km]	Flight Altitude [m]	Endurance [hr]	Max. Take-Off Weight [kg]	Example
Micro	<10	250	1	<5	Wasp III
Mini	<10	150 - 300	<2	<30	Raven
Medium Range	70 - 200	5000	6 - 10	1250	Sky Spirit
Medium Altitude Long Endurance	>500	14000	24 - 48	1500	Predator
High Altitude Long Endurance	>2000	20000	24 - 48	12000	Global Hawk



(a) Wasp



(b) Raven



(c) Sky Spirit



(d) Predator



(e) Global Hawk

Figure 1.5: Examples for the UAV types: (a) Micro, (b) Mini, (c) Medium Range, (d) Medium Altitude Long Endurance, (e) High Altitude Long Endurance

1.3 Mini UAV System Built In Aerospace Engineering Department

Following the increasing trend in aerospace industry, an unmanned aerial vehicle research center is founded in the Aerospace Engineering Department in the Middle East Technical University. For a project financed by the State Planning Organization, a mini UAV system, named “Güventürk”, is designed and produced in the research center. The UAV was designed to accomplish the missions of observation, reconnaissance and surveillance autonomously within a range of 10 kilometers through the use of day or infrared camera. It is hand launched, and is capable of belly landing on a flat surface. Some specifications of the mini UAV are given in Table 1.3.

Table 1.3: Specifications of Güventürk

Wing Span	2.2 m
Length	1.35 m
Aspect Ratio	10
Maximum Take-off Weight	4.5 kg
Empty Weight	3 kg
Maximum Range	10 km
Maximum Endurance	1.5 hr
Payload	Day/Infrared Camera
Engine	Brushless electric motor
Battery Type	Lithium-Polymer

The mini UAV has been made up of 100 % composite materials. Considering the loads that will be exerted on the aircraft; e-glass, carbon, and kevlar type woven fabrics are used. These are plain weave balanced fabrics with 0/90 degrees fiber orientation. For the matrix material epoxy is used since it is available in the market plentifully. The fuselage, which carries the autopilot and other electronic components has been made of carbon fiber and has been strengthened by kevlar for landing loads. Wing structure was manufactured from e-glass, and carbon fabrics in addition to balsa wood and styrofoam layers with different thicknesses which are used for increasing the stiffness of the structure where necessary. As for the manufacturing method, details of which is explained in Chapter 2 thoroughly, vacuum bagging method with curing at room temperature is used. A view of the UAV taken in operation is shown in Figure 1.6.



Figure 1.6: Mini UAV system, Güventürk in operation.

1.4 Aim and Scope of the Thesis

The main objectives of this thesis can be listed as:

- i. Detailed manufacturing process of the UAV wing out of composite materials, including the molds used.
- ii. Characterization of the materials used in the UAV.
- iii. Preliminary structural analysis of the wing.

Establishing a composite manufacturing workshop is one of the milestones of this study. Implementing vacuum bagging system, preparing molds of the UAV wing, and building the wing from these molds are some of the main goals of this work. In Chapter 2, preparing the male and female molds of the wing, and manufacturing the wing structure is explained in detail.

Unlike metals, composite materials are very sensitive with the manufacturing process. With different manufacturing procedure, they tend to have different structural characteristics. Therefore, it is important to know the aspects of the composite material used. As a preliminary work, several mechanical tests can be performed to obtain some properties in order to have an approximate information. In this study, longitudinal tensile testing is used to obtain the elastic

modulus and maximum strength of the materials. Additionally, the properties are obtained using micromechanics of composites and another approximate approach. Material characterization is explained in Chapter 3. These three different modulus information is used as a material input in the finite element analysis of the wing structure, and the results are compared.

Finite element analysis is performed using MSC Patran 2006¹ and MD Nastran 2006 r1¹ programs. The fibers used in the UAV are plain weave fabrics, which have a complicated structure and detailed meso scale models are required for the analysis. However, some practical methods can be used for a preliminary analysis. In this study, two different methods are used for modeling the woven structure. First method is modeling the woven lamina as a two layer cross ply laminate where the thickness of each layer is taken as half thickness of actual woven lamina. Second method is modeling the woven lamina as a single equivalent layer by assuming $E_1 = E_2$. In the analyses, these two methods are used with the material properties obtained from three different ways. For a case study of simulating level flight conditions, spanwise distribution of wing loading is obtained using a program of ESDU [10], and the wing is analyzed with distributed loading. Additionally, the front spar of the wing is analysed with two approaches: transformed section method, and finite element analysis. Details of the analyses and the results obtained from finite element analysis are given in Chapter 4.

In Chapter 5, the results of this study are discussed, concluding remarks are made, and recommendations on the future work are presented.

¹ Licenced to METU Aerospace Eng. Dept.

CHAPTER 2

MANUFACTURING OF THE UAV WING

Building a UAV wing out of composite materials is one of the main aims of this study. For this scope, a composite workshop is founded in the Department of Aerospace Engineering at METU. The composite wing is manufactured using male and female molds with vacuum bagging technique by a group of people consisting of aerospace engineers and technicians. In the following sections of this chapter detailed descriptions of manufacturing process is available. Firstly, the composite manufacturing method, vacuum bagging, is explicated. Then, manufacturing of the male mold and female molds of the wing is explained. Finally, the manufacturing of the wing structure is elucidated at the end of this chapter.

2.1 Vacuum Bagging Method

The fabrication process is one of the most important steps in the application of composite materials. Because, every step in the manufacturing process affects the final mechanical properties of the composite structure. There are several manufacturing techniques for preparing a composite material from continuous fiber and non-metallic matrix material. Some of them are vacuum bagging, matched die molding, filament winding, and resin transfer molding. Vacuum bagging method was the manufacturing technique that was applied in the manufacturing of the

UAV wing. In this section, manufacturing with vacuum bagging method will be explained in detail.

Vacuum bagging, basically, is a process applied after laying-up the fiber material over the mold surface and wetting with the matrix material. The mold is covered by a bag that prevents the air passage, and vacuum is applied during the curing period of the matrix material.

One of the main advantages of vacuum bagging method is that it is relatively cheaper to set up, especially when compared to curing in autoclave. Other advantages can be listed as follows:

- i. Laminates with higher fiber content can be achieved than with standard wet lay-up techniques, since the excess resin is absorbed from the laminate surface. By reducing the resin/fiber ratio, brittleness of the final structure is reduced; because most thermoset resins are brittle materials.
- ii. Minimizing the voids due to trapped air within the laminate, and therefore avoiding possible crack initiation points; composite structures with higher strength can be achieved.
- iii. Owing to the applied pressure, a better distribution of resin throughout the fibers is achieved. This results in a more homogeneously wetted fibers which gives opportunity to have a better estimation of the mechanical characteristics of the laminate using numerical or analytical methods.
- iv. Due to the pressure applied, the layers will compress each other, that leads to a composite structure with well connected, or cohered layers. Consequently, the shearing strength between the layers will be increased.

There are several items used in the vacuum bagging process. They are mainly used for preparing a well sealed vacuum environment, collecting excess resin from the composite material, having a desired surface quality, and taking the composite product out of the mold easily. In the

market, vast amount of these items having different characteristics are available. Here, some of the main items that can be used in a basic application of vacuum bagging are listed and described below. Also, in Figure 2.1, a schematic drawing the vacuum bagging method is shown.

1. **Release agent:** is a kind of chemical that is applied to the tool surface for preventing the sticking of the laminate to the mold surface.
2. **Peel ply:** is a tightly woven fabric, often nylon, and impregnated with some type of release agent. It is used to give the laminate a rough surface, rather than a smooth finish.
3. **Release film:** is a thin plastic which has been treated so it will not bond to the laminate. There are small holes on it allowing the matrix material to pass through.
4. **Breather:** is a thick layer of cloth used for collecting the excess resin from the laminate that passed through the peel ply and the release film. It also provides the uniform vacuum distribution.
5. **Vacuum bagging film:** is a relatively thick plastic layer which is used for isolating the laminate. It provides the necessary vacuum environment.
6. **Sealant tape:** is a putty-like sticky material. It is used for sticking the vacuum bagging film to the tool surface, and it prevents air leakage.
7. **Vacuum pump:** is used for supplying necessary vacuum pressure.

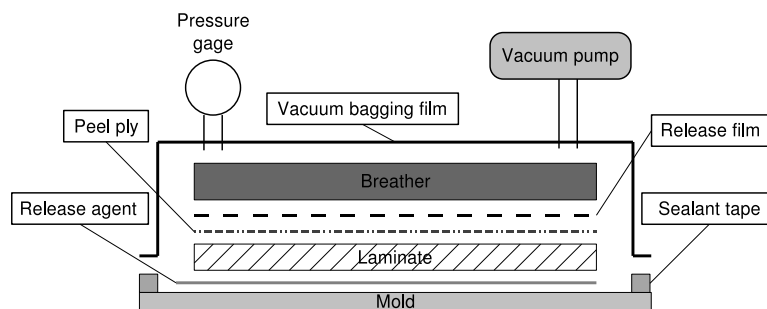


Figure 2.1: Schematic drawing of vacuum bagging process.

2.1.1 Manufacturing a Composite Plate with Vacuum Bagging Method

As shown in Figure 2.1, vacuum bagging is a quite simple method to apply for manufacturing composite structures. However, building structures successfully requires some labor intensive work and some practice. In this section, manufacturing a composite plate with vacuum bagging method will be described in detail by supporting with photographs taken. Composite plate was manufactured with the intention of preparing coupons for tensile testing.

For the plate manufacturing, a glass table surface is used as the mold surface. Before starting, it should be assured that the mold surface is free from any foreign objects, particles, oil or other chemicals.

In the beginning, sealant tape is adhered to the boundaries of the area that the lay-up process will take place. For the example manufacturing, double sided tape is used as the sealant tape (Figure 2.2 (a)). It should be noted that, the upper side of the tape is not opened yet; considering the possible sticking of the composite fabrics or other items while setting up the system.

After defining the boundary of application area, release agent is applied over the enclosed mold surface. Here, care must be taken that there should remain no surface that the release agent is not applied. In other case, the laminate will stick to the mold surface, and it can be cracked or broken when releasing it from the mold. To be on the safe side, it is recommended to apply the release agent twice. Some time must be allowed for the release agent to dry totally. The surface after the application of the release agent is shown in Figure 2.2 (b).

Afterwards, some resin mixture is applied to the bare mold surface with a brush. The reason for this action is to prevent the slipping of the fiber cloth over the mold surface when applying the resin mixture. Then, the first layer of the fabric is placed over the pre-wetted mold surface. These steps are shown in Figures 2.2 (c) and (d). The resin mixture is applied with the brush, and the layer is wetted thoroughly as shown in Figure 2.2 (e). The other layers of fabric can

be placed over the first layer with the desired orientation, and each layer is wetted in the same manner. Figure 2.2 (f) illustrates the placement of the second layer over the first one.

After the desired stack-up sequence is obtained, a layer of peel ply can be placed over the laminate if a rough surface is desired in the final product. Here, in the example manufacturing peel ply layer was unnecessary to use since it is a coupon fabrication, and a rough surface is not essential. A layer of release film is laid-up over the laminates for the excess resin to pass through as shown in Figure 2.2 (g).

Over the release film, a layer of breather is placed (Figure 2.2 (h)). The function of the breather is to absorb the excess resin, and to disperse vacuum under the bag. After this process, thicker layers of breather are placed on top of the breather layer. These thicker breather layers are placed to the locations where the vacuum ports are going to be put. In this way, it is assured that the vacuum ports are kept away from excess resin that might choke up the vacuum port. In addition, the thicker layers of breather prevent the final composite part from being squeezed by the metal ends of the vacuum port. Failure to do so, may induce unwanted wrinkles at the locations of the composite plate which coincides with the vacuum port. Over these thicker breathers, bottom halves of the vacuum ports are placed (Figure 2.2 (i)).

Subsequently, paper coverings on the top of the double sided tapes are peeled off (Figure 2.2 (j)), and vacuum bagging film is adhered to the double sided tape. Choosing the right size of the vacuum bagging film is critical. Too small of a vacuum bagging film may cause the film to stretch which could cause a rupture during the cure. Allowing for approximately 30% to 40% excess vacuum bagging film is recommended.

It should be stressed that, it is very important to entirely seal the vacuum bagging film, and to have a perfect vacuum medium. Therefore, to provide this, the sticking of the vacuum bagging film to the double sided tapes is started from one edge and continued with the consecutive edge

after totally sticking the first edge. Since excess vacuum bagging film is used, there are some pleats formed. These pleats are processed in the final edge. Approximately, a 10 cm part of the edge is remained unsticked. At this location, a strip of double sided tape is stuck inside the vacuum bagging film covering the pleat and it is stuck to itself first, and then over the tape on the edge of the mold (Figures 2.2 (k), (l), (m), (n)).

After adhering the vacuum bagging film, small slits are cut on the film at the points where the top halves of the vacuum ports will be connected to the bottom halves (Figure 2.2 (o)). Over these slits, top halves of the vacuum ports are placed, and the top parts are twisted firmly to fix the ports (Figures 2.2 (p) and (q)).

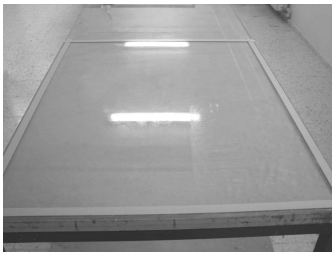
Vacuum gage is installed to the one of the vacuum ports (Figure 2.2 (r)), and the hose of the vacuum pump is installed to the other one (Figures 2.2 (s) and (t)). Vacuum pump is started while the hose of the vacuum pump is held straight and perpendicular to the surface until the vacuum reaches everywhere under the vacuum bagging film (Figure 2.2 (u)).

After reaching a certain pressure, it should carefully be checked whether there is leakage of air from the vacuum ports or the sealant tapes. For this, hose of the vacuum pump is unplugged and the pressure gage is controlled for possible pressure drop in the dial. In addition to pressure gage check, the mold surface is examined by eye check, and it is also controlled with ear to hear if there is a noise of air leakage. If any defects are detected in the vacuum bagging film, those locations must be treated with sealant tapes properly.

After the leakage check, the hose of the vacuum pump is plugged again, and the pump is restarted. During the curing of the resin, it is recommended that the vacuum pump is kept working; even though there is no air leakage. Depending on the resin material used, it is advised to preserve the laminate under vacuum environment for about 12 hours. Considering the capacity of the vacuum pump, the vacuum environment is held under almost -1 atmosphere

pressure (Figure 2.2 (w)).

Finally, the cured composite plates (Figure 2.2 (x)) are removed from the mold surface after finalizing vacuum process and removing the vacuum bagging film and the other items. In the removal process of the plates, thin, sharp edged tools like a spatula, or a blade are used. The edges of the composite plates are trimmed, and the plates are cut to the desired size and prepared for use.



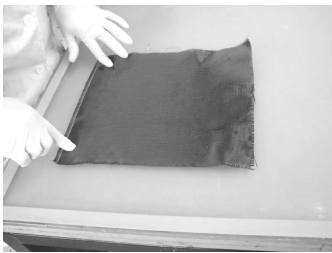
(a)



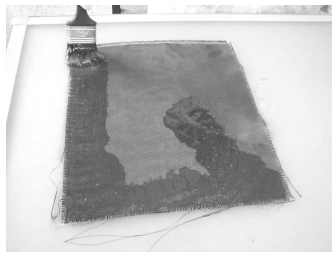
(b)



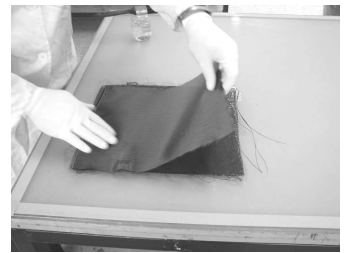
(c)



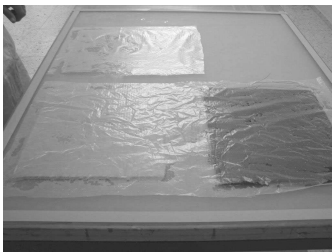
(d)



(e)



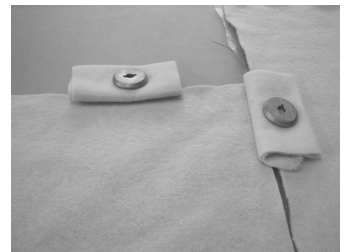
(f)



(g)



(h)



(i)



(j)



(k)



(l)

Figure 2.2: Manufacturing steps of a composite plate with vacuum bagging method.



(m)



(n)



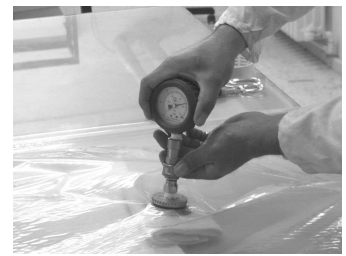
(o)



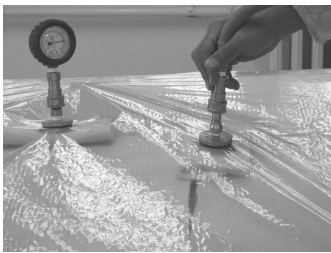
(p)



(q)



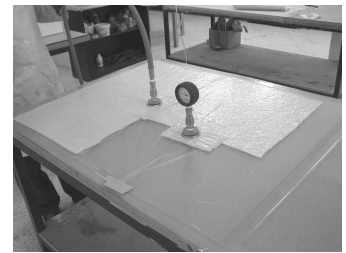
(r)



(s)



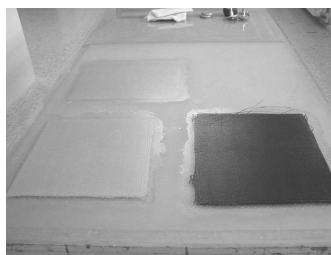
(t)



(u)



(w)



(x)

Figure 2.2: Manufacturing steps of a composite plate with vacuum bagging method (continued).

2.2 Manufacturing of the Skin Molds of the Mini UAV Wing

2.2.1 Manufacturing Process of Male Models of the Wing

In this section, the detailed manufacturing process of the male models of the wing will be explained. Male wing model will serve for the purpose of manufacturing the female wing molds which will be used in the manufacturing of the upper and lower wing skins. 3-D drawings of the wing is shown in Figure 2.3.



(a) Isometric view



(b) Front view

Figure 2.3: 3-D model of the wing.

As shown in the wing drawings, the wing is designed with a 3° dihedral at the outer wings. To handle this difficulty, in the final design the wing was planned to be composed of three parts: a center wing and two outer wings. For this, male foam models of the center wing and outer wings have been cut by utilizing the numerically controlled foam cutting machine which is shown in Figure 2.4.

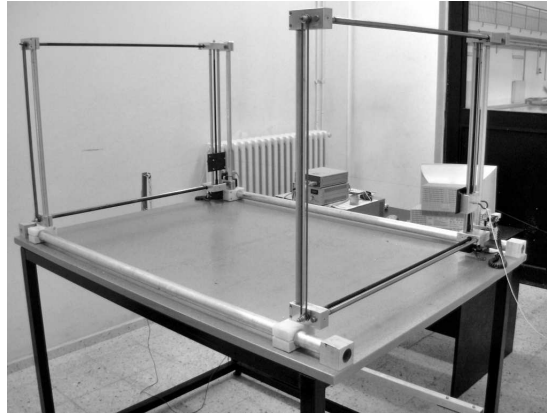


Figure 2.4: Numerically controlled foam cutting machine.

Foam cutting machine is a practical CNC machine used for cutting polystyrene foams easily and accurately. The cutting action is done by a hot cutting wire which is numerically controlled from the two ends via feeds. The driving mechanisms of both feeds are controlled by the software installed on the PC. The software also controls the current and the voltage in the cutting wire, as well as the speed and x-y location of each of the feeds. A schematic set-up of the foam cutting machine is shown in Figure 2.5.

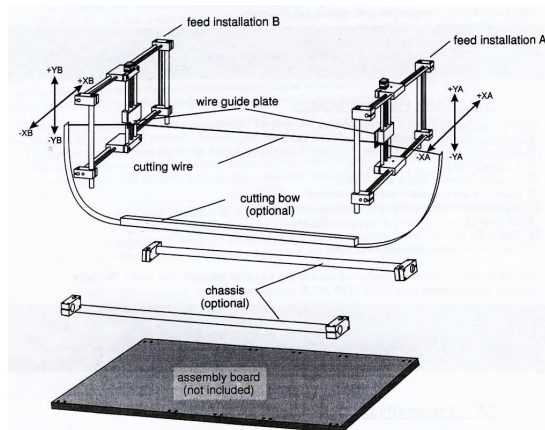


Figure 2.5: Schematic set-up of the foam cutting machine.

For cutting a wing model from polystyrene, the airfoil geometry files of the tip and root sections of the wing are loaded to the PC. Then, with proper feed speed and wire temperature

the model is cut from the foam block. It is important that, while cutting the foam, the block should not move. For this reason, the foam block is suitably fixed to the assembly board of the cutting machine. Regarding the opening between the feeds, models with long span can not be cut in one operation; instead, they must be cut in sections with narrower spans which are to be assembled later on.

For the two outer wings and the center wing the wing profile is cut from block of foam material which is in the form of rectangular prism. Since the wing will be composed of three parts the three blocks were cut to same size except for the length which is different for the center and outer wing. The three wing profiles were cut from the foam material such that the starting point of the cutting wire was adjusted to the same location on the foam blocks. Figure 2.6 shows the schematic drawing of the chordwise cross section of the male mold and the resulting female foam molds.

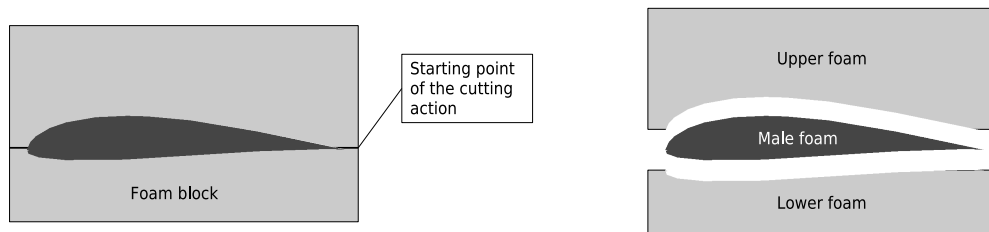


Figure 2.6: Male and female wing molds prepared from the foam material.

At the end of the cutting operation, three male foam molds and their counterpart upper and lower female molds are made ready.

Adjustment for the dihedral:

The dihedral is adjusted by providing the half of the dihedral angle on the center wing and the other half on the outer wing. To do this, the outer and center wing is cut at 1.5° along the chord line at the locations corresponding to the connection of the center wing and the outer wings as shown schematically in Figure 2.7.

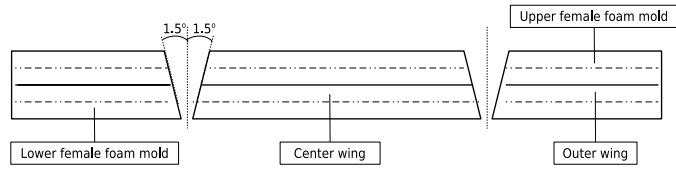


Figure 2.7: Adjustment of the dihedral angle in the male-female foam mold assembly.

When the three pieces of the total molds assemblies for the outer and center wing are placed on a smooth tool table the dihedral angle is formed as shown in Figure 2.8.

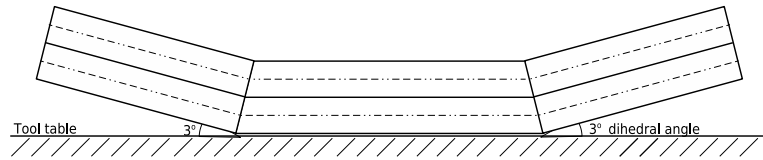


Figure 2.8: Final dihedral angle formed.

Before the start of the production of the actual male model of the aircraft, the wing molds have to be positioned properly. The positioning of the outer wing molds with respect to the center wing molds is accomplished by adjusting the right tip height of the outer wing mold assembly from the tool table. In this process, foam supports and polyurethane foam are used to adjust the tip height of the molds such that the required dihedral angle is attained. In the meantime, in order to prevent the movement of the center wing lower mold on the tool table, the lower female molds are stuck to the tool table by double sided bands as shown in Figure 2.9.

After the tip height adjustment of the outer wing mold assembly with respect to the center wing, the outer and center wing molds are positioned by using bands. At the same time, the male molds are also secured to the lower female molds by double sided bands in order to prevent unexpected movement of the male foam molds.

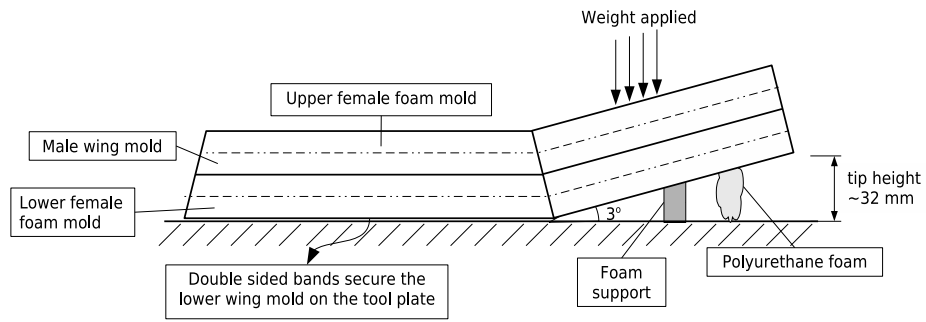


Figure 2.9: Positioning of the outer wing with respect to the center wing.

It should also be noted that because of the expansion of the polyurethane foam during curing, some weight is put on the upper female foam mold. This way, position change of the outer wing molds during the curing period of the polyurethane foam is prevented.

The mold assembly is left for some period of time in order to allow time for the polyurethane foam to cure. Once the polyurethane foam is cured, the upper female molds are removed as shown in Figure 2.10 which shows the schematic side view of the mold assembly.

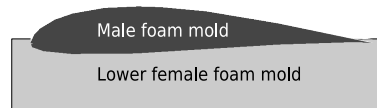


Figure 2.10: Side view of the mold assembly after the upper female foam mold is removed.

4 layers of E-glass fabric are laid-up over the male foam mold together with the application of epoxy resin between each fabric layer. This process is shown schematically in Figure 2.11.

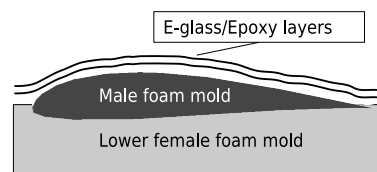


Figure 2.11: Application of composite layers on one side of the male foam mold.

The hand lay-up assembly is left for curing for one day. After the curing of the assembly, the upper surface of the wing is initially treated by sandpaper and a layer of polyester paste is applied over the wing surface. The goal of smearing a layer of polyester over the wing is to fill in the pores of the composite fabric. This way, a smooth wing surface is achieved. After the application of the polyester paste, the wing structure is treated by different grade sandpapers. Initially, the wing surface is treated in dry conditions. The last sandpaper treatment is performed with a higher grade sandpaper wetted with water in order to achieve a very smooth wing surface.

After all the treatments of the wing surface is completed, the complete wing is removed away from its lower female foam mold mold. Schematic view of the removed wing is shown in Figure 2.12.

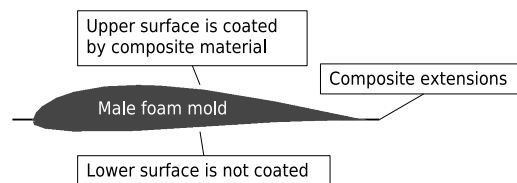


Figure 2.12: Male wing mold removed from the mold assembly.

During the removal of the wing from the lower female foam mold assembly, care should be taken in order not to give harm to the lower foam mold. Because lower female mold can be used for various other purposes later on. Therefore, the wing is separated from the lower female foam mold by pulling the wing away from the banded regions. At this point, it should be stressed that the wing should be secured to the lower female foam mold by the double sided bands only for a very short distance at certain locations. If a long band length is used, then it will be very difficult to separate the male wing mold away from the lower female foam mold.

The cured composite material extensions at the leading and trailing edges are cut, and the

edges are treated by the sandpaper to smooth out the irregularities. After the control of the wing profile by the wing profile templates, the wing is turned upside down, and it is placed on the upper female foam mold. This process is shown schematically in Figure 2.13.

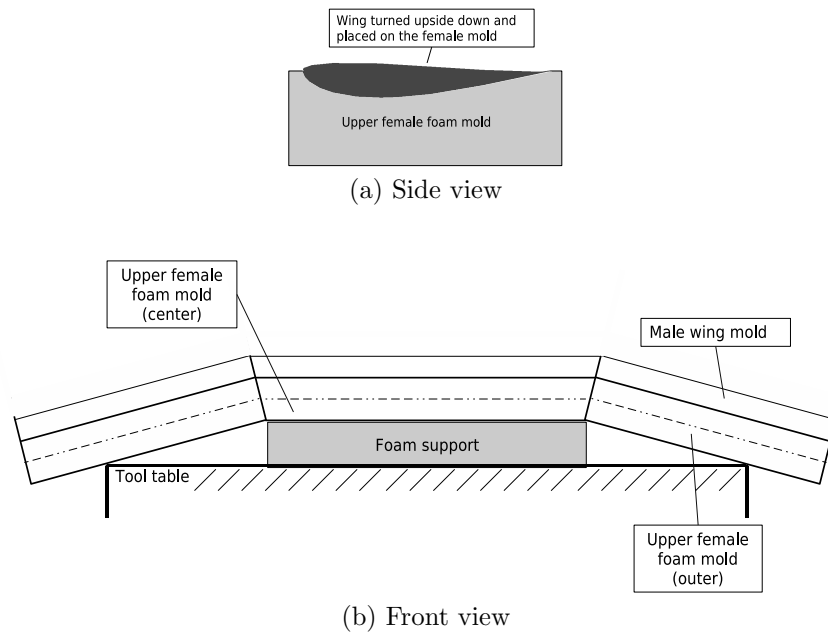


Figure 2.13: Adjustment of the male wing mold in the upper female foam mold.

At this point, it should be noted that after the application of the composite material over one surface of the male foam mold, the wing becomes one integral piece. The wing is then placed onto the center female foam mold and the whole assembly is brought to a higher altitude by the help of foam support, in order to clear the outer female mold from the edge of the tool table. At this point, the outer female molds are secured to center mold and dihedral angle is checked. If the required dihedral angle is not met, the outer wing female molds are stretched downwards or upwards depending on the deviation of the dihedral angle from the true value.

The stretched molds are secured to the tool table from the sides of the molds by polyurethane foam. In order to prevent any slight movement of the male wing mold in its female mold, the male mold is secured to the upper female foam mold by double sided band at certain locations, paying attention not to use too long length of the band in order to ease the removal of the male

mold from the female mold after the operation.

4 layers E-glass fabric is lay-up over the male foam mold together with the application of epoxy resin between each fabric layer. This process is shown schematically in Figure 2.14.

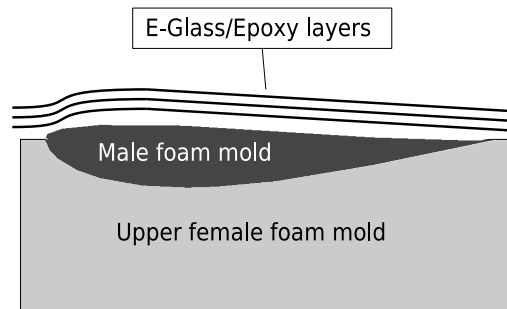


Figure 2.14: Application of composite layers on the foam side of the male mold.

Similar to the sequence of operations applied for the other side of the male mold, the whole assembly is left for curing approximately for one day. After the curing, the bands which are used to position the male wing mold on the female molds are removed. The wing is pulled away from the upper female foam mold and separated from the double sided bands which were used to secure the male mold in the female mold. The composite fabric extensions at the leading and trailing edges are cut and the remaining irregularities are smoothed out with sandpaper. In order to close the pores of the composite fabric, the lower face of the wing is also smeared by polyester paste. After the paste is dried, the surface of the wing is treated by sandpaper in dry and later on in wet conditions.

Two wooden wing templates, made of balsa wood, were prepared by using a metal wing profile. These wooden templates are connected to the right and left wing tips as shown schematically in Figure 2.15.

The wooden wing templates are stuck to the foam by polyurethane foam and by means of paper

bands the tip profiles are secured to the wing tip, and the whole assembly is left for the cure of the polyurethane foam as shown in Figure 2.15 (b).

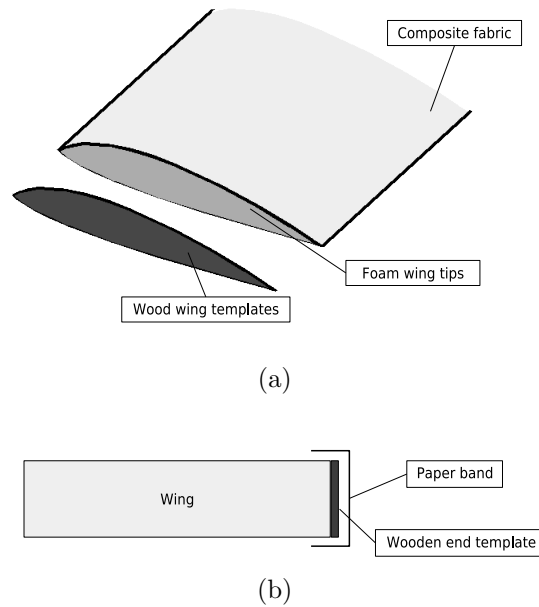


Figure 2.15: Preparation of wing tip profiles.

After the end plates are assembled, the whole leading edge of the wing is covered by 2 or 3 layers of slice of E-glass/Epoxy composite material as depicted schematically in Figure 2.16.

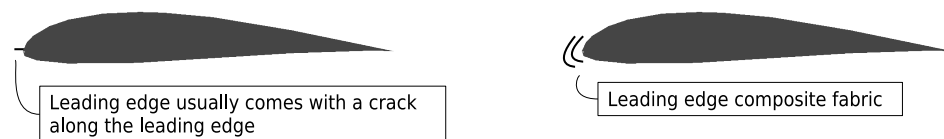


Figure 2.16: Application of leading edge composite fabric.

After the curing of the leading edge composite material, the leading edge and wing tips are treated by sandpaper and these surfaces are smoothed out.

Finally, the wing leading edge and wing tips are covered by polyester paste to close the pores of composite fabric and any opening that might exist, especially at the wing ends. After the application of the polyester paste, the wing tips and leading edge is treated by different grade sandpapers in sequence and the surfaces are treated to be as smooth as possible. As in the other surfaces of the wing sandpaper treatment is performed first in dry conditions and then in wet conditions in order to produce a very smooth surface.

The last operation of the preparation process of the male wing mold is the painting of the wing by a primer. This operation is shown schematically in Figure 2.17.

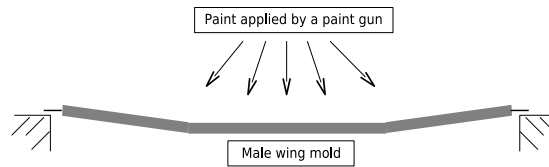


Figure 2.17: Final painting operation of the male wing model.

Primer application on the wing surface serves for the purpose of detecting the indented areas of the wing surface. Detection of indented areas of the wing surface is accomplished by first smearing the polyester paste over the painted wing surface. Afterwards, the paste is scraped over the wing surface by a sharp edged metal sheet. Thus, the indented areas are filled with the paste and they can be easily visualized because of the color change of those areas. The correct surface areas preserve their true color. This operation is shown schematically in Figure 2.18.

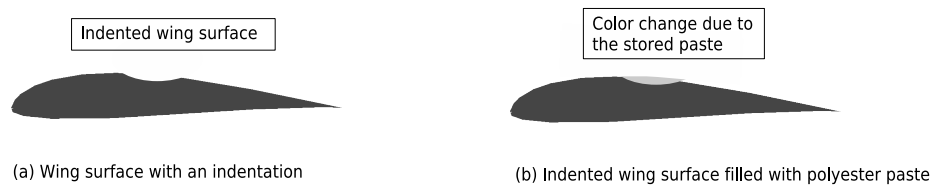


Figure 2.18: Final surface finishing operation of the surface of the male wing model.

Following the correction of the irregular areas of the wing surface by the method described above, the whole wing is left for the dry-out period of the polyester paste.

As for the final operations, the wing surface is treated with a high grade sandpaper for smoothing the paste particles which remained on the wing surface. Grade 600 is used for this purpose. Then, one layer of paint is applied again with a paint gun over the whole wing surface. After the final painting, the whole surface is again treated with a higher grade sandpaper in wet condition this time. Sandpaper with grade 800 is used for this purpose. The picture of the male wing model is shown in Figure 2.19.

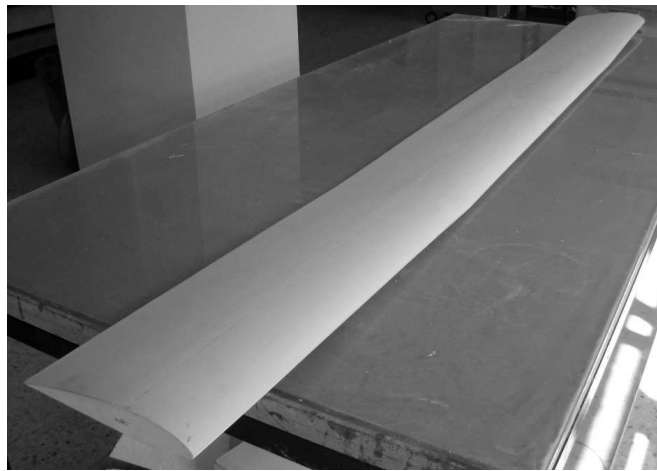


Figure 2.19: Picture of the male wing model after final operations.

It should be emphasized that achieving a very smooth and correct male wing surface is essential for manufacturing correct female molds which will be used for the production of wing skins. Therefore, in this section the sequence of surface treatment operations are introduced in detail to emphasize the need for achieving high quality surface finish of the male wing model.

2.2.2 Manufacturing Process of the Upper and Lower Wing Skin Female Molds Using the Male Wing Model

In this section, the detailed manufacturing process of the female wing skin molds will be described. The female molds will be used in the production of the upper and lower wing skin for the purpose of building up the total wing structure. The manufacturing process of the female mold will be described by referencing schematic drawings which will aid the understanding of the detailed steps of the process.

Initially, the male wing model is placed on the tool table for the purpose of positioning for the female mold production. Figure 2.20 shows the two schematic views of the male model placed on the tool table.

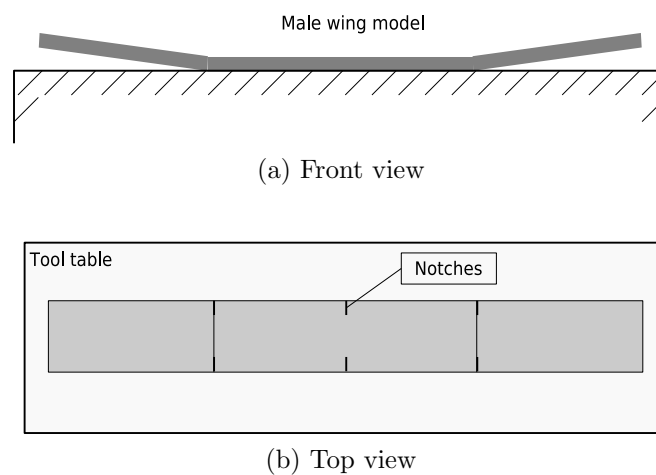


Figure 2.20: Positioning of the male wing model on the tool table.

As shown in Figure 2.20 (b), notches are created with a knife at the center/outer wing connection points, and at the center of the wing on the male model. This way, after the production of the female molds, these positions will be generated automatically on the female molds.

After the initial marking and control of the male model, the model is positioned on the tool table as shown schematically in Figures 2.21 and 2.22. Figure 2.21 shows the sectional view

taken at the center wing location.

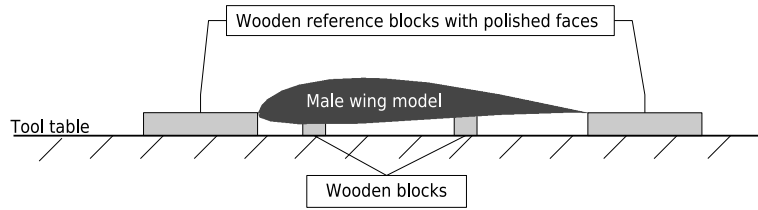


Figure 2.21: Section of the center wing/reference block assembly.

As shown in Figure 2.21, male wing model is lifted up from the tool table by the help of wooden blocks which are positioned underneath the wing. The height adjustment of the male model from the tool table is done such that the leading and trailing edges of the wing model are brought in line with the two reference blocks. The reference blocks in the end will form the flange surface of the female molds. The top view of the assembly given in Figure 2.21 is shown in Figure 2.22. This figure shows that, the wooden blocks completely surrounds the male wing model, and total of 8 wooden blocks are used around the male wing model.

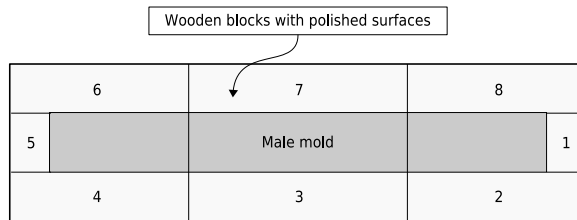


Figure 2.22: Top view of the wing model and reference blocks.

The critical point in the positioning of the male wing model with respect to the reference blocks is to bring the leading edge and trailing edge of the wing in line with the edges of the reference blocks around the wing. To accomplish this, fine tuning of the height adjustments is done by placing paper bands on the wooden blocks which are placed underneath the wing model (Figure 2.21). Figure 2.23 shows the front view of the assembly of the wing and the reference blocks.

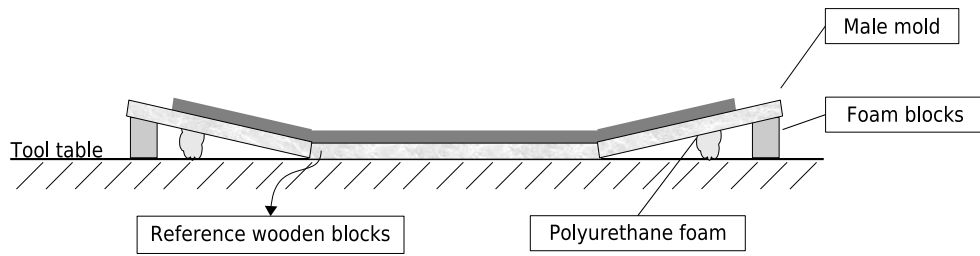


Figure 2.23: Front view of the wing mold and reference blocks.

The foam blocks are used to position the reference wooden blocks surrounding the outer wings. At the same time, polyurethane foam is injected underneath the reference blocks and underneath the outer wings to secure the wing and the surrounding reference wooden blocks to the tool table. It should be noted that polyurethane foam, once cured, provides the sticking action of the wing and the reference wooden blocks with the tool table. Figure 2.24 shows the side view of the wing/reference block assembly.

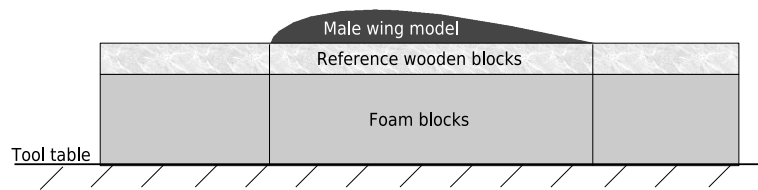


Figure 2.24: Section of the outer wing/reference block assembly; tip section.

As it is seen in Figure 2.24, foam blocks are used at the tip section to support the reference wooden blocks. Again, the critical point here is to bring the leading and trailing edges of the outer wing in line with the inclined edge of the reference wooden blocks. To achieve the accurate positioning, wood shims are placed between the reference wooden blocks and the edge foam blocks. Thus, the whole wing, including the center and outer wing, is brought in line with the upper edges of the reference blocks.

Before the application of the polyester layer over the wing surface and the reference blocks, the connection lines between the reference blocks and the wing are sealed with a suitable sealant.

The sealed regions are shown schematically in Figure 2.25.

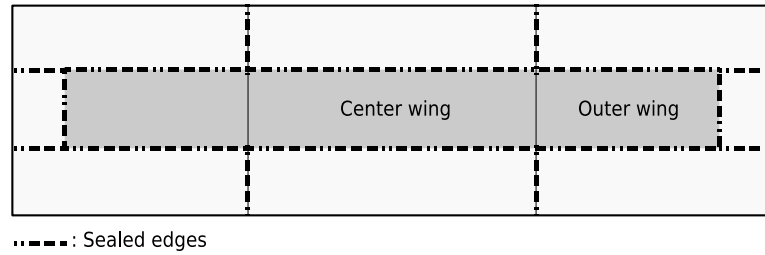


Figure 2.25: Sealed edges of the wing/reference block assembly.

After the sealing operation, the wing surface and the faces of the reference blocks are smeared with 2 or 3 layers of mold release agent. The role of the release agent is to provide the release of the female mold which is to be produced from the wing surface and the reference wooden blocks. After the release agent application, 2 thin layers of polyester resin is smeared over the wing surface and the reference blocks. These layers will form the actual surface of the female molds. The choice of using polyester resin as opposed to epoxy resin is due to its fast curing time. This way, two layers of polyester resin could be applied in sequence in a short time after the curing of the first layer is achieved. The mold assembly is left for one night for complete curing to occur.

The next day, one more layer of polyester resin, which is made denser by applying baby powder, is applied. Following the third layer of polyester application, a fourth layer is applied after the third layer is hardened. The fourth layer of polyester is applied again similar to the third layer. Figure 2.26 shows the schematic drawing of the polyester resins applied and their composition.

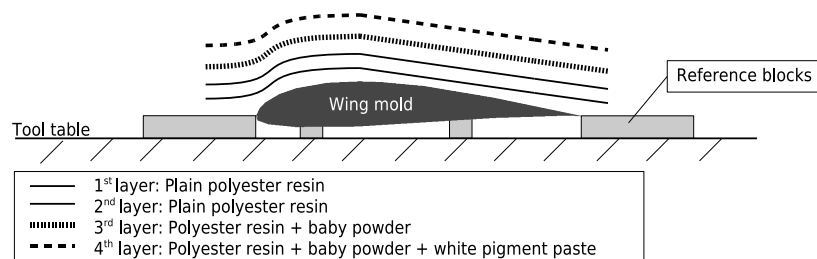


Figure 2.26: Application of polyester resin layers over the wing mold and reference blocks.

It should be noted that, the third and fourth polyester layers are made denser by adding baby powder in it. This way the strength of the polyester is tried to be increased. Application of baby powder in the polyester resin in a way resembles to adding powder material into a matrix in order to generate a composite material. Wood dust, or chopped balsa wood could also be used in combination with the resin material to increase the strength of the base polyester resin. In the fourth layer, white colored pigment paste is applied in the polyester resin to turn the color of the resin into white to have a white-colored mold.

After fourth layer of polyester application, 2 layers of E-glass fabric (86 g/m^2) has been applied over the male wing mold and the reference blocks. As the resin material, again polyester resin is used to allow for fast curing times. The use of low weight grade fabric makes it possible to conform better to the curved surface of the male wing mold, thereby providing the first two layers of composite material of the female mold wall.

It should be noted that, the application of polyester resin over the fabric material generates an exothermic reaction and heat is emitted. This is a characteristic of the polyester resins which are thermoset resins ([11]). Therefore, after the application of a layer of polyester resin and fabric material, some time has been allowed for the heat to dissipate. In certain circumstances air cooling has been applied to speed up the cooling operation. If no time has been allowed for the cool down of the polyester plus fabric mixture, and a second layer is applied, then due to the additional heat emission, temperatures may rise further. Thus, upon cooling down of the system, the resin material may exhibit cracks due to the residual stress built up. Therefore, it is recommended to allow time for each layer of polyester resin plus fabric material to cool down before the application of the next layer.

The remaining thickness of the female mold wall is built up by using cheap, chopped fiber E-glass material in combination with polyester resin. Schematic drawing showing this process is shown in Figure 2.27.

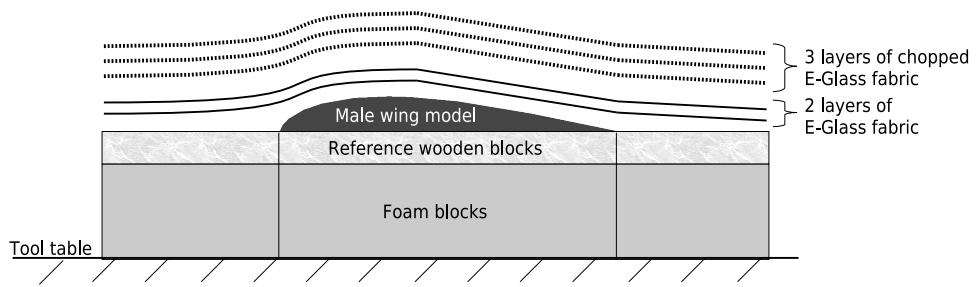


Figure 2.27: Application of fabric layers to form the thickness of the female mold; side tip view.

3 layers of cheap, chopped fiber and polyester were laid down to provide sufficient wall thickness of the female mold of one side of the wing skin. It should be noted that, away from the inner surface of the female mold, composite fabric with higher weight per square meter can be used. Because, these layers will only be used to get sufficient thickness for the female mold, and provide a rigid structure.

With the application of 4 layers of polyester, 2 layers of E-glass and polyester application and 3 layers of chopped fiber and polyester layers, a wall thickness of approximately 1 cm was achieved. Schematically, the resulting female mold wall thickness is shown in Figure 2.28.

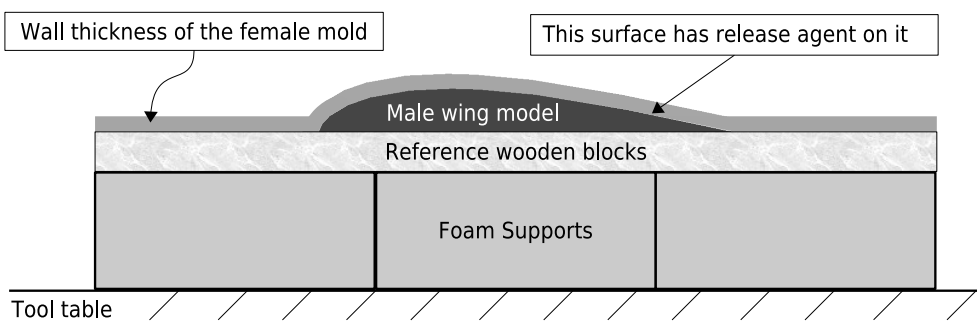


Figure 2.28: Wall thickness of the female mold; side tip view.

Assembly of the back-up structure of the female mold:

After the curing of the composite layers forming the wall thickness of the female mold, a back-up structure is built up to provide a rigid box structure for the female mold. The outline of the

back-up structure is given in Figure 2.29.

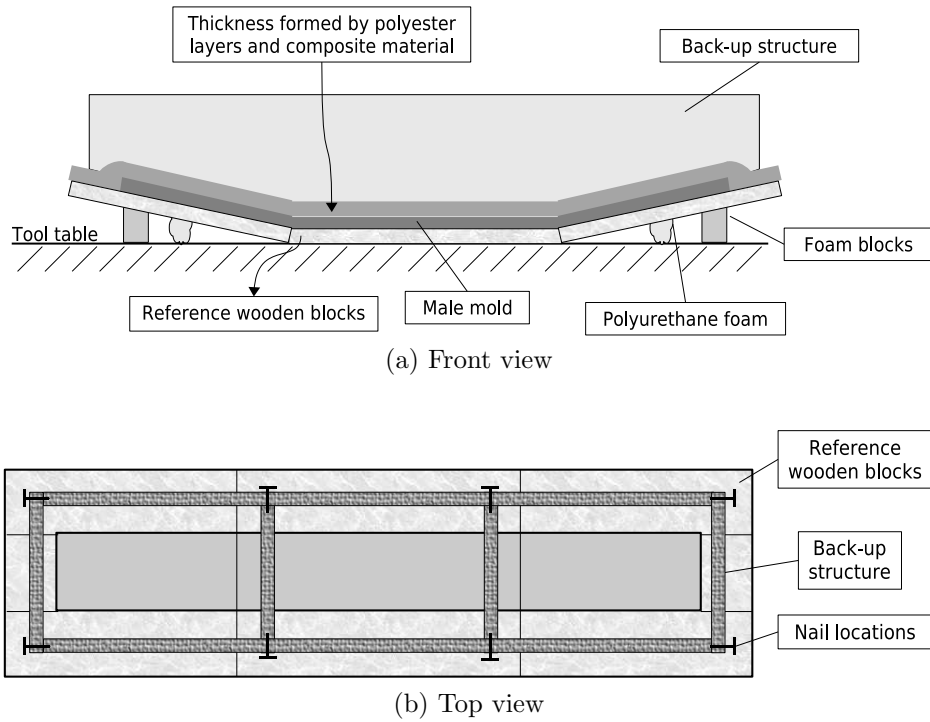


Figure 2.29: Schematic view of the back-up structure of the female mold.

Notice that the top view of the schematic drawing of the back-up structure is drawn such that the wing and the reference blocks are made clear. The back-up structure consists of wooden blocks nailed to each other at the nail locations indicated in Figure 2.29 (b). The base of the back-up structure is connected to the base of the female mold by chopped fiber plus polyester resin mixture along the sides. The base connection regions are shown in Figure 2.30.

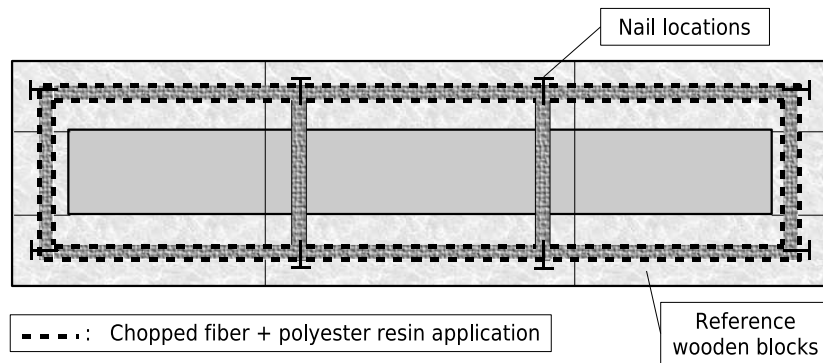


Figure 2.30: Connection of the back-up structure to the female mold by chopped fiber/polyester resin combination.

As shown in Figure 2.30, the chopped fiber plus polyester resin combination is applied all around the back-up structures to fix the structure to the female mold. By means of the back-up structure, female mold becomes more rigid and possible deformation of the mold wall is reduced to a minimum value.

By letting the whole assembly for cure, one side of the female mold together with its back-up structure has been made ready. For the manufacturing of the other side of the female mold, the whole assembly is first let free from the foam supports and polyurethane foams which are used for fixing the mold to the tool table. Later on, the mold assembly is turned upside down and placed on the pool table. It should be noted that, since a certain wall thickness of the female mold is reached, the reference blocks are no longer needed, and they are removed from the mold assembly by inserting sharp edged objects, preferably wooden, into the mating surfaces of the female mold and the reference wooden blocks. Figure 2.31 shows the schematic drawing of the mold assembly after it is turned upside down and placed on the tool table.

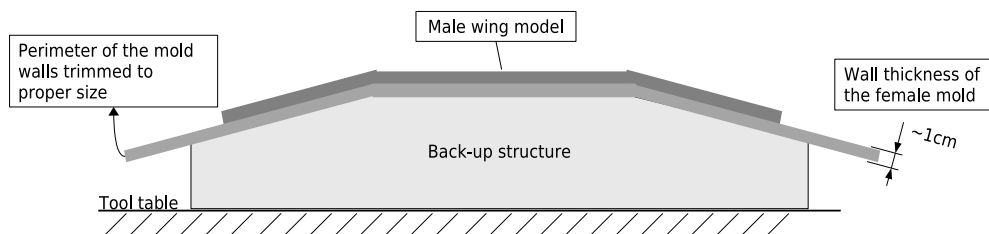


Figure 2.31: Front view of the mold assembly after it is turned upside down.

As shown in Figure 2.31, after the reference blocks are all removed, the polyester layers plus the composite fabric layers form a flange whose thickness is approximately 1 cm thick. It should further be stressed that, after the removal of the reference blocks, the other side of the male wing model stands out by itself, and it is firmly pushed into its female cavity if any movement of the male mold has occurred during the removal of the reference blocks.

At this step, the free face of the male wing is treated with sandpaper if any surface irregulari-

ties has occurred after the removal of the polyurethane foam. In addition, the perimeter of the flange of the female mold is trimmed to a proper size and treated with sandpaper. This process is very critical because, improper treatment of the sides of the flange wall by sandpaper may leave hardened chopped fibers sticking out, and these may cause injuries if the mold is handled from these areas with bare hands.

After the mold assembly is prepared, similar procedures were followed as in the other side of the mold to make up the other half of the female mold. These processes are summarized here in sequence.

- A thick layer of release agent is applied over the male wing surface and the complete flange area of the mold. Schematic drawing of the top view of the mold assembly shows the related surfaces (Figure 2.32).

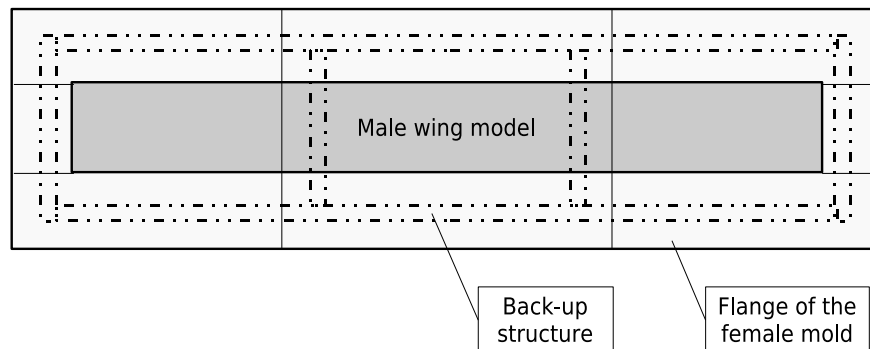


Figure 2.32: Schematic top view of the mold assembly showing the flange of the female mold and the male wing.

- 4 layers of polyester has been applied over the complete male wing model and flange of the female mold. After each layer of polyester application, some time has allowed for the partial curing of the resin.
- On top of the 4 plain polyester resin layers, 2 layers of 86 g/m^2 woven E-glass fabric is laid down and wetted with polyester resin to conform to the curved surface of the wing mold.

- Several layers of E-glass chopped fiber is placed over the mold and wetted with polyester resin. This way, the required wall thickness is achieved in a similar process as the other side of the female mold. This operation is shown schematically in Figure 2.33.

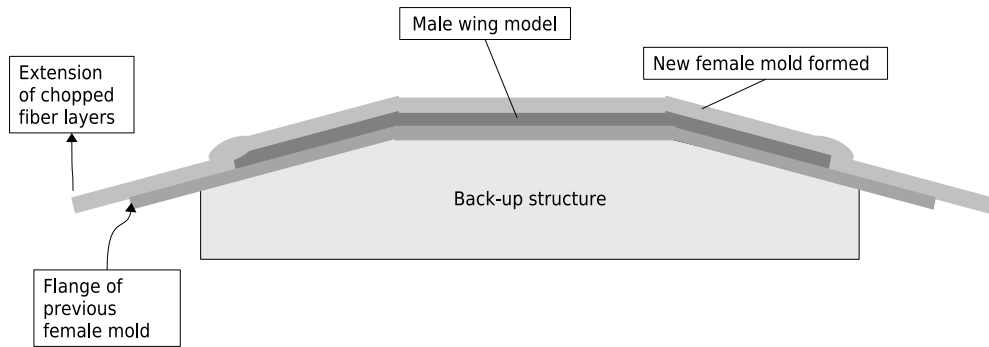


Figure 2.33: Front view of the mold assembly after the built-up of the wall of the female mold.

- After the curing of the mold assembly, the perimeter of the new female mold flange is trimmed and treated with sandpaper. Following this operation, a similar back-up structure is built-up, and this is shown in Figure 2.34.

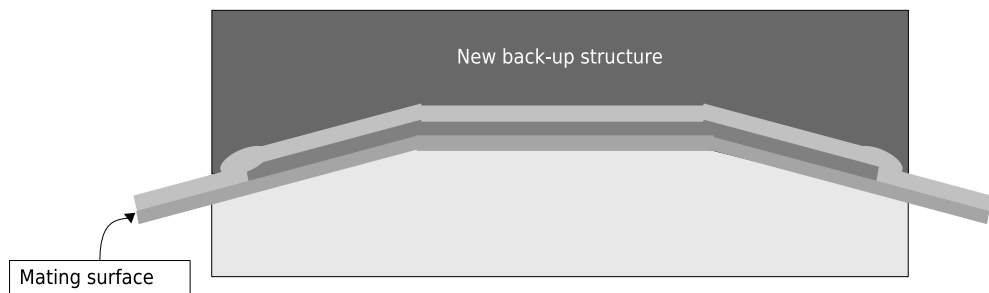


Figure 2.34: Back-up structure built on the new female mold surface.

- The same built-up procedure of the back-up structure as the other side is followed for the new back-up structure.

At this point, both female molds and their back-up structures are ready. However, the molds and the male mold are not separated from each other. Before dismantling of the molds, two

diagonal holes were drilled for the guide pins. Schematically, the positions of the guide pin holes are shown in Figure 2.35.

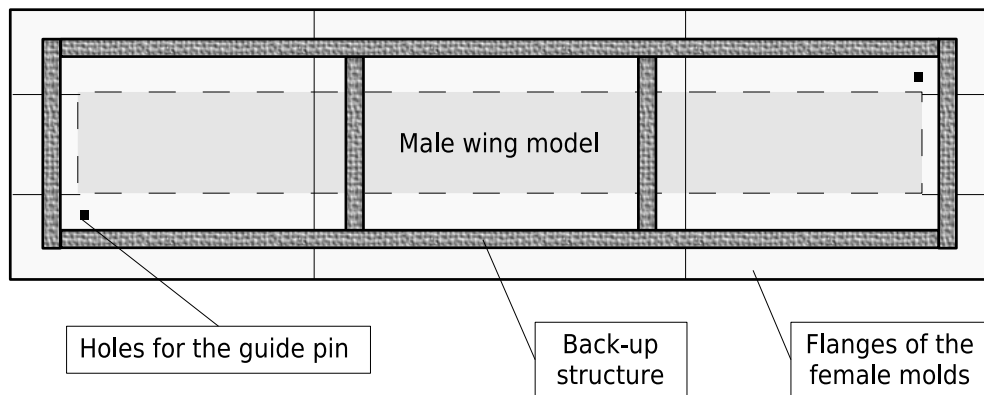


Figure 2.35: Position of the holes of the guide pins.

The guide pins are drilled inside the back-up structure as shown in Figure 2.35. The detail view of the guide pin hole is shown in Figure 2.36.

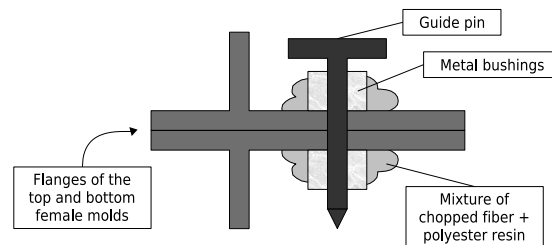


Figure 2.36: Detail view of the guide pin connection.

As shown in Figure 2.36, two metal bushings are used on both sides of the female molds to guide the guide pin through the hole. The bushings were connected to the mold by the mixture of chopped fiber and polyester resin. In order to position the bushings correctly with respect to the pin hole, the guide pin was smeared with the release agent and it was passed through the bushings and the guide pin. The whole assembly was left one night for curing of the polyester resin which was applied around the bushing. The next day, the guide pin was removed, and the mold assembly was ready for dismantling.

It should be noted that, the guide pins are necessary to locate both female molds correctly with respect to each other during the manufacturing of the actual wing structure. The actual manufacturing process of the wing will be explained in the next section and the role of the guide pins will be clear.

The last process is to separate the two female molds from each other. This separation is accomplished by inserting thin female sheets of wood, into the mating surface of the two female molds shown in Figure 2.34. Since the release agent was smeared over this mold surface, the sticking of the two molds was prevented. However, the separation of the two molds take some time, because care is needed not to exert excessive force to separate the female molds from each other.

After the molds were separated, the male model usually remains inside the one of the female molds. The male mold is separated from the female mold by carefully applying force between the mating surface of the male wing model and the female mold surface. This force is again applied by means of thin sheets of wood, which are slid into the mating surface at various locations all around the male model. This operation is shown schematically in Figure 2.37.

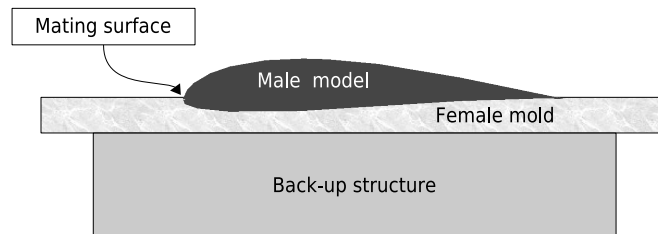


Figure 2.37: Side view of the male model and female mold with its back-up structure.

The actual pictures of the two female molds and back-up structure are presented in Figure 2.38.

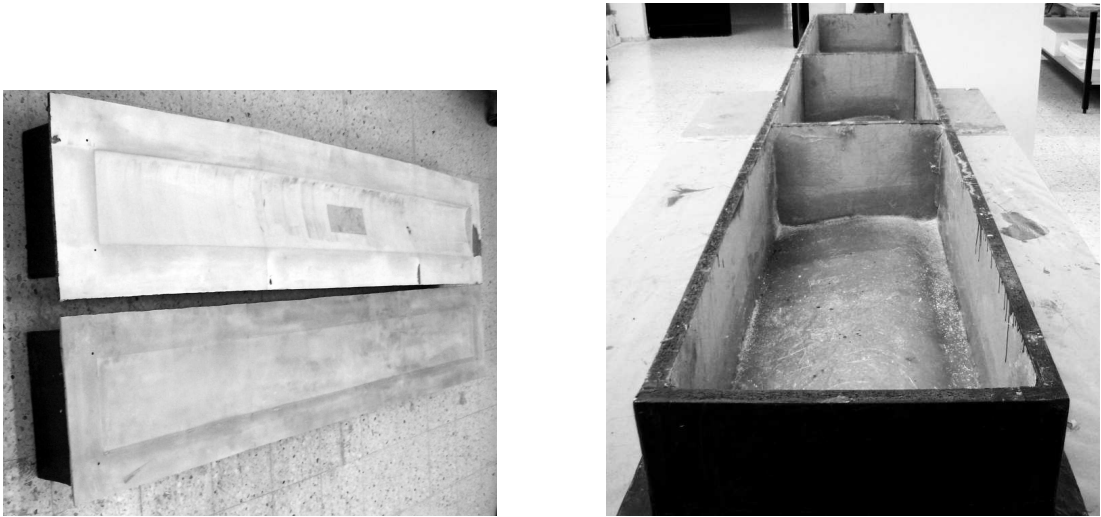


Figure 2.38: Upper and lower wing skin female molds, and the back-up structure.

2.3 Manufacturing the UAV Wing

Manufacturing of the wing consists of two parts: manufacturing the components of the wing, and assembling the components.

2.3.1 Manufacturing the Components of the Wing

The wing consists of three parts; the center wing, and two outer wings. Each part is built up from several parts; namely, upper and lower skin, front and rear spar, and ribs.

Manufacturing the skins:

The skins are manufactured as a sandwich structure. The female molds of upper and lower skin are used as the mold surface. A 1-mm-thick styrofoam layer is placed in between two layers of e-glass fabric. The aim of using a styrofoam layer is to increase the stiffness of the wing skin. Additionally, a strip of carbon fabric with approximately 5 cm width is laid up on the top surface of the upper skin at the location where the front spar will be placed. It should be noted that, this carbon strip does not extend to the tips of the skin. There remains approximately 15 cm uncovered from each wing tip. Vacuum bagging is used as the manufacturing

technique. At the end of the process, the edges of the composite skin are trimmed to the actual wing geometry. Schematic drawing of the configuration of the materials used in the wing skin are shown in Figure 2.39. Properties of the materials used in the wing skin are given in Table 2.1.

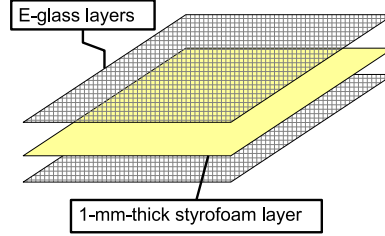


Figure 2.39: Configuration of the wing skin.

Table 2.1: Properties of the materials used in the wing skin.

Material type	Density	Amount used
E-glass fabric	86 g/m^2	2 layers
Styrofoam	31 kg/m^3	1 layer with 1 mm thickness
Carbon fabric	98 g/m^2	1 layer strip with 5 cm width

Some of the electronic equipment of the UAV is kept in the middle of the main wing. In order to have an access to the equipment, a lid is needed. Position and the geometry of the lid is provided using a metal insert plate with a rectangular cross section. The insert is placed in the female mold of the upper skin during the manufacturing process of the skins. After the manufacturing, the lid is cut off from the upper skin using a sharp-edged knife.

Manufacturing the front spar:

Front spar is manufactured from styrofoam and carbon fabric. Manufacturing method is nearly the same as the plate manufacturing method described in Section 2.1.1. Glass table surface is used as the mold surface; a 15-mm-thick styrofoam panel is put over a layer of carbon fabric which was pre-wetted with epoxy, and another layer of carbon fabric is laid up over the styrofoam plate and epoxy is applied. Then, the plate is cured in vacuum bagging at room temperature. Final shape is obtained by cutting the desired shape from the plate. In Figure 2.40, a schematic representation of the front spar configuration is shown. Properties of the

styrofoam plate and carbon fabric used in the front spar are given in Table 2.2.

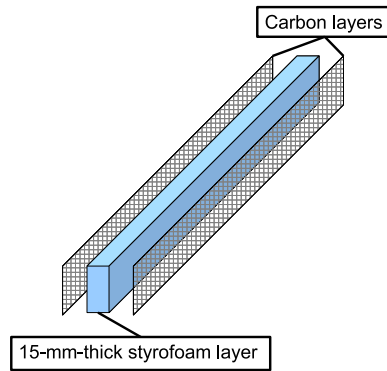


Figure 2.40: Configuration of the front spar.

Table 2.2: Properties of the materials used in the front spar.

Material type	Density	Amount used
Carbon fabric	98 g/m^2	2 layers
Styrofoam	33 kg/m^3	1 layer with 15 mm thickness

Manufacturing the ribs and the rear spar:

The structures of the ribs and the rear spar are identical. Manufacturing method is the same as the manufacturing of the front spar. This time, a 3-mm-thick balsa wood is covered with a single layer carbon fabric at each side surfaces, and cured in vacuum bagging at room temperature. Finally, from the composite plate ribs and the rear spar of the wing are cut out. Configuration of the materials used in the rear spar and the ribs is shown in Figure 2.41. Properties of the balsa wood and carbon fabric used in the ribs and rear spar are given in Table 2.3.

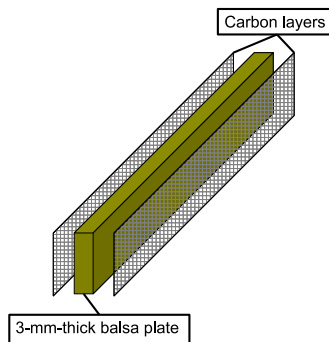


Figure 2.41: Configuration of the rear spar.

Table 2.3: Properties of the materials used in the ribs and rear spar.

Material type	Density	Amount used
Carbon fabric	98 g/m^2	2 layers
Balsa wood	160 kg/m^3	1 layer with 3 mm thickness

2.3.2 Assembling the Inner Components of the Wing

The UAV wing consists of three parts; one main wing and two outer wings. The assembling of the inner components is maintained separately in three parts.

2.3.2.1 Assembly of the main wing inner structure

All the processes explained in this section are applied on the lower skin of the wing. The reason behind working on the lower skin is that, during flight, the lower skin of the wing is subjected to tensile forces. Therefore, it is important that the connection between lower wing skin and inner structural components is strong enough. In addition to this, lower wing skin has less curvature when compared to upper skin, that enables easier assembly of inner components. After all components are set up, the upper skin is adhered to the lower skin at the end of the processes.

The Figure 2.42 shows the schematic view of the main wing configuration. The front spar is located such that its mid-point is at the quarter chord of the wing (approximately 55 mm apart from the leading edge). The rear spar location is 45 mm apart from the trailing edge, which corresponds to 80% of the wing chord. There are two ribs, that extend throughout the chord, placed at the tips of the main wing. Additionally, there is a wood block placed at the mid-span of the wing next to the front spar at the leading edge side. This block is used as the slot of the bolt, which connects the wing structure to the body of the UAV.

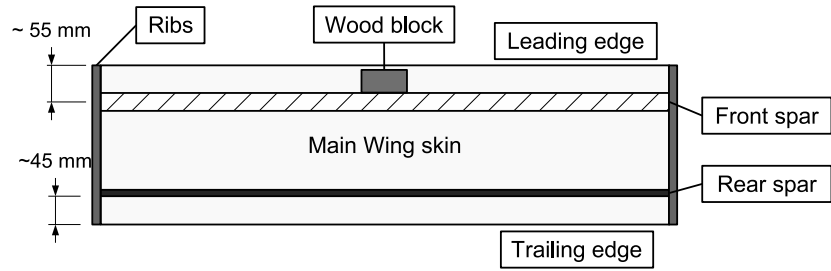


Figure 2.42: Inner configuration of the main wing (top view)

In the manufacturing of the components phase, the skins of the wing are produced as main wing and outer wings combined together as a single piece. Thus, as a first step, the lower skin is cut from the starting points of the dihedral of the wing into three pieces in the female mold using a sharp-edged knife. In Figure 2.43, this cutting process is shown schematically.

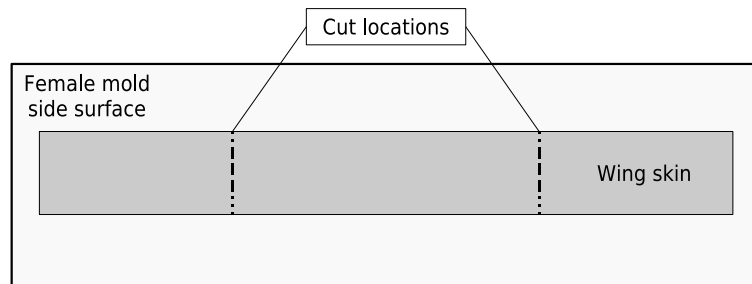


Figure 2.43: Cutting process of the lower skin in the female mold (top view)

After the lower skin is cut, the outer wing skins are taken out of the female mold. In order to assure that the spars and the ribs perfectly match and fit into the lower skin, the spars are trimmed off from the tips as the thickness of the ribs. Spars and the ribs are placed in the lower skin properly. For positioning the ribs perpendicular to the main wing skin, two wood sticks are fixed to the mold surface using double sided bands and paper bands. The locations of these sticks are dictated using the ribs. Using small clamps, the ribs are temporarily attached to the positioning sticks. In Figure 2.44, this process is demonstrated.

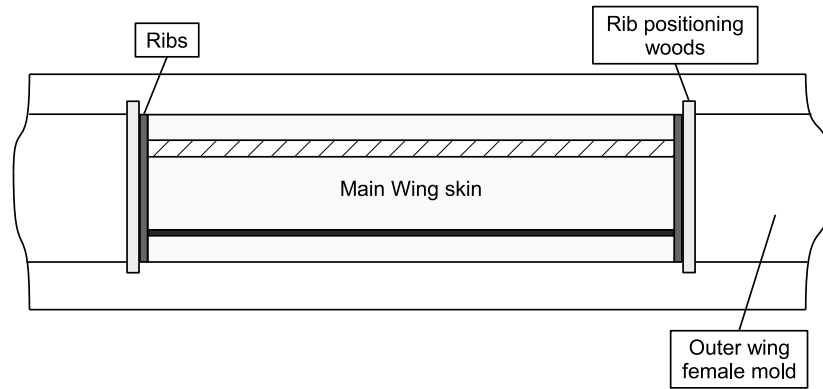


Figure 2.44: Positioning the ribs in the upper skin of the main wing (top view)

Next, the front spar is dislocated, and cream-like mixture of epoxy material (same as the one used in the composite manufacturing) thickened with baby powder is smeared throughout the span and the front spar is repositioned. This process is repeated for the rear spar after the front spar is positioned. Then, some weight is applied over the spars, and this caused some excess adhesive mixture to leak from the sides of the spars. Strips of e-glass, with approximately 25 mm width for the front spar and 15 mm width for the rear spar, are laid down over this excess epoxy mixture at both sides of the spars for additional strength, and this is shown in Figure 2.45.

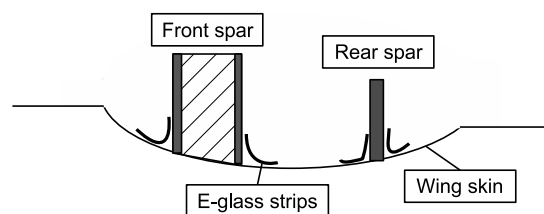


Figure 2.45: Placing strips of e-glass to the sides of the spars (side view)

Before fixing the ribs in position, a strip of e-glass is placed below the ribs for obtaining extra strength under the ribs. Then, ribs are adhered to the lower skin using the same cream-like mixture, and weight is applied. Similarly, strengthening e-glass strips are put between ribs, skin and spars, as shown in Figure 2.46.

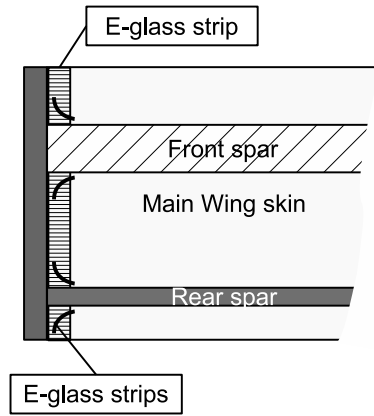


Figure 2.46: Placing strips of e-glass to the sides of ribs, skin and spars (top view)

2.3.2.2 Assembly of the outer wings inner structures

In the assembly of the right and left outer wings inner structures, the same procedure is applied as in the assembly of the main wing structure. Here, the front spar, unlike rear spar, extends up to the end of the carbon strip, not to the wing tip. There are, again, two ribs at each end of the outer wings. Figure 2.47 shows the general configuration of the outer wings.

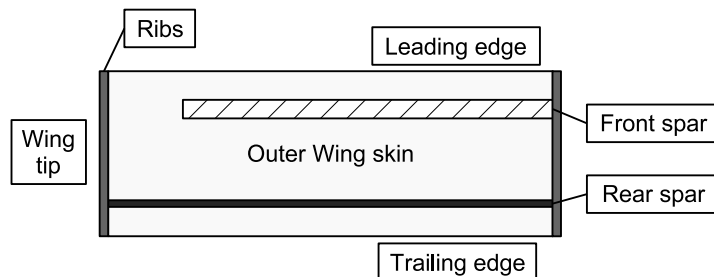


Figure 2.47: Inner configuration of the outer wings (top view)

Here, it should be stressed that, the ribs are manufacturing by cutting out of a composite plate using a wing profile made of metal. This metal profile has exactly the same geometry as the model wing profile. Thus, when the ribs are placed inside the wing, they will not fit in tightly due to the thickness of the upper and lower skins. This problem will be handled by reducing the sizes of the ribs using sand papers.

Another important issue here is that, the rib at the connection between the main wing and the

outer wing is placed perpendicular to the main wing skin, not to the outer wing skin. Because, if it was placed perpendicular to the outer wing skin, the ribs at the connection would not be parallel to each other due to the dihedral.

2.3.2.3 Setting up the connection parts between the main and outer wings

The connection between outer wings and the main wing is obtained using carbon tubes passing through the ribs and the spars. Two different carbon tubes are used in the connection. A solid (male) tube with 6 mm diameter, and a hollow (female) tube with inner and outer diameters of 6 and 8 mm respectively. In order to drill the holes, that the carbon tubes will pass through, accurately and without too much effort, a wing profile is cut out of wood plate with 18 mm thickness. The wood profile is placed next to the rib of the main wing, and about 5 cm of styrofoam core is removed from the tip of the front spar. This process is shown in Figure 2.48.

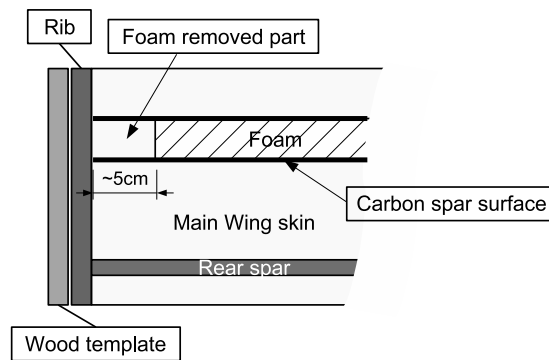


Figure 2.48: Styrofoam removal process (top view)

Using the guide hole of the wood template, a hole with 6 mm diameter is drilled at the rib of the main wing. Then, the male tube is placed to the hole and release agent is applied on the male tube for preventing the possible sticking to the rib of the main wing or to the female carbon tube. Afterwards, a female carbon tube with 5 cm length is cut, and male tube is placed in it. This tube assembly is positioned in the hole of the front spar as shown in Figure 2.49. The remaining volume between the tube assembly and the carbon layers of the front spar is filled with a strong adhesive thickened and reinforced with balsa wood sawdust.

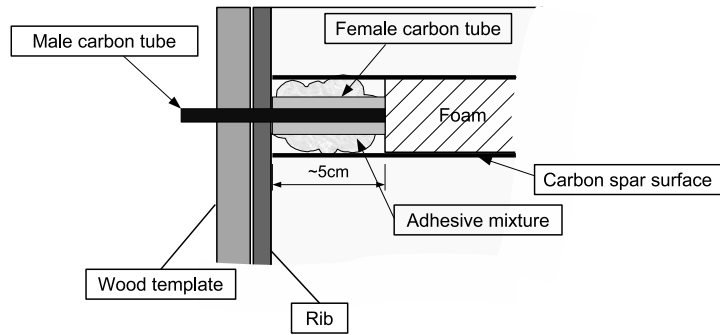


Figure 2.49: Positioning the tube assembly in the front spar (top view)

In the assembly of the carbon tube connection at the rear spar, the same procedure is followed. Since the rear spar is not thick enough to allow the carbon tube pass through, the hole is drilled 3 mm apart from the side (the one close to the front spar) of the rear spar. A small piece of plate is cut from the same composite plate which the ribs are cut before, and is placed between the female carbon tube and the side of the rear spar in order to support the carbon tube assembly. The male tube is positioned and covered with release agent. Then, it is placed in the female tube, and positioned next to the support plate. Finally, the tube assembly is fixed in position using the same adhesive mixture. In Figure 2.50, detailed view of the positioning of rear connection is shown.

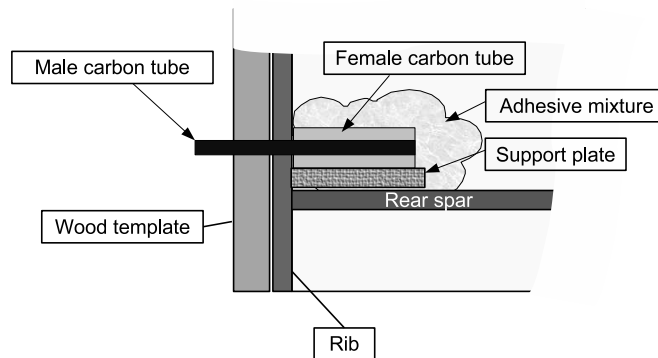


Figure 2.50: Positioning the tube assembly next to the rear spar (top view)

After the adhesives are totally cured, the male carbon tubes are disconnected from the female tubes. Using a similar process as explained above, the male carbon tubes are fixed to the outer wings. For the tube at the front spar, some of the styrofoam core is removed and the male tube

is positioned using the wood profile. Then, same adhesive is applied to fill the voids at the core of the front spar between the carbon tube and the carbon layers of the spar.

Likewise, for the tube at the rear spar, a supporting plate is placed between the carbon tube and rear spar. The carbon tube is positioned using the wood plate, and adhesive is applied to fix the connection. After the adhesive is totally cured, the connection between the main and the outer wing is obtained.

It should be stressed that, the axis of the holes drilled on the rib of the outer wings is not parallel to the longitudinal axis of the outer wings; instead, it is parallel to the longitudinal axis of the main wing. Because, as explained before, the rib of the outer wing is not perpendicular to the skin of the outer wing.

There is another mechanism between the main and the outer wings, that mechanically constrains the wings and prevents accidental dislocating of the wings. This mechanism is basically a metal fastener consisting of two parts. The schematic drawing of the fastener is shown in Figure 2.51.

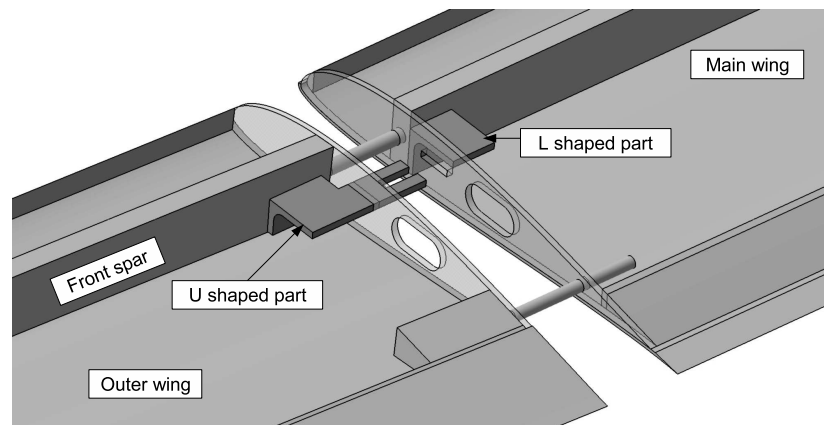


Figure 2.51: Fastener mechanism at the wing connection (isometric view)

The part having the U shape at the end is fixed to the front spar of the outer wing. For this,

a slit is opened on the rib of the outer wing, and the part is adhered to the front spar after U shaped end is fitted from the slit. The counterpart is placed in the main wing. Initially, a nutplate is riveted to the upper horizontal surface of the L shaped metal part. A bolt is placed in the nutplate. The diameter of the bolt is almost the same as the opening of the U shape. Likewise, a slit is opened at the rib of the main wing and the metal part is adhered to the front spar. In order to reach that bolt, a small hole is drilled on the lower skin of the main wing.

2.3.3 Assembling the Wing

After all the structural components are fixed in the wing structure, and wiring harness is put, the upper and lower skin can be fixed together. As explained before, due to the thickness of the skins and the adhesives used for fixing the components, the upper and lower skins may not fit together perfectly. Using a sand paper, excess parts are removed and perfect matching is obtained. It should be stressed that, unlike the lower skin, the upper skin is not cut into three pieces from the locations where dihedral begins. Instead, it is assembled as a single part, and will be separated using a sharp-edged knife after assembling the wing.

In order to provide additional sticking surface, and to increase the stiffness foam plates in the shape of the leading edge and the trailing edge are put in the wing structure between the spars and the edges.

For assembling the wing, the main wing and the outer wings are connected together and placed in the female mold of the lower skin. Over the edges of ribs, spars and additional foam plates at the leading and trailing edges, a very strong adhesive thickened and reinforced with balsa wood sawdust is smeared. Then, the upper skin is placed properly and carefully over the lower skin. With the purpose of applying uniformly distributed pressure, and preventing the slippage of the upper and lower skins, the female mold of the upper skin is placed upside down on the upper skin. The molds are fixed together with clamps. During the female mold manufacturing, two guide holes were drilled on the flanges of the molds at two corners on the diagonal line.

Using the guide pins, it is guaranteed that upper and lower female molds perfectly match and do not slip. The female molds clamped together is shown in Figure 2.52.



Figure 2.52: Female molds clamped during wing assembly.

After the adhesive is totally cured, the guide pins removed and the female molds are separated. Then, using a sharp-edged knife, the upper skin is cut into three pieces from the small gaps between ribs located at the connection of the main and outer wings. Finally, the parts are separated and prepared for post-manufacturing processes like painting, system integration, etc. In Figure 2.53, the main and the outer wings are shown after post-manufacturing.

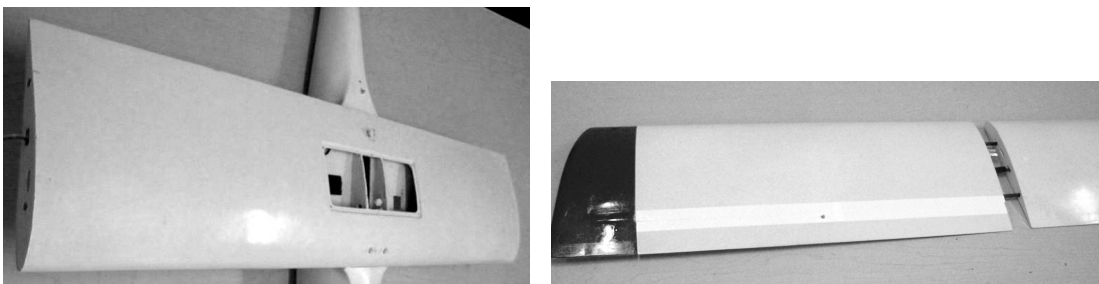


Figure 2.53: Pictures of main and outer wing after post-manufacturing.

CHAPTER 3

CHARACTERIZATION OF THE MATERIALS USED IN THE UAV

When compared to traditional metallic materials used in the structures, composite materials offer better mechanical properties like high stiffness, high strength, and long fatigue life. In the market there are extensive amount of different composite fibers and matrix material types which can be used with different combinations and compositions. As there are many different alloys exhibiting different mechanical properties, composites with different constituents evince diverse mechanical properties. Even with the same fiber and matrix material, the properties may differ due to the stacking sequence, or other environmental factors, etc.

The mechanical properties of the composites are also very sensitive to the manufacturing as well. Any imperfection that may happen during the manufacturing process like voids or any kind of foreign particles within the laminate can cause cracks which will reduce the strength of the structure. Moreover, differences in the treatments may end up in very different characteristics. For example, different curing cycles affects the dimensional stability, and strength of the composite products.

When working with the traditional metallic materials, it would be quite sufficient to look up

the mechanical properties from the material handbooks. Whereas, in the composite case one can estimate the mechanical properties by using mathematical formulations such as rule of mixtures applying on the data given by the fiber and matrix material manufacturers. However, it is always recommended to perform coupon tests for predicting the mechanical properties of the composites due to their highly sensitive characteristics.

In this chapter, determination of the mechanical properties of the composites, used in the mini UAV, through mechanical tests is explained.

3.1 Determination of Tensile Properties of Woven Fabric Lamina

As described in the previous chapter in detail, the mini UAV is manufactured from e-glass, kevlar, and carbon fibers accompanied with a thermosetting resin, epoxy; hand lay-up and vacuum bagging is used as the fabrication method. Therefore, in order to simulate the same conditions, test specimens are manufactured following the same procedure using the same materials.

The fibers used are plain weave balanced fabrics manufactured by Hexcel. Using woven fabrics, instead of unidirectional fibers, is mainly due to their ability to provide good reinforcement in all directions within a single layer, to their better impact resistance, better-balanced properties, easier handling and fabrication, and good ability to conform surfaces with complex curvatures. However, their complex architecture makes the analysis of their behavior much more challenging. Specifications of the fabrics used in the UAV, and the mechanical properties of the fibers of which the fabrics are composed are given in Tables 3.1 and 3.2, respectively.

Table 3.1: Specifications of the woven fabrics used in the mini UAV.

Fabric type	Style	Weight [g/m ²]	Weight distribution Warp / Weft %	Fiber count		Thickness [mm]
				Warp [yarns/cm]	Weft [picks/cm]	
E-glass	235	86	49 / 51	12	12.5	0.06
Kevlar	20796	60	50 / 50	13.5	13.5	0.07
Carbon	G0801	98	50 / 50	7.4	7.4	0.10

Table 3.2: Mechanical properties of the fibers composing the fabrics.

Fiber type	Density [g/cm ³]	Tensile Modulus [GPa]	Ultimate Tensile Strength [MPa]	Elongation %
E-glass	2.6	74	2500	4.5
Aramid	1.45	130	2900	1.9
Carbon	1.76	230	3530	1.5

The matrix material used is an epoxy system, which is widely used in aerospace and industrial composites, tooling, and aircraft repair. It is called as “Cold-curing epoxy system based on Araldite LY 5052 / Aradur 5052”, manufactured by Huntsman. Some features of this epoxy system can be listed as follows [12];

- Low viscosity that allows impregnation of reinforcement materials easily.
- Long potlife (2 hours for 100 ml at ambient) that allows production of big objects.
- High glass transition temperature; after ambient cure: 60°C, after post-cure at 100°C: 120°C.
- High mechanical and dynamic properties after ambient cure with potential for even higher properties after post-cure at elevated temperatures.

For the specimen production, square plates with 300 mm edge length are manufactured with vacuum bagging method. The E-glass plate is prepared from 6 layers of e-glass, whereas this layer number is 4 for kevlar plate and 3 for carbon plate. In the selection of the number of layers, the maximum testing capacity of the tensile testing machine is considered. The fabrics are laid-up in 0°/90° orientation. Details of plate manufacturing are demonstrated in Figure

2.2 in the previous chapter. From the composite plates, specimens are cut into the shape of a thin flat strip as specified in the standard in detail [13].

3.1.1 ASTM Standard and Test Procedure

Tensile properties of the composites used in the UAV are determined through mechanical testing according to the ASTM standard D 3039/D 3039M-00, “*Standard Test Method of Tensile Properties of Polymer Matrix Composite Materials*”. The scope of this standard is to determine the in-plane tensile properties of continuous or discontinuous fiber reinforced polymer matrix composite materials, which are required to be balanced and symmetric with respect to test direction. Basically, the specimen having a constant cross section is positioned in the grips of a mechanical testing machine. Specimens are loaded monotonically in tension, and loading is recorded as well as the change in the grip separation. The ultimate strength of the tested material is determined from the maximum load carried before failure, and the stress-strain behavior of the material is obtained from the recorded load and change in grip separation data.

Testing at least five specimens per test condition is recommended unless valid results can be obtained with less number of specimens. Specimen geometry is not strictly dictated in the standard; however, there are some general requirements and some specific recommendations for specimen geometry.

For the general requirements, it is stated that the coupon must have a constant rectangular cross section, and the minimum length of coupon should be summation of gripping length, gage length and twice of the specimen width. It is also stated that, specimen must be flat, and tabs may be used at the grip locations as necessary.

In the specific recommendations section, it is advised to select specimen cross section such that the failure occurs in the gage section, and there exists adequate number of fibers in the cross section statistically representing the bulk material. The use of tabs depends on the material

configuration, but it is strongly recommended when testing unidirectional materials. However, tabs may also be required for preventing gripping damage. Tab material may be steel or other metals, or the same composite material as the specimen.

Typical specimen geometries meeting the minimum requirements are outlined in Table 3.3 for different configurations. Considering the remarks and recommendations explained in the standard, a specimen geometry shown in Figure 3.1 is chosen for this study. It should be stated that, in the decision of the specimen thickness the major concern was the capability of the test machine to be used in the experiments. In order not to exceed the limits of the test machine, specifications of which is given in the following sections, several tests are done and proper thickness is selected for testing the materials used in the UAV.

Table 3.3: Tensile specimen geometry recommendations.

Fiber orientation	Width [mm]	Overall length [mm]	Thickness [mm]	Tab length [mm]
0° unidirectional	15	250	1.0	56
90° unidirectional	25	175	2.0	25
balanced and symmetric	25	250	2.5	emery cloth
random-discontinuous	25	250	2.5	emery cloth

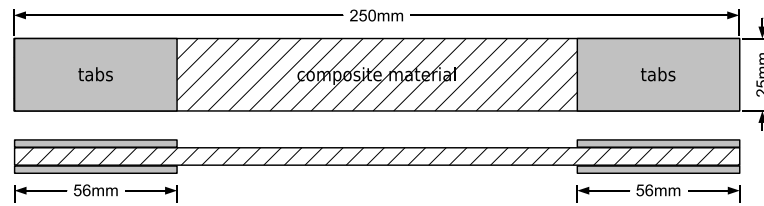


Figure 3.1: Tension test specimen geometry.

Test machine used in this study is Zwick/Roell Z010 Universal Static Testing Machine. This machine is used for tensile, compression and bending tests on material specimens, as well as function testing on machine components such as springs, wheels, etc [14]. Z010 has a drive unit powered by an electric motor, and is capable of testing loads up to 10kN. It can be operated using function keys on the testing machine, or alternatively it can be operated with a PC via

a software, named *testXpert*[®]. This software increases the usability of the machine, and helps making tests more standardized and well documented. It gives stress-strain diagram, elastic modulus, failure stress, elongation at break, etc. as outputs. Unfortunately, there were not any extensometer available; thus, displacement of the gages is used for strain data. Some pictures of the testing machine are shown in Figure 3.2.

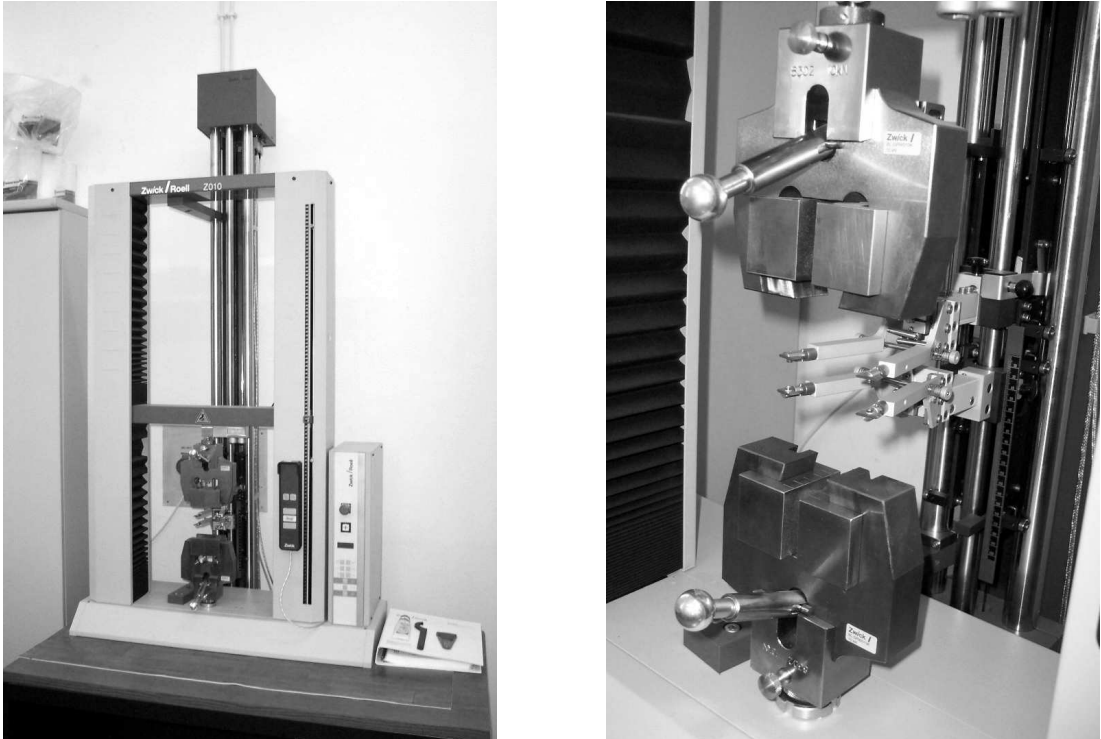


Figure 3.2: Zwick/Roell Z010 Universal Static Testing Machine.

Before starting testing, dimensions of the specimens must be recorded. The standard recommends to determine the specimen area as the average of three places in the gage section. In addition to the dimensions, weight of coupons are measured before sticking the tabs to the composites in order to calculate the fiber volume fraction of the composites. Average values of the measured data are given in Table 3.4. Detailed information about the specimens are supplied in Appendix A.

Table 3.4: Average specimen geometry and mass data

Material type	Number of layers	Average width [mm]	Average thickness [mm]	Average mass [g]
E-glass	6	25.52	0.48	4.6
Kevlar	4	25.56	0.48	2.8
Carbon	3	25.60	0.40	3.0

After preparing specimens and measuring required data, specimen is clamped to the grips. It is important that, the specimen must be aligned properly with respect to the vertical axis of the test machine, which is the testing direction. In order to assure this, a centerline is drawn on the specimen, and this line is matched with the centerline of the grips. After fixing the specimen, inputs are entered to the software controlling the testing machine. Main inputs are thickness and width of the specimen, speed of testing, and grip separation. Speed of testing, which is constant throughout the test, is defined as $2\text{ mm}/\text{min}$ by the standard.

Test is started after all the input parameters are entered. The software records the stress-strain diagram, and calculates the elastic modulus of the material. Also, the stress and percent elongation values at the instant that the specimen is failed are recorded. All data is presented in a tabulated form, and statistical information such as standard deviation and average values are supplied as well.

3.1.2 Tensile Tests Performed and Results

In the scope of this study, several specimens are manufactured using three different fiber materials, namely, e-glass, kevlar, and carbon. Vacuum bagging with hand lay-up method is used with different curing cycles. Curing cycles are selected according to the data sheet of the resin used. Three different curing schemes are applied, that are room temperature (RT), 1 day RT + 4 h 100°C, 1 day RT + 8 h 80°C. This type curing is called as *post-curing*. Specimens are prepared at room temperature, and kept under vacuum for 12 hours. After keeping the specimens at room temperature under atmospheric pressure for another period of 12 hours, they are post-cured in a heat controlled oven. In order to make a controlled experiment, half

of the specimens, which are manufactured from the same composite plate, are post-cured while the other half is kept at room temperature. The aims of these experiments are to obtain the mechanical properties, and to see the effect of post-curing on the mechanical properties of the composite materials used in the UAV. Later, the mechanical properties obtained from the tests will be used in the finite element analysis, and the post-curing method may be applied in the further manufacturing processes if the results come out such that there is an improvement in the mechanical properties.

Three different cases are examined through the mechanical tests:

- Case I: Specimens are cured at room temperature.
- Case II: Specimens are initially cured at room temperature and half of them are post-cured at 100°C for 4 hours while keeping the other half at room temperature.
- Case III: Specimens are initially cured at room temperature and half of them are post-cured at 80°C for 8 hours while keeping the other half at room temperature.

The composite materials tested, exhibited brittle characteristics. That is, the stress-strain curve is almost a straight line, and there occurs no yielding. A typical stress-strain curve output is shown in Figure 3.3. The failure happens suddenly with a lateral type failure¹ (perpendicular to the testing axis) at different locations of the specimens. Samples of fractured specimens are shown in Figure 3.4.

In the following sections, the averages of the results obtained from the tests are presented and discussed. All the data is supplied in Appendix A explicitly.

¹ Refer to [13] for failure types.

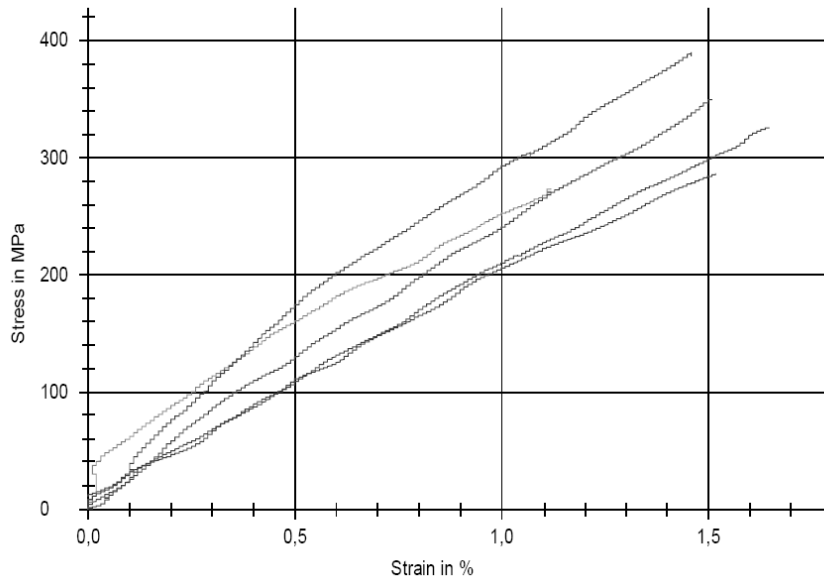


Figure 3.3: Stress-strain curves for a set of composite specimens.

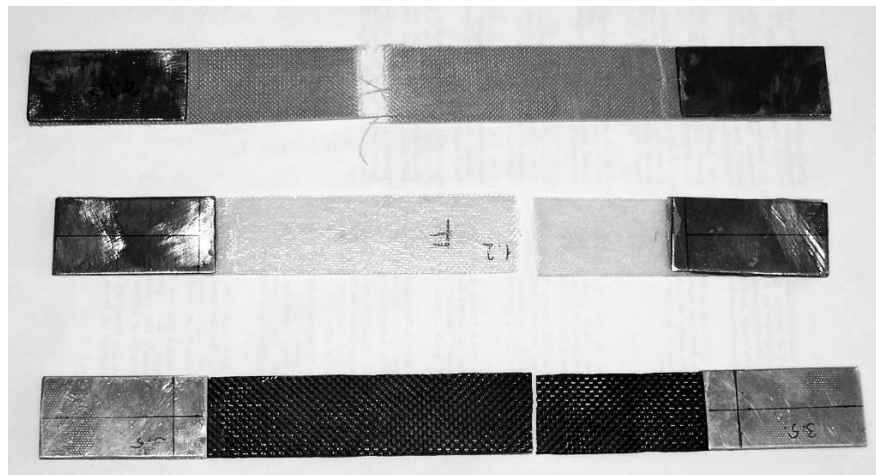


Figure 3.4: Samples of fractured specimens (namely, kevlar, e-glass, and carbon from top to bottom).

3.1.2.1 Results of Case I

From a statistical point of view, it is better to have more data included in the analysis. Since half of the specimens manufactured for Cases II and III are cured at room temperature, the results of those specimens are combined with the ones specifically manufactured for Case I. In Table 3.5, average values of tensile modulus, tensile strength, and percent elongation at break

are given in a tabulated form.

Table 3.5: Test results of the specimens cured at room temperature.

Fabric type	\overline{E}_t [GPa]	St.Dev.	$\overline{\sigma}_{max}$ [MPa]	St.Dev.	% Elongation	St.Dev.
E-glass	22.29	5.16	268.17	39.97	1.51	0.47
Kevlar	24.13	3.54	314.61	45.03	1.49	0.24
Carbon	46.26	11.76	428.33	60.96	0.82	0.24

3.1.2.2 Results of Case II

This case is prepared for investigating the effects of post-curing on the mechanical properties of the composites. Post-curing scheme is selected as curing the specimens at 100°C for 4 hours. This is one of the suggested curing cycles defined in the data sheet of the epoxy used. In Table 3.6, summary of the results obtained from this case is given.

Table 3.6: Test results of Case II.

Fabric type	\overline{E}_t [GPa]	St.Dev.	$\overline{\sigma}_{max}$ [MPa]	St.Dev.	% Elongation	St.Dev.
E-glass RT	21.03	2.38	275.13	54.15	1.31	0.55
E-glass Pc100	21.85	1.83	275.61	39.26	1.29	0.45
Kevlar RT	24.12	3.02	293.63	53.94	1.33	0.33
Kevlar Pc100	23.99	4.49	304.68	23.39	1.31	0.36
Carbon RT	50.56	15.95	404.97	68.16	0.77	0.27
Carbon Pc100	47.36	8.24	403.31	56.85	0.77	0.23

Here, Pc100 stands for the specimens post-cured at 100°C, and RT stands for the specimens cured at room temperature for the purpose of comparison.

In Table 3.7, percent changes in the material properties after post-curing with respect to room-temperature-cured values are given.

Table 3.7: Percent changes of the mechanical properties when post-curing at 100°C for 4 hours is applied.

Fabric type	ΔE_t (%)	$\Delta \sigma_{max}$ (%)	ΔE_l (%)
E-glass	3.87	0.17	-3.85
Kevlar	-0.55	3.77	-1.56
Carbon	-6.33	-0.41	-0.63

3.1.2.3 Results of Case III

This case is prepared, again, for investigating the effects of post-curing on the mechanical properties of the composites. Post-curing scheme is selected as curing the specimens at 80°C for 8 hours, as suggested in the data sheet of the epoxy used. Additionally, this case will give a chance to compare two different post-curing schemes. In Table 3.8, summary of the results obtained from this case is given.

Table 3.8: Test results of Case III.

Fabric type	\bar{E}_t [GPa]	St.Dev.	$\bar{\sigma}_{max}$ [MPa]	St.Dev.	% Elongation	St.Dev.
E-glass RT	24.11	7.38	272.76	20.09	1.74	0.35
E-glass Pc80	20.66	4.23	285.74	20.91	1.48	0.45
Kevlar RT	24.54	4.37	338.31	48.05	1.54	0.20
Kevlar Pc80	25.95	4.57	327.27	32.03	1.49	0.19
Carbon RT	47.01	11.24	444.62	72.21	0.77	0.31
Carbon Pc80	44.21	10.23	414.99	66.56	0.77	0.18

Likewise, Pc80 stands for the specimens post-cured at 80°C, and RT stands for the specimens cured at room temperature for the purpose of comparison.

In Table 3.9, percent changes in the material properties after post-curing with respect to room-temperature-cured values are given.

Table 3.9: Percent changes of the mechanical properties when post-curing at 80°C for 8 hours is applied.

Fabric type	ΔE_t (%)	$\Delta \sigma_{max}$ (%)	ΔE_l (%)
E-glass	-14.32	4.76	-15.19
Kevlar	-2.08	-0.32	-3.45
Carbon	-5.96	-6.66	-0.78

3.1.3 Discussion of the Results

Results obtained throughout tensile testing of several specimens are reasonable and acceptable. First of all, the results are consistent to some extent. The results are ranging approximately in a 10% margin. Also, the results of this study are in accordance with the experimental results available in the literature. In Ref.[15], tensile moduli of an e-glass/epoxy laminate and a

carbon/epoxy laminate are given as 13.8 GPa, and 49.3 GPa respectively. The results are 18.6 GPa for e-glass/epoxy laminate, and 46.3 GPa for carbon/epoxy laminate in Ref.[16].

When the effects of post-curing on tensile modulus and strength are considered, it is difficult to come up with a suitable correlation. In some cases, it turned out that post-curing is enhancing the mechanical properties. However, in some cases it is observed that post-curing reduces the mechanical properties. At a first glance, one can deduce that the mechanical properties will improve with post-curing processes. This is correct to a certain extent. Actually, post-curing is a process related with the resin material. Therefore, with post-curing resin dominated properties like degree of curing, viscoelastic properties and glass transition temperature are quite affected; whereas, fiber dominated properties, tensile modulus and strength for example, are not significantly affected. This point is also reported in the literature [17].

In the data sheet of the epoxy, some experimental results are supplied. For the post-curing at 80°C for 8 hours case, the tensile strength of the resin is increased to 85 MPa, while the result of room temperature cured case is 60 MPa. On the other hand, tensile modulus is decreased from 3.45 GPa to 3.10 GPa. Another result for a post-curing scheme at 50°C for 15 hours is given such that the the tensile strength is increased to 84 MPa, and tensile modulus is increased to 3.55 GPa. By considering the results given in the data sheet, post-curing has an improving effect on tensile strength. However, it is not possible to decide whether post-curing has an enhancing or worsening effect on tensile modulus.

Even if post-curing has ameliorating effect on both tensile strength and modulus of the resin material, it would not imply that it would also increase the properties of the composite laminate. Because, the mechanical properties of the fibers in the laminate are not notably affected from post-curing. The increase in the properties of resin is quite negligible when compared with the mechanical properties of fibers (see Table 3.2). Hence, it would be inappropriate to expect an improvement in the tensile properties of composites when post-curing applied.

When the results of the tests performed are studied, one can notice a scatter in the tensile modulus and tensile strength values obtained in three different test cases. The results of the three test cases belong to the test coupons which are manufactured at different times. The reasons for the scatter in the mechanical properties are thought to be due to the following items:

- i. *Non-identical test conditions:* The variation in temperature at the manufacturing laboratory could be one factor affecting the properties. In addition, same vacuum conditions may not have been adjusted during the three different manufacturing activities.
- ii. *Specimen preparation:* Although specimens were manufactured by referencing the ASTM standard [13], the final specimens were cut to their standard sizes from the composite plates by sharp edged knives, because water jet cutting type professional equipment were not available. Specimens cut by sharp edge knife are prone to edge cracks, delaminations depending on the skill of the person performing the cutting action. This factor is deemed to be one of the major reasons for the existence of scatter in the data, because one can not expect to make repeatable cutting actions since the specimen cutting is made by a person but not by a machine.
- iii. *Possible misalignment of the test specimens in the tensile test machine:* This effect could also be one reason for the scatter in the test values. Because, in the tensile test machine used, the person performing the test aligns the specimen himself and the machine does not allow automatic alignment. Therefore, one is again restricted with the skill of the person attaching the specimen to the tensile test machine. Changes in the alignment of the different specimens could generate extra forces which are different from specimen to specimen, and this may cause scatter in the test values.
- iv. *Dissimilar void content achieved during the vacuum bagging process:* It is very possible that specimens manufactured at different times can have different void content due to the possible non-repeatable process environment that results during the preparation of the vacuum bagging system. Because of the non-automatic process of preparing the whole vacuum

bagging assembly, and reliance on the skill and experience of the person preparing the assembly, differences in the void content may occur in the composite structures manufactured at different times. This situation may directly affect the test coupons since they are prepared from the composite plates produced by vacuum bagging method.

To summarize, non-repeatability in the manufacturing process, test coupon preparation and alignment/attachment of the test coupons in the tensile test machine are deemed out to be the primary factors affecting the scatter in the test values. It is thought that, specimen cutting to final coupon size is very critical to get similar specimens without any defect, and cutting systems like water jet cutting, etc. should be used in specimen preparation.

More work should be done on material testing in order to have more reliable data. Number of the specimens tested should be increased to improve the quality of data from statistical point of view. Additionally, specimen preparation should be performed in a more delicate manner to minimize the possible defects in the specimens. If these conditions are not satisfied, one has to be conscientious in the design when using experiment data.

CHAPTER 4

FINITE ELEMENT MODEL AND ANALYSIS

4.1 Finite Element Model

For finite element analysis of the composite wing MSC Patran 2006 is used for pre- and post-processing, accompanied with MD Nastran 2006 as the solver. Half span of the wing is modeled with quad type shell elements properly. After meshing, 11695 nodes and 12028 elements are obtained. Boundary condition is defined as the wing is clamped at the root section. Figure 4.1 shows the isometric view of the half span wing model, and Figure 4.2 shows the detailed views of main and outer wing.

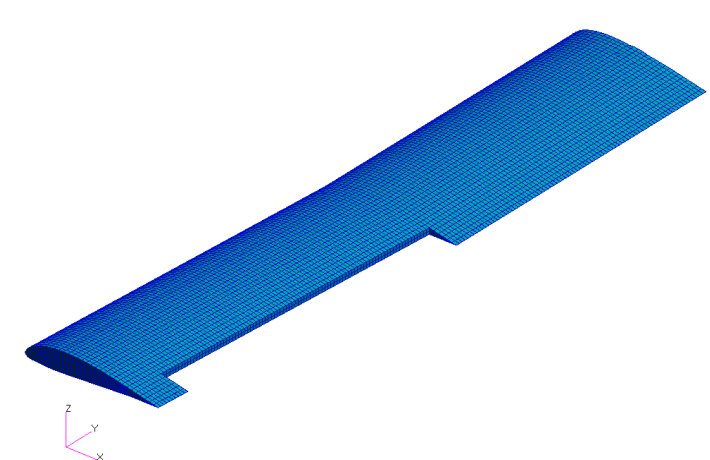


Figure 4.1: Finite element model of the wing.

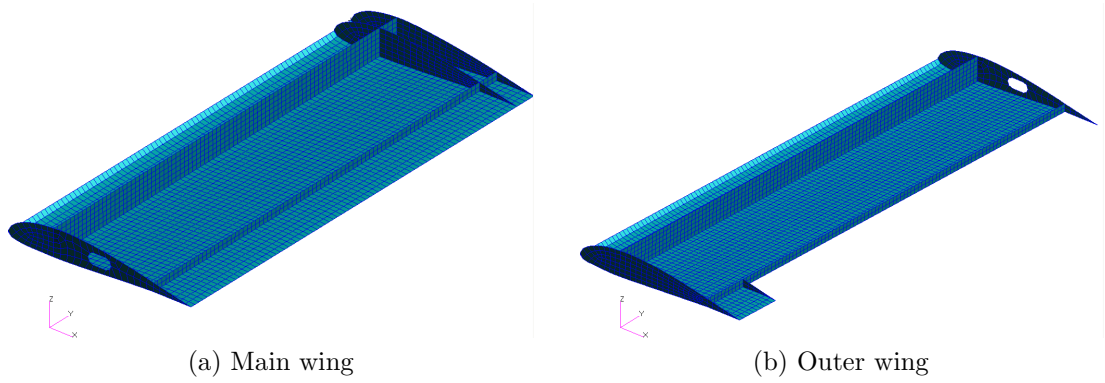


Figure 4.2: Detailed views of outer and main wing.

As seen in Figure 4.2, the wing structure has different components such as front and rear spar, and ribs with different geometries at different locations. Moreover, these components also differ in terms of the configurations of the materials used. The skin is made of 2 layers of e-glass with a 1-mm-thick styrofoam plate in between. The front spar, which is the main force carrying member, is formed by covering the two sides of a 15-mm-thick styrofoam core with carbon fabric. The rear spar and the ribs are manufactured with 2 layers of carbon fiber and a 3-mm-thick balsa wood as the core material. Schematic drawings of the configurations of components of the UAV are given in Figure 4.3.

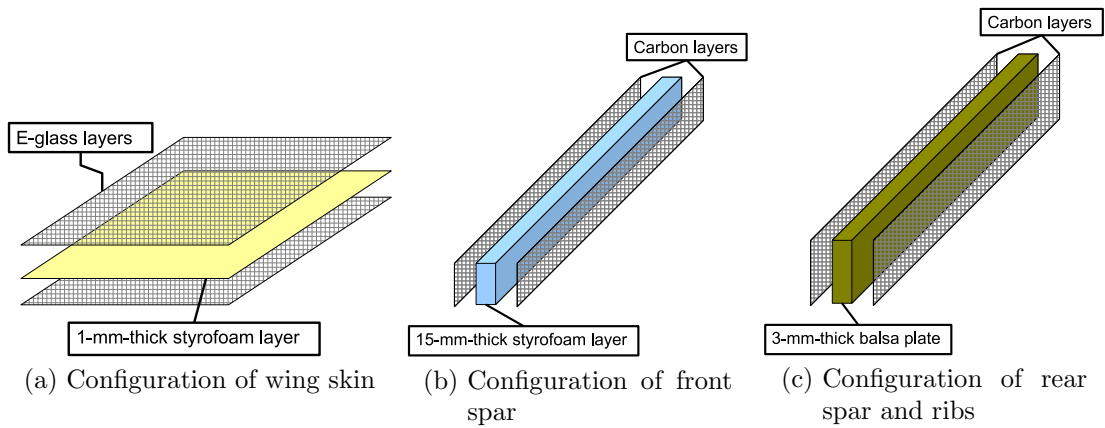


Figure 4.3: Schematic drawings of the configurations of components of the UAV.

It should be stressed that, the wing model used in this study is a simplified version of the actual wing. The actual wing has complicated connections, and has different discontinuities on the surface at different locations. However, the main aim of the analysis is to establish an equivalent

material model by comparing different approaches. Thus, this simple model is sufficient for this study.

4.2 Determination of Elastic Modulus

The elastic modulus of the composites used in the wing structure is determined using three different approaches. Firstly, mechanics of materials approach is employed for the characterization unidirectional composites. In the second approach, elastic modulus of the woven fabric is obtained through mechanical testing. The third method is based on approximate approaches.

4.2.1 Mechanics of Materials Approach

The elastic properties of the composites can be determined using the mechanics of materials approach of the micromechanics of composites. The properties of the composite are determined in terms of the material properties and the volume fractions of the constituent materials used in composite.

The following equations are derived for a unidirectionally reinforced fibrous composite material by assuming that the strains in both the matrix and the fiber are the same. Derivations of these equations are available in any mechanics of composite materials textbooks [4].

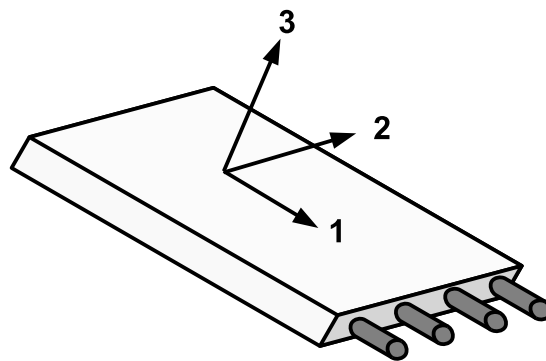


Figure 4.4: Axis system used.

$$E_1 = E_f V_f + E_m V_m \quad (4.1)$$

$$E_2 = \frac{E_f E_m}{V_m E_f + V_f E_m} \quad (4.2)$$

$$\nu_{12} = V_m \nu_m + V_f \nu_f \quad (4.3)$$

$$G_{12} = \frac{G_f G_m}{V_m G_f + V_f G_m} \quad (4.4)$$

Here, E is elastic modulus, G is shear modulus, ν is Poisson's ratio, and V is the volume fraction where $V_m = 1 - V_f$. The subscripts f and m represents the properties of fiber and matrix respectively, 1 and 2 are material directions, and 12 is 1-2 plane.

The mechanical properties of the fibers and the matrix material supplied by the manufacturers [18, 12], and the fiber volume fractions obtained at the end of the manufacturing process are given in Table 4.1, and the calculated elastic properties are given in Table 4.2.

Table 4.1: Mechanical properties of the fibers and matrix material used in the UAV.

Material	E [GPa]	ν	G [GPa]	V_f
E-glass	74	0.22	30	0.5
Kevlar	130	0.35	2.9	0.47
Carbon	230	0.2	10	0.49
Epoxy	3.45	0.35	1.25	

Table 4.2: Unidirectional Elastic properties of the composites used in the UAV based on micromechanics of composites.

Composite type	E_1 [GPa]	E_2 [GPa]	ν_{12}	G_{12} [GPa]
E-glass/Epoxy	38.73	6.59	0.29	2.4
Kevlar/Epoxy	62.3	6.3	0.35	1.7
Carbon/Epoxy	115.14	6.71	0.28	2.2

Notice that these elastic properties are calculated for a unidirectionally reinforced composite material; whereas, the UAV is built with plain weave woven fabrics. In this approach, for comparison purposes, woven layer is modeled as a two layered biaxial cross ply laminate with the

half thickness of the actual one layer woven lamina. It should be noted that the results of this section is only used to see how off the biaxial modeling is from the results obtained based on the experimental determination of the elastic constants.

4.2.2 Mechanical Testing of Composites

The details of material characterization through mechanical testing are discussed in Chapter 3 comprehensively. In this section, the average elastic moduli of the specimens obtained through tensile testing are given in Table 4.3. It should be noted that, the properties used in the finite element analysis belong to the specimens cured at room temperature.

Table 4.3: Average elastic moduli of the specimens obtained from tensile testing.

Fabric type	\overline{E}_t [GPa]
E-glass/Epoxy	22.29
Kevlar/Epoxy	24.13
Carbon/Epoxy	46.26

4.2.3 An Approximate Method for Obtaining Elastic Properties

The equations presented in the micromechanics approach relate to unidirectional materials and cannot be applied directly to woven fabric layers. The complex nature of the woven structure mean requires unit cell approaches to come up the elastic constants of the composite material composed of resin and woven fabric [19]. However, especially in preliminary design studies, simple relations may be used to calculate the elastic modulus of the lamina. In References [20, 21], for woven fabric layers, it is suggested to use a modified rule of mixtures relation to calculate the elastic modulus of the composite material. Modification involves the multiplication of the fiber modulus by an efficiency factor, η as shown in Equation 4.5.

$$E_1 = \eta E_f V_f + E_m V_m \quad (4.5)$$

For plain weave balanced fabrics the efficiency factor is usually taken as 0.5. Using the material properties given in Table 4.1, the elastic modulus of the composites obtained as follows:

Table 4.4: Elastic moduli of the composites obtained from an approximate method.

Composite type	E_1 [GPa]
E-glass/Epoxy	20.23
Kevlar/Epoxy	30.07
Carbon/Epoxy	58.44

Using three different approaches some of the elastic properties of the composites used in the UAV are determined. The composite materials are defined as 2-D orthotropic materials in MSC Patran, and shear moduli in 1-2, 2-3 and 1-3 planes are required as well. Those missing data are obtained from the experimental results available in the literature [17]. Additionally, except for the micromechanics approach, the Poisson's ratio in 1-2 direction could not be obtained. To solve this problem, a square plate is modeled in Patran as a biaxial cross ply laminate using the material properties obtained from the micromechanics approach. The boundary conditions are set to a unit displacement in 1 direction and deflections in 2 direction are set to be free. In the results, deflection in 2 direction are obtained, and from the displacements in 1 and 2 directions the Poisson's ratio is obtained.

In the wing structure, two types of styrofoam plate and balsa wood are used as the core materials in the sandwich-like structure. The styrofoam plates are modeled as isotropic materials with the elastic properties obtained from the manufacturer [22]. The balsa wood is modeled as a 2-D orthotropic material with the elastic properties obtained from [23].

To sum up, the elastic properties which are to be used in the finite element analysis are presented in Table 4.5. Properties obtained from different methods are indicated with VF, Test, and App. which refer to micromechanics approach, tensile testing, and approximate method respectively.

Table 4.5: Material properties to be used in the finite element analysis.

Material Type		Properties
E-glass/Epoxy	VF	$E_{11} = 38.73$ GPa, $E_{22} = 6.59$ GPa, $\nu_{12} = 0.29$, $G_{12} = 2.4$ GPa, $G_{23} = 2.4$ GPa, $G_{13} = 2.4$ GPa, $\rho = 1.45 \times 10^{-6}$ kg/mm ³
	Test	$E_{11} = 22.29$ GPa, $E_{22} = 22.29$ GPa, $\nu_{12} = 0.08$, $G_{12} = 3$ GPa, $G_{23} = 2.4$ GPa, $G_{13} = 2.4$ GPa, $\rho = 1.45 \times 10^{-6}$ kg/mm ³
	App.	$E_{11} = 20.23$ GPa, $E_{22} = 20.23$ GPa, $\nu_{12} = 0.08$, $G_{12} = 3$ GPa, $G_{23} = 2.4$ GPa, $G_{13} = 2.4$ GPa, $\rho = 1.45 \times 10^{-6}$ kg/mm ³
Carbon/Epoxy	VF	$E_{11} = 115.14$ GPa, $E_{22} = 6.71$ GPa, $\nu_{12} = 0.28$, $G_{12} = 2.2$ GPa, $G_{23} = 2.7$ GPa, $G_{13} = 2.7$ GPa, $\rho = 1.19 \times 10^{-6}$ kg/mm ³
	Test	$E_{11} = 46.26$ GPa, $E_{22} = 46.26$ GPa, $\nu_{12} = 0.03$, $G_{12} = 3.8$ GPa, $G_{23} = 2.7$ GPa, $G_{13} = 2.7$ GPa, $\rho = 1.19 \times 10^{-6}$ kg/mm ³
	App.	$E_{11} = 58.44$ GPa, $E_{22} = 58.44$ GPa, $\nu_{12} = 0.03$, $G_{12} = 3.8$ GPa, $G_{23} = 2.7$ GPa, $G_{13} = 2.7$ GPa, $\rho = 1.19 \times 10^{-6}$ kg/mm ³
Balsa wood		$E_{11} = 3378$ MPa, $E_{22} = 50.67$ MPa, $\nu_{12} = 0.229$, $G_{12} = 125$ MPa, $G_{23} = 17$ MPa, $G_{13} = 182$ MPa, $\rho = 0.16 \times 10^{-6}$ kg/mm ³
Foam (blue)		$E = 10$ MPa, $\nu = 0.35$, $\rho = 3.3 \times 10^{-8}$ kg/mm ³
Foam (yellow)		$E = 10$ MPa, $\nu = 0.35$, $\rho = 3.1 \times 10^{-8}$ kg/mm ³

It should be noted that the elastic moduli calculated based on the micromechanics approach are the unidirectional properties, therefore one should not compare the unidirectional properties with the elastic properties based on the test and approximate method.

4.3 Analysis of the Wing

The fibers used in the UAV wing are plain weave balanced fabrics with $0^\circ/90^\circ$ orientation. As shown in Figure 4.5, woven fabrics have a complex architecture, and for a detailed analysis, one has to implement meso scale models, like unit cell or quarter cell models. However, this is a very complicated job, and some practical methods can be used for preliminary structural analysis.

In this study, for modeling the woven structure, two methods are introduced. One is modeling the woven lamina as a two layer biaxial cross ply laminate with each layer having half thickness of the single woven lamina. Second method is modeling with a single equivalent layer by assuming $E_1 = E_2$. Schematic drawings of the two models are shown in Figure 4.6.

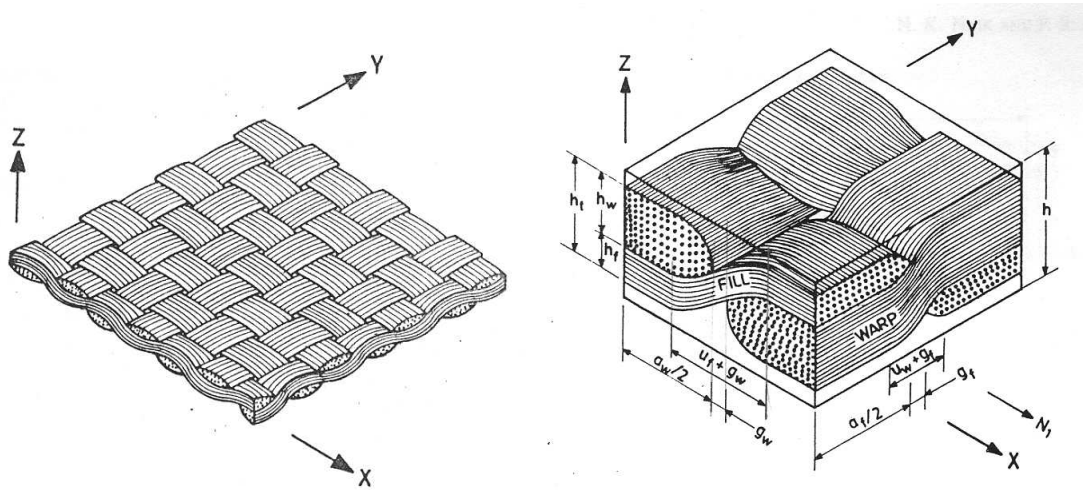


Figure 4.5: A general and a detail view of woven architecture.

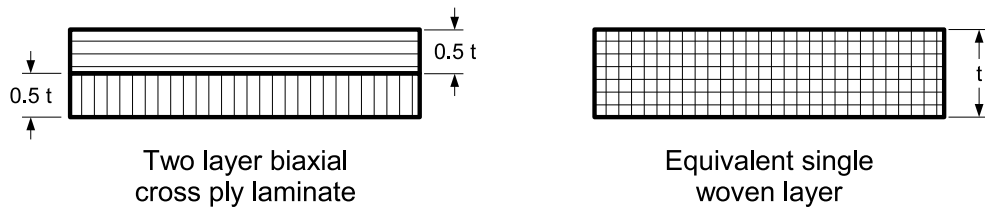


Figure 4.6: Two different approaches for modeling woven lamina used in this study.

In the structural analysis, these two material models are used with the material properties obtained from three different methods as discussed in previous section. The following cases are analyzed:

- Case I: The material properties obtained from micromechanical approach are used for modeling the single woven layer as a biaxial cross ply laminate with half thickness of actual thickness of the woven lamina. For control purpose, a single layer of woven composite is modeled with $[0^\circ/90^\circ]$ and $[90^\circ/0^\circ]$ stacking orientations to see if stacking sequence of cross ply laminate affects the solution. A sketch of stacking sequence of Case I is shown in Figure 4.7.

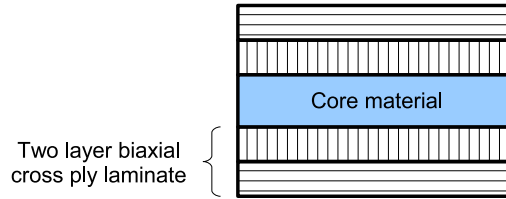


Figure 4.7: Stacking sequence used in Case I.

- Case II: The material properties obtained from tensile testing are used for modeling the single woven layer with Young's moduli in 1 and 2 directions being the same. This approach is also suggested by MSC as well [24]. Stacking sequence of this case is shown in Figure 4.8.

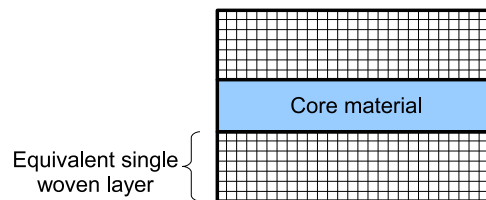


Figure 4.8: Stacking sequence used in Cases II and III.

- Case III: The material properties obtained from approximate approach are used in the same manner as in Case II.

During the structural analysis, the wing is assumed to be clamped at root section. Two types of analyses are performed: linear static analysis and modal analysis. In the linear static analysis, the loading is applied as total load uniformly distributed to the elements at the tip of the upper skin of the outer wing. This load case simulates lifting up the air vehicle from the tips of the wing. Thus, half weight of the air vehicle is applied from the wing tips. The loading and the boundary condition, which are applied, is shown on Figure 4.9.

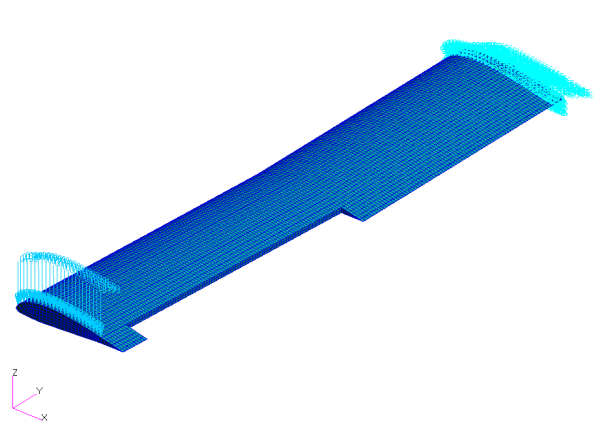
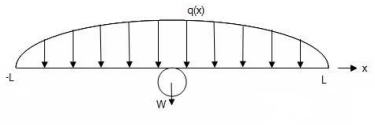
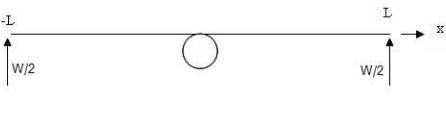


Figure 4.9: Loading and the boundary condition defined in the wing model.

This load case simulates a $2.35g$ flight condition. If the lift distribution over the wing is assumed as an elliptical distribution, which is the ideal case, the bending moment at the wing root comes out to be $0.21WL$, whereas, for the tip loading case it is $0.5WL$ (see Table 4.6). Therefore, tip loading case simulates a $2.35g$ flight condition at the root of the wing.

Table 4.6: Comparison of distributed elliptic loading and tip loading cases.

Distributed elliptic loading	Tip loading
 $q(x) = \frac{2}{\pi} \frac{W}{L} \sqrt{1 - \frac{x^2}{L^2}}$ $M_{root} = \int_0^L \frac{2}{\pi} \frac{W}{L} \sqrt{1 - \frac{x^2}{L^2}} x dx = 0.21WL$	 $M_{root} = 0.5WL$

4.3.1 Results of Case I

In this case woven composite is modeled as biaxial cross ply laminate with $[0^\circ/90^\circ]$ orientation. The analysis is repeated for $[90^\circ/0^\circ]$ orientation for control purpose. In Table 4.7 results of this case are summarized.

Table 4.7: Results of linear static and modal analyses of Case I.

Material property	Results
VF $[0^\circ/90^\circ]$	Max. Deflection = 44.6 mm
	Max. Stress @Skin = 119 / 41.6 / 0.517 / 32.7 / 127 MPa
	Averaged Max. Stress = 80.3 / 0.517 / 79.75 MPa
	Max. Stress @FrontSpar = 160 / 20.4 / 0.0983 / 15.6 / 172 MPa
	Averaged Max. Stress = 90.2 / 0.0983 / 93.8 MPa
VF $[90^\circ/0^\circ]$	1st modal frequency = 0.56171 Hz. (bending)
	2nd modal frequency = 2.6583 Hz. (torsion)
	3rd modal frequency = 3.0515 Hz. (bending)
	Max. Deflection = 44.7 mm
	Max. Stress @Skin= 42.4 / 121 / 0.525 / 128 / 33.3 MPa
VF $[90^\circ/0^\circ]$	Averaged Max. Stress = 81.7 / 0.525 / 80.65 MPa
	Max. Stress @FrontSpar = 21.1 / 162 / 0.098 / 173 / 15.7 MPa
	Averaged Max. Stress = 91.55 / 0.098 / 94.35 MPa
	1st modal frequency = 0.56095 Hz. (bending)
	2nd modal frequency = 2.6606 Hz. (torsion)
	3rd modal frequency = 3.0517 Hz. (bending)

There are five stress values given as ‘Max. Stress’ and three stress values given as ‘Averaged Max. Stress’ in Table 4.7. As explained before, in this case a single layer woven lamina is modeled as a biaxial cross ply laminate. Thus, the first two and last two stress values correspond to maximum stress at each layer of cross ply laminate. The third one corresponds to the maximum stress at the core material. In order to compare the stress values of this case with the other two cases, the stresses at the layers of cross ply laminate are averaged, and the average maximum stress outlines this result.

The following figures show the stress and displacement contours of the wing structure obtained from the finite element analysis with $[0^\circ/90^\circ]$ orientation. Figure 4.10 is the stress and displacement contours of the wing. In Figure 4.11, detail views of stress contours at each layer of cross ply laminate are presented. In Figure 4.12, stress and displacement contours of the front spar are shown. The detail views of stress contours at each layer of cross ply laminate at the

front spar are demonstrated in Figure 4.13. The first three mode shapes of the wing obtained from the modal analysis are presented in Figure 4.14.

Similarly, the same contour plots are presented in Figures 4.15, 4.16, 4.17, 4.18, 4.19 for $[90^\circ/0^\circ]$ orientation.

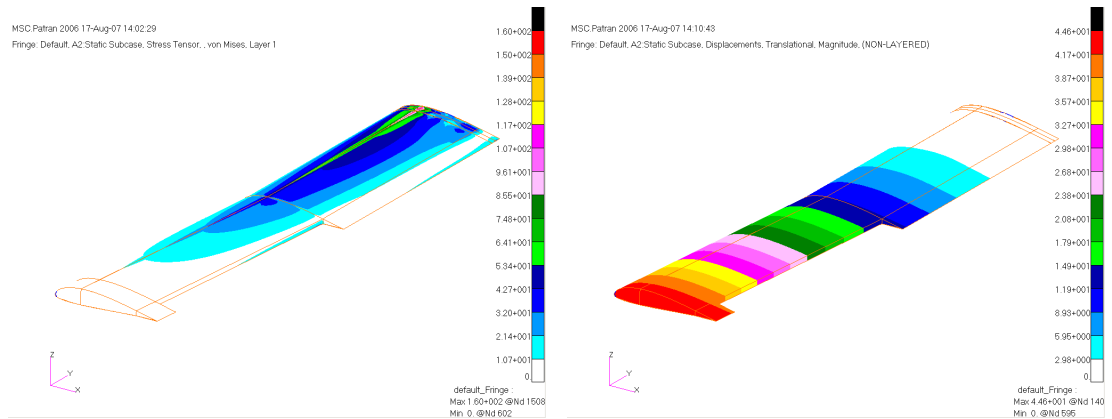


Figure 4.10: Stress and displacement contours of the wing (material orientation: $[0^\circ/90^\circ]$).

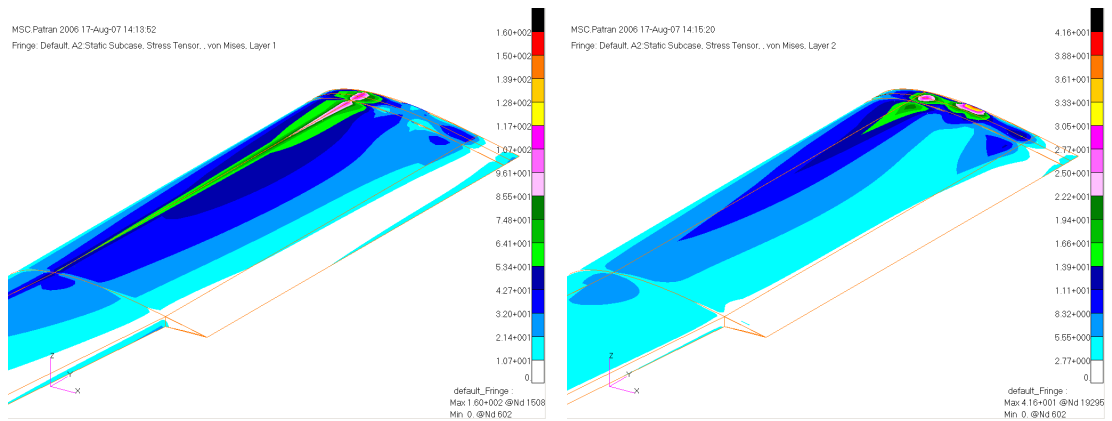


Figure 4.11: Detailed views of stress contours at Layer 1 and Layer 2 of the wing (material orientation: $[0^\circ/90^\circ]$).

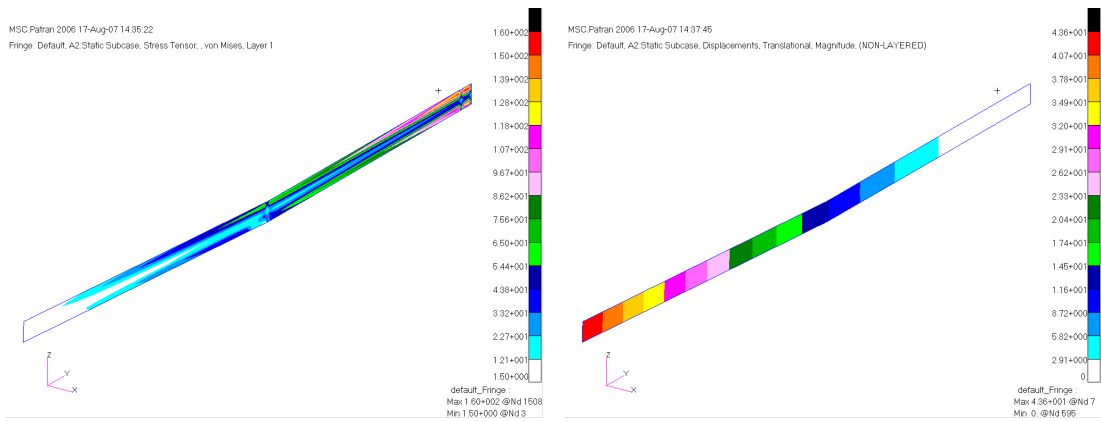


Figure 4.12: Stress and displacement contours at the front spar (material orientation: $[0^\circ/90^\circ]$).

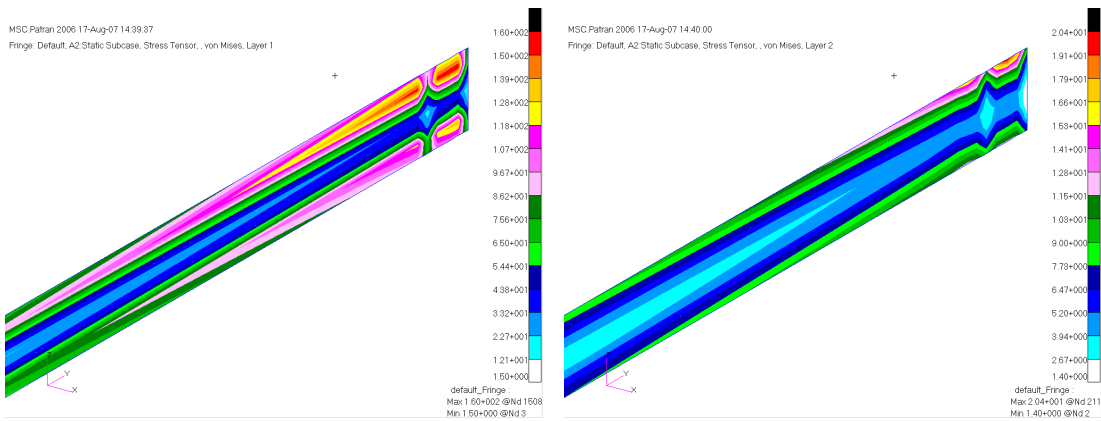


Figure 4.13: Detailed views of stress contours at Layer 1 and Layer 2 at the front spar (material orientation: $[0^\circ/90^\circ]$).

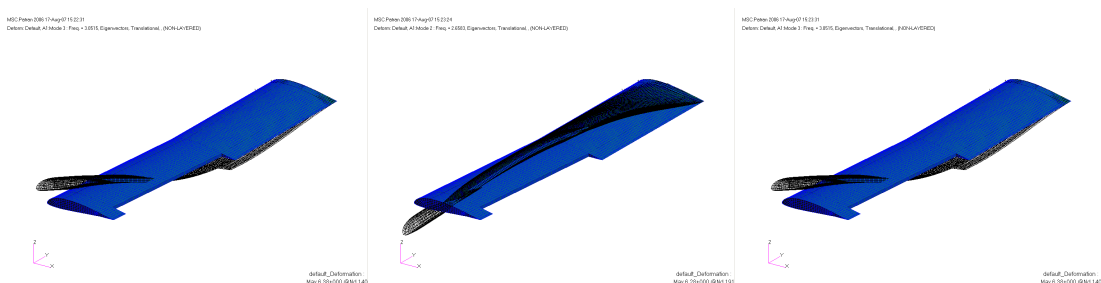


Figure 4.14: First three mode shapes of the wing structure (material orientation: $[0^\circ/90^\circ]$).

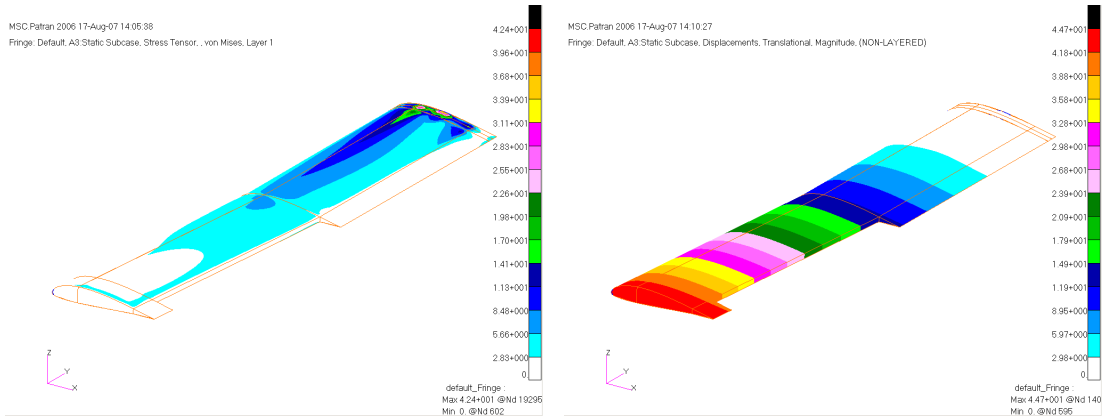


Figure 4.15: Stress and displacement contours of the wing (material orientation: $[90^\circ/0^\circ]$).

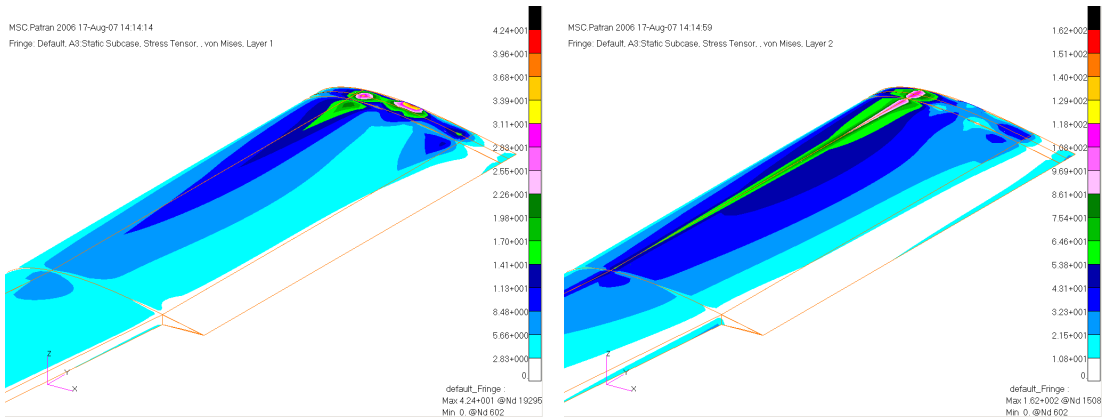


Figure 4.16: Detailed views of stress contours at Layer 1 and Layer 2 of the wing (material orientation: $[90^\circ/0^\circ]$).

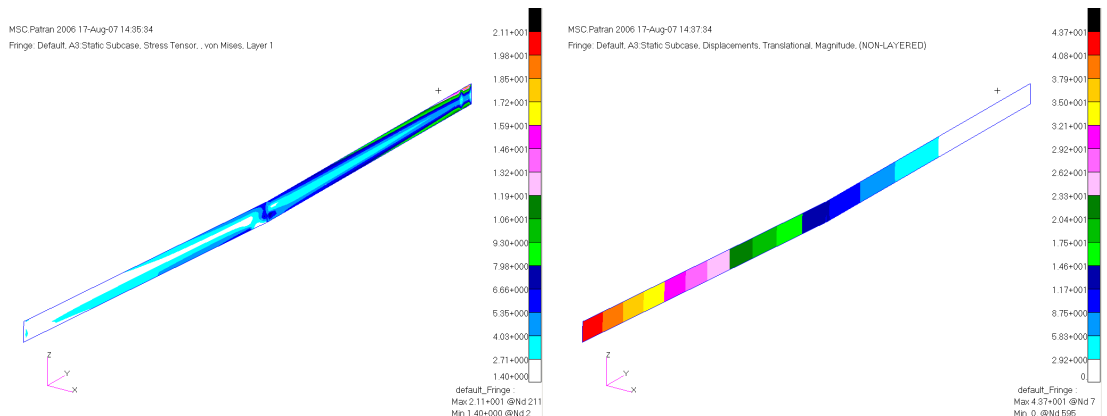


Figure 4.17: Stress and displacement contours at the front spar (material orientation: $[90^\circ/0^\circ]$).

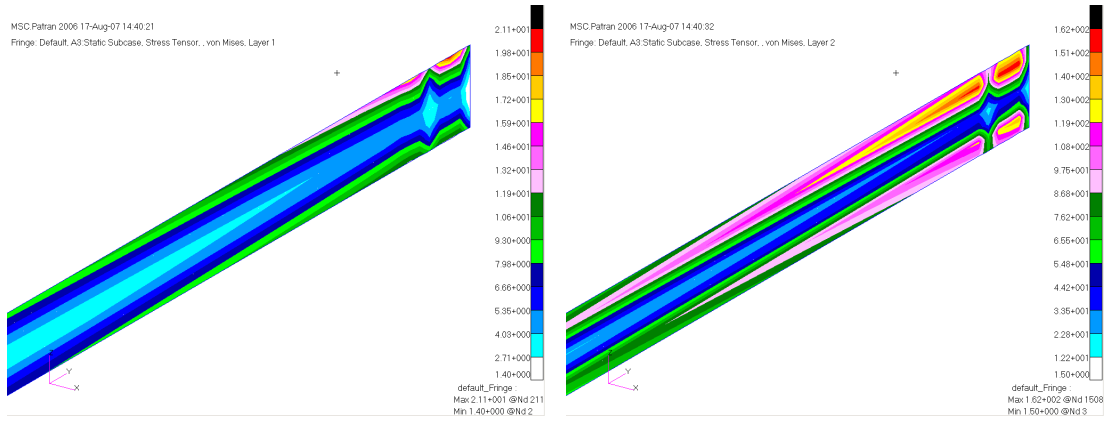


Figure 4.18: Detailed views of stress contours at Layer 1 and Layer 2 at the front spar (material orientation: $[90^\circ/0^\circ]$).

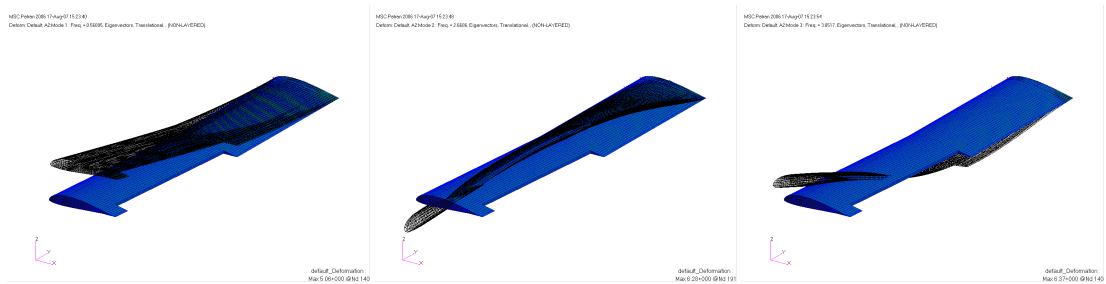


Figure 4.19: First three mode shapes of the wing structure (material orientation: $[90^\circ/0^\circ]$).

4.3.2 Results of Case II

In this case the material properties used in the analysis are obtained through tensile testing. The composite woven layers are modeled as 2-D orthotropic layers, and E_1 and E_2 are taken as same. The results are given in Table 4.8.

Table 4.8: Results of linear static and modal analyses of Case II.

Material property	Results
Test	Max. Deflection = 46.9 mm
	Max. Stress @Skin= 65.7 / 0.558 / 66.4 MPa
	Max. Stress @FrontSpar = 73.1 / 0.0722 / 75.6 MPa
	1st modal frequency = 0.57521 Hz. (bending)
	2nd modal frequency = 2.8839 Hz. (torsion)
	3rd modal frequency = 3.2044 Hz. (bending)

In Table 4.8, similar to the previous table, maximum stresses at each layer of composite laminate are given for the total wing and front spar separately. In the last row, first three modal frequencies are given.

The following figures present the stress and displacement contours of the wing and front spar obtained from the linear static analysis. Figure 4.20 shows the stress contour of the wing from isometric and detail views. Figure 4.21 shows the displacement contour of the wing and the spar. Figure 4.22 shows the stress contour of the front spar from isometric and detail views. Figure 4.23 shows the first three mode shapes of the wing.

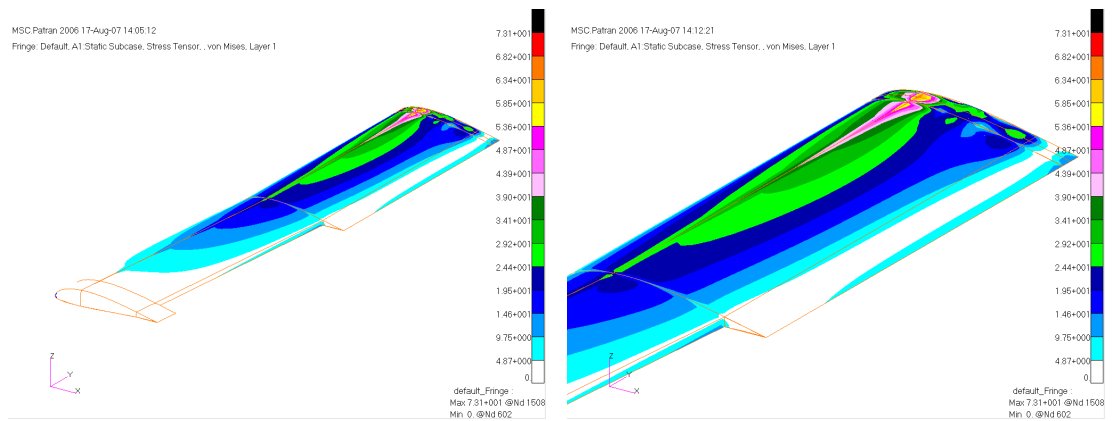


Figure 4.20: Isometric and detail views of stress contour of the wing.

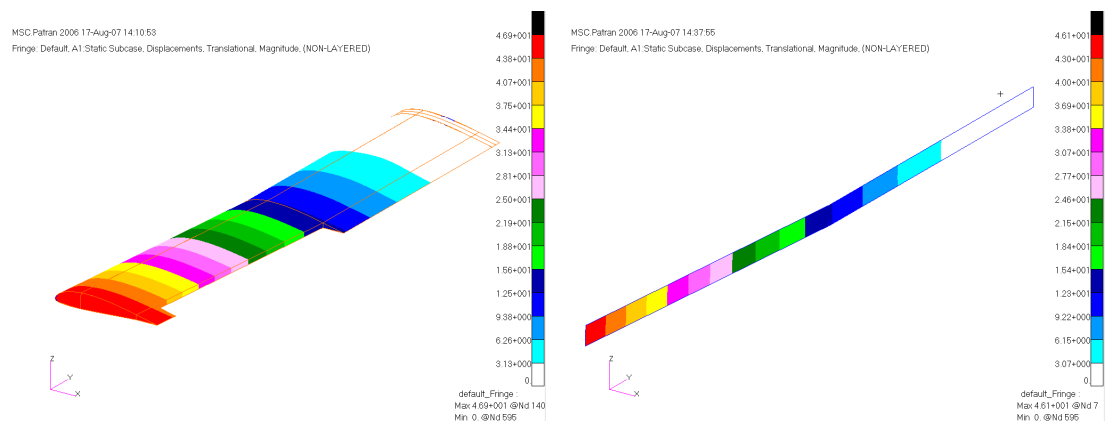


Figure 4.21: Displacement contours of the wing and the front spar.

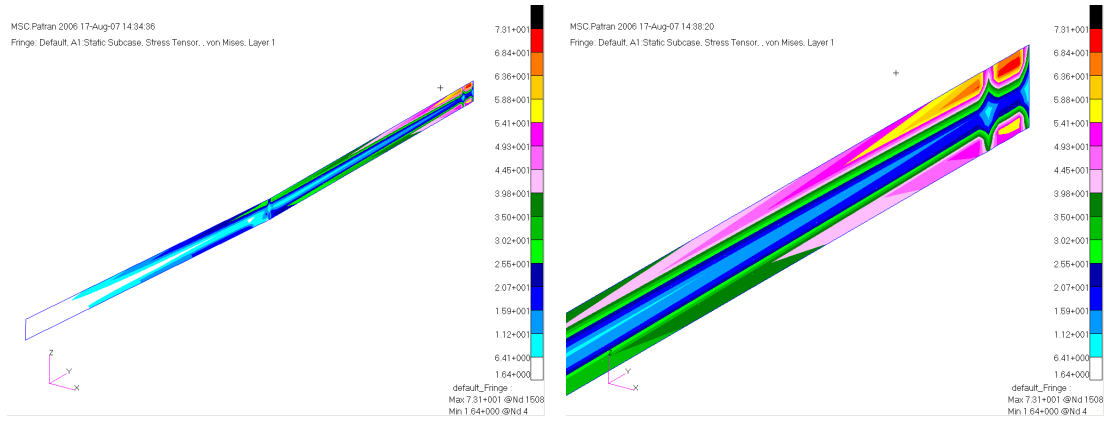


Figure 4.22: Isometric and detail views of stress contour of the front spar.

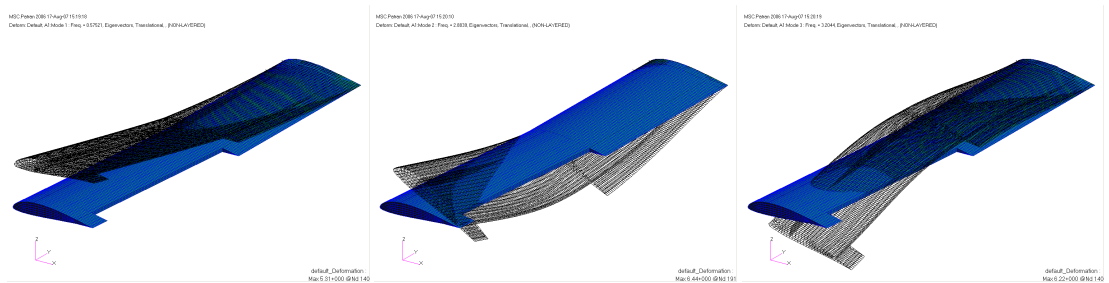


Figure 4.23: First three mode shapes of the wing structure.

4.3.3 Results of Case III

In this case the material properties used in the analysis are obtained through an approximate approach. The composite woven layers are modeled as 2-D orthotropic layers, and E_1 and E_2 are taken as same. The results are given in Table 4.9.

Table 4.9: Results of linear static and modal analyses of Case III.

Material property	Results
App.	Max. Deflection = 48.7 mm
	Max. Stress @Skin= 70.6 / 0.557 / 72.1 MPa
	Max. Stress @FrontSpar = 93.0 / 0.0929 / 95.4 MPa
	1st modal frequency = 0.56499 Hz. (bending)
	2nd modal frequency = 2.8561 Hz. (torsion)
	3rd modal frequency = 3.1713 Hz. (bending)

In Table 4.9, similar to the previous table, maximum stresses at each layer of composite laminate are given for the total wing and front spar separately. In the last row, first three modal

frequencies are given.

The following figures presents the stress and displacement contours of the wing and front spar obtained from the linear static analysis. Figure 4.24 shows the stress contour of the wing from isometric and detail views. Figure 4.25 shows the displacement contour of the wing and the spar. Figure 4.26 shows the stress contour of the front spar from isometric and detail views. Figure 4.27 shows the first three mode shapes of the wing.

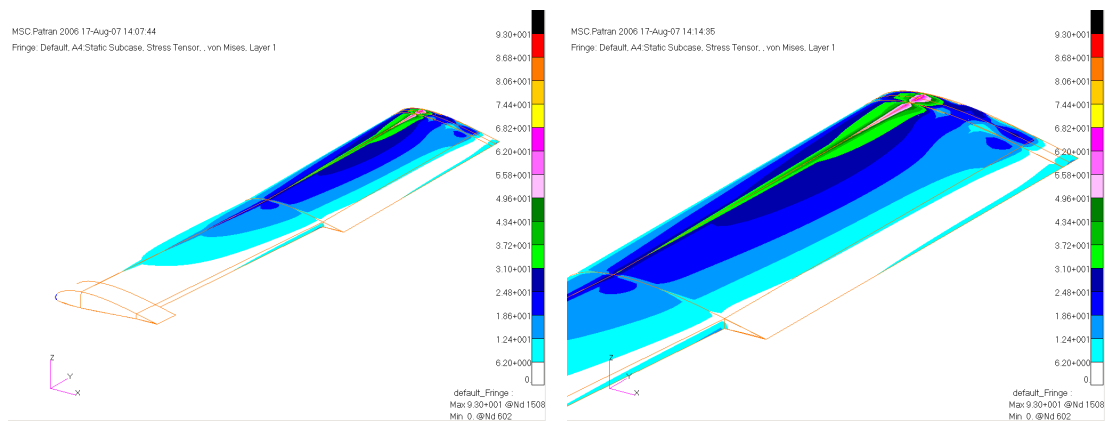


Figure 4.24: Isometric and detail views of stress contour of the wing.

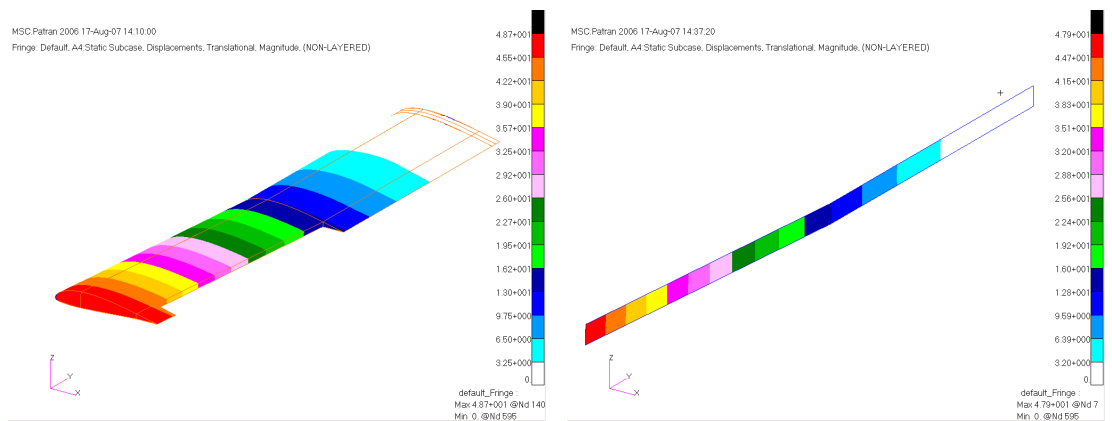


Figure 4.25: Displacement contours of the wing and the front spar.

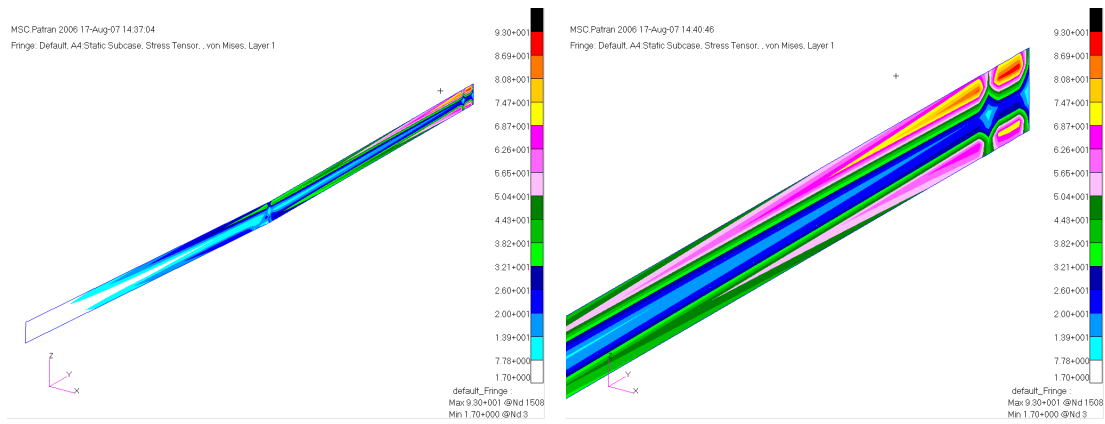


Figure 4.26: Isometric and detail views of stress contour of the front spar.

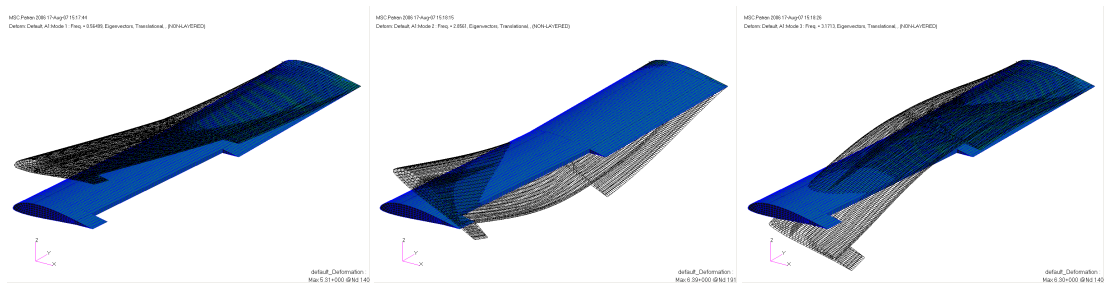


Figure 4.27: First three mode shapes of the wing structure.

4.3.4 Discussion of Results

When the results are observed, it can be seen that the results are close to each other. Especially, the maximum deflections and modal frequencies came out to be nearly the same. For the stress results, stresses in Cases I and III are close; whereas, in Case II, stress results obtained are approximately 20% less than the other two cases. Nevertheless, all stress results are well below the tensile strength values obtained from tensile tests. It should be noted that modeling a woven layer as a biaxial composite is not the correct way. However, as the results show, biaxial modeling approach approximates the stiffness of the wing quite accurately when the thickness of each layer is taken as one half of the thickness of the woven layer. Therefore, in the preliminary design study satisfactory wing stiffness can be obtained by approximating the woven layer by a biaxial laminate. The stress results of the three cases give averaged out stresses, and these stresses can only be used for global analysis. For initial and progressive damage analysis

appropriate micro models should be used. However, for initial sizing and for deciding on the composite layer configuration and fabric/resin selection, the stress analysis results of the three cases can be used.

In Case I, the results of both $[0^\circ/90^\circ]$ and $[90^\circ/0^\circ]$ orientations yielded very close results. Thus, it can be concluded that stacking sequence of the cross ply laminate does not affect the solution in this problem.

4.4 Case Study: Spanwise distributed wing loading

During the design phase of the aircraft, in the wing geometry design stage, spanwise lift and moment coefficient distributions are calculated for 4 different level flight conditions using ESDU wing loading program [10]. The data obtained from the program is plotted as shown in Figure 4.28.

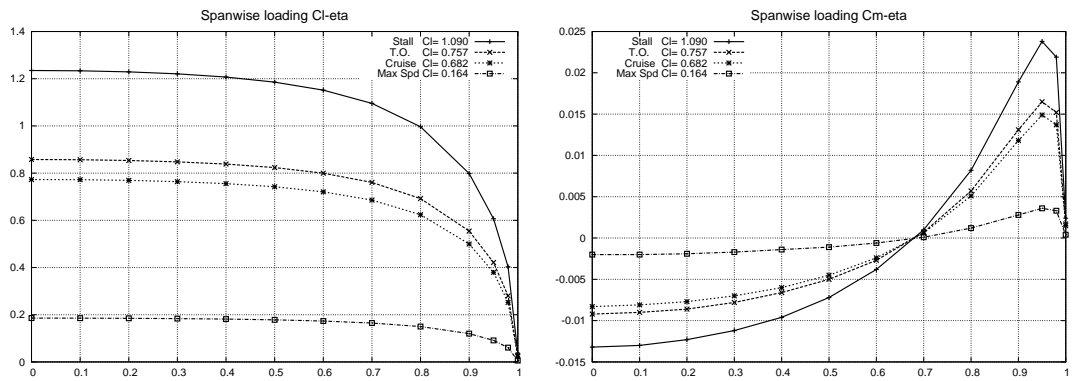


Figure 4.28: Spanwise wing loadings for 4 different level flight conditions.

For the case study, level flight with stall speed is selected and finite element analysis performed for this distributed loading. The ESDU program calculated lift and moment coefficients at 13 stations over the span. Between these stations, lift force and pitching moment are calculated with the Equations 4.6 and 4.7, respectively, using trapezoidal rule. The calculations are performed for a stall speed of $V_\infty = 11 \text{ m/s}$, with half wing span (1.1 m) and 0.2 m chord at sea

level conditions. Then these force and moment results are distributed between 13 stations over the front spar, whose location is at the quarter chord. A close-up view of distributed force and moment applied on a section over the front spar is shown in Figure 4.29.

$$L = \frac{1}{2}\rho V_{\infty}^2 S C_l \quad (4.6)$$

$$M = \frac{1}{2}\rho V_{\infty}^2 S c C_m \quad (4.7)$$

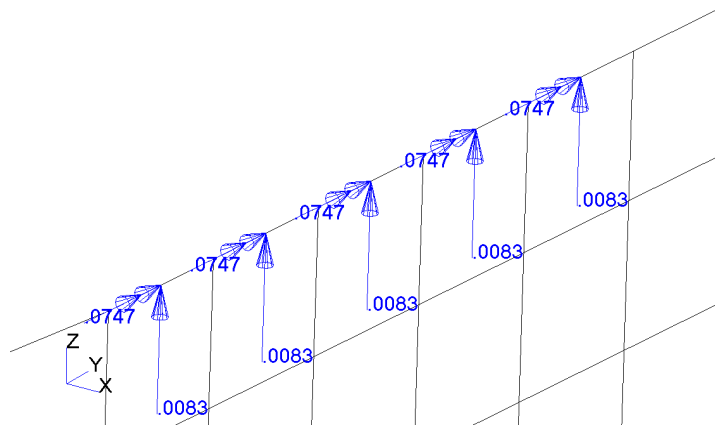


Figure 4.29: Close-up view of distributed force and moment applied on a section over the front spar.

The results obtained from the finite element analyses are given in Table 4.10.

Table 4.10: Results of stall case analysis using different material definitions.

Material property	Results
VF [0°/90°]	Max. Deflection = 11.9 mm
	Max. Stress @Skin = 46.4 / 13.9 / 0.179 / 11.0 / 49.1 MPa
	Averaged Max. Stress = 30.15 / 0.179 / 30.05 MPa
	Max. Stress @FrontSpar = 61.5 / 7.56 / 0.0206 / 5.90 / 65.2 MPa Averaged Max. Stress = 34.53 / 0.0206 / 35.55 MPa
Test	Max. Deflection = 12.5 mm
	Max. Stress @Skin= 25.1 / 0.194 / 25.8 MPa
	Max. Stress @FrontSpar = 28.3 / 0.0198 / 29.2 MPa
App.	Max. Deflection = 13.0 mm
	Max. Stress @Skin= 27.0 / 0.193 / 27.6 MPa
	Max. Stress @FrontSpar = 35.5 / 0.0193 / 36.4 MPa

Here, it should be stressed that the wing loading data was obtained during the conceptual design phase. At that time, take-off weight of the aircraft was estimated to be 3.5 kg; whereas, the actual take-off weight is 4.5 kg. Since, linear static analysis is performed in the finite element program, the stress and displacement results are proportional to the load applied. One can observe that, the stress and displacement results obtained from the tip loading cases, which are given in Tables 4.7, 4.8 and 4.9, are approximately twice as much as the results obtained from the distributed loading case; provided that the difference between the design take-off weight and actual take-off weight is taken into account. Therefore, it can be concluded that the assumption that ‘the tip loading is simulating approximately 2.35 *g* flight case’ is reasonable.

The general distributions of stress and displacement contours obtained from the analyses are conformable for each material definition. The plots of the results obtained using properties calculated with micromechanics approach are given in the following figures.

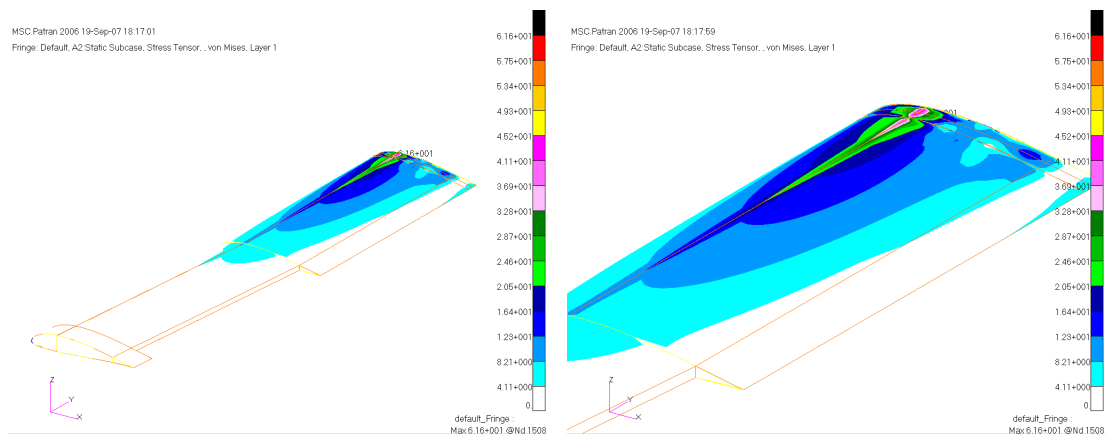


Figure 4.30: Isometric and detail views of stress contour of the wing.

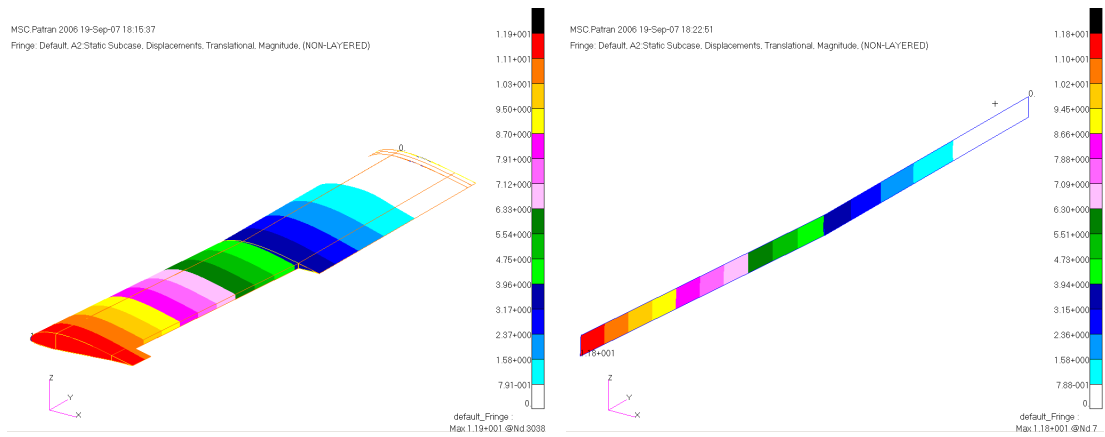


Figure 4.31: Displacement contours of the wing and the front spar.

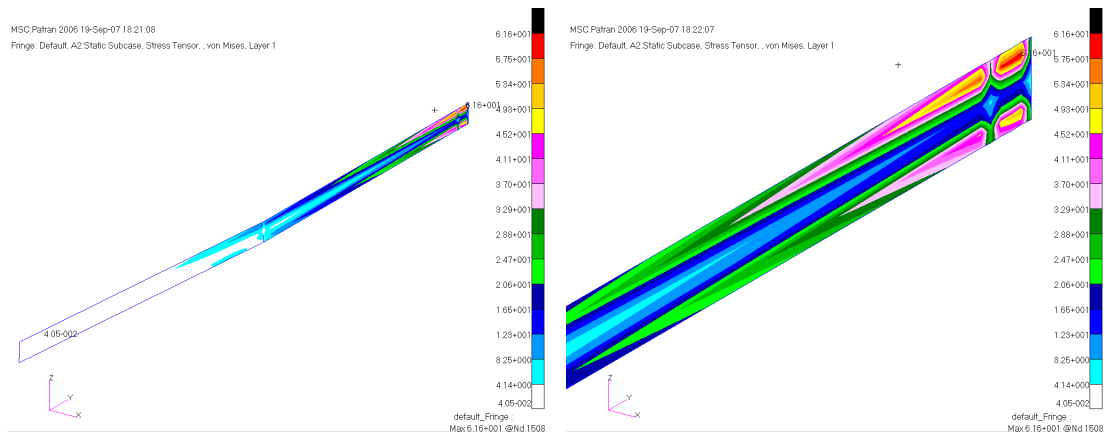


Figure 4.32: Isometric and detail views of stress contour of the front spar.

4.5 Analysis of Front Spar

In these kind of lightweight aircraft, for an initial sizing study, it can be assumed that all the wing loading is carried by the main spar. Following this assumption, the front spar of the UAV wing is analyzed separately with two methods. The front spar is first analyzed with method of transformed sections, and the results of the transformed section method are compared with the results obtained by the finite element analysis.

4.5.1 Analysis with Transformed Section Method

Transformed section method is used for calculating the stress and displacement in a beam made of two or more different materials. The procedure is to transform the cross section into an equivalent cross section composed of only one material. Then, the transformed section is analyzed in the usual manner for a beam of one material. The transformed section must have the same neutral axis and the same moment-resisting capacity as the original beam if it is to be equivalent. The transformation is made by multiplying the thickness of the material, which is to be transformed, by the ratio of Young's modulus of the material and the Young's modulus of the material to which transformation will be performed. It can easily be shown that changing the thickness of materials in a cross section does not change the location of neutral axis [25].

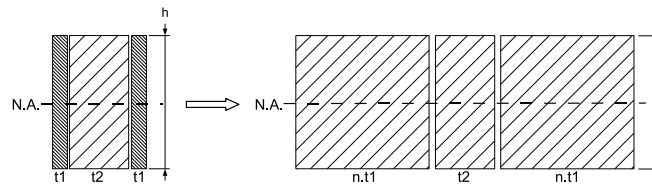


Figure 4.33: Method of transformed section.

Consider the front spar of the UAV shown in Figure 4.33. It has a cross section as shown in the left hand side of Figure 4.33. A 15-mm-thick styrofoam plate is covered with woven carbon fabric at both side surfaces. Here, carbon laminae are transformed into styrofoam, thus, their thickness is multiplied by n , where $n = E_{carbon/epoxy}/E_{styrofoam}$. Then, the second moment of inertia is calculated with new cross section, and using the equations of mechanics of materials stress and maximum deflections are obtained. The stress obtained is the stress value in the material to which the whole cross section is transformed into. Hence, in order to find the stress in the carbon laminate, the obtained stress result must be multiplied with n again. Hence, in order to find the stress in the carbon laminate, the obtained stress result must be multiplied by the ratio of the Young's moduli, n , and back transformation has to be performed [25].

The analysis is done with following configuration: a tip load of 22.07 N , which is the half weight of the UAV, is applied to the beam which is 1100 mm long and clamped at one edge; height of the cross section is 30 mm and thicknesses of carbon layers and foam core are 0.13 mm and 15 mm respectively; elastic modulus of carbon layer is 46.26 GPa and foam layer has a modulus of 10 MPa . The results obtained are given in Table 4.11.

4.5.2 Analysis with Finite Element Method

The front spar of the wing is analyzed separately with finite element program, MSC Patran as well. In the analysis, material properties used are the ones obtained from mechanical testing, same as the Case II of previous section. The results obtained are given in Table 4.11. Stress contours in carbon and styrofoam layers, and displacement contours are presented in Figures 4.34, 4.35.

Table 4.11: Comparison of results obtained from the front spar analysis.

Analysis method	Results
Transformed Section	$\sigma_{max}@carbon/epoxy = 614.89\text{ MPa}$ $\sigma_{max}@foam = 0.13\text{ MPa}$ $\delta_{max} = 357.41\text{ mm}$
Finite Element	$\sigma_{max}@carbon/epoxy = 405\text{ MPa}$ $\sigma_{max}@foam = 0.09\text{ MPa}$ $\delta_{max} = 360\text{ mm}$

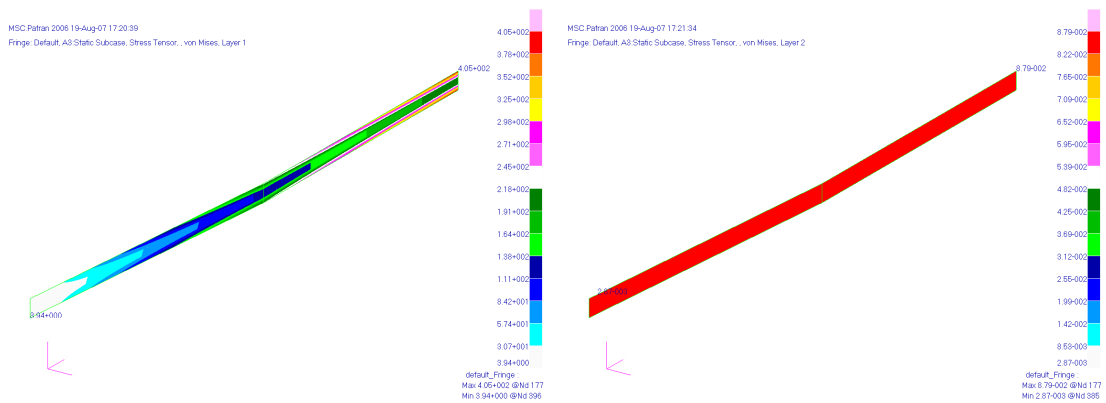


Figure 4.34: Stress contours at carbon and styrofoam layers of the front spar.

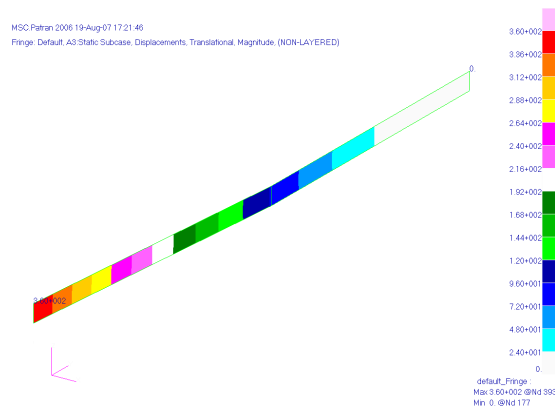


Figure 4.35: Displacement contour of the front spar.

It can be concluded from the results that, in terms of deflection, transformed section method gives close results to the results of finite element. Thus, the stiffness of the spar is approximated very accurately by the transformed section method. However, stress values of transformed section method are found out to be overestimating the results of finite element analysis.

It should also be stated that, the results of front spar analysis are not close to the stresses and deflections found in the total wing analysis. The reason for this is the same load is applied to the spar only in the front spar analysis; whereas, in the total wing analysis, the load is applied to the full wing structure.

Here, one can expect to have very close results in terms of the stresses as well, since the front spar has rather a simple rectangular geometry. In order to check the reliability of the method, a simple test case is analyzed. A composite beam composed of 2 mm thick aluminum plate as core material in between two 1 mm thick steel plates. In the finite element analysis, the geometry is modeled with solid elements, as shown in Figure 4.36. The results, which are outlined in Table 4.12, found out to be very close.

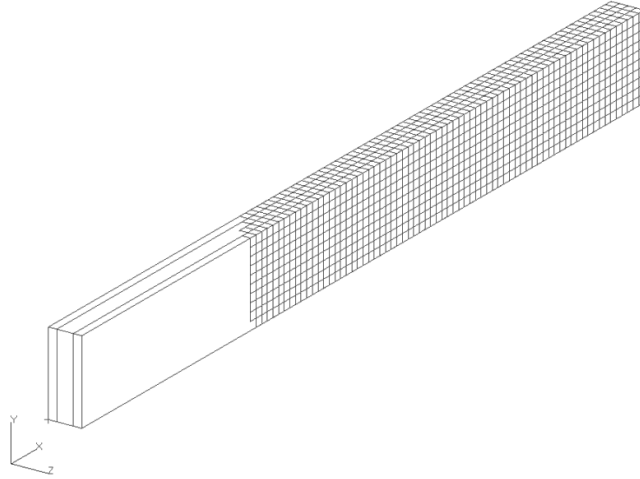


Figure 4.36: Geometry and mesh structure of the test case

Table 4.12: Comparison of results of the test case.

Analysis method	Results
Transformed Section	$\sigma_{max}@steel = 220.59 \text{ MPa}$ $\sigma_{max}@aluminum = 79.41 \text{ MPa}$ $\delta_{max} = 0.74 \text{ mm}$
Finite Element	$\sigma_{max}@steel = 205.74 \text{ MPa}$ $\sigma_{max}@aluminum = 73.97 \text{ MPa}$ $\delta_{max} = 0.73 \text{ mm}$

From the test case it can be deduced that transformed section method also predicts the stress values accurately. It appears that modeling the spar with shell elements yields less realistic results, possibly due to the elements being not oriented perpendicularly to the bending axis.

The front spar problem can be modeled with solid elements so as to obtain comparable results with the transformed section method. However, the element size of solid mesh must be as small as the thickness of carbon/epoxy layer. When the ratio of length-to-thickness and width-to-thickness is examined, it is obvious that this would require very powerful workstations, which would be unnecessary to deal with for such a trivial problem.

CHAPTER 5

DISCUSSION AND CONCLUSION

In this study, manufacturing a lightweight composite UAV wing is introduced. For composite manufacturing, a composite workshop is founded and vacuum bagging system is established. Manufacturing process of the UAV wing from mold production to ultimate wing structure is explained in detail with the aid of supporting schematic drawings and pictures. During manufacturing, hand lay-up method is used, and the curing process took place at room temperature.

Material characterization was another main aspect of this study. In order to design the structure strong enough to carry design loads, mechanical characteristics and limits of the materials used in the structure must be known. For composites, there are no exact material information available since the material properties are highly affected by manufacturing, compositions of the constituents, stacking sequence of the layers, and other factors. Therefore, one has to perform mechanical tests for obtaining the material properties of the composites.

In this study, tensile testing of coupon specimens are performed in order to obtain the elastic moduli of the composites used in the UAV. Several tests are performed with specimens having three different post-curing schemes for the purpose of examining the effects of post-curing on the mechanical properties. After the tests, satisfactory results in accordance with the literature

are obtained. However, it was observed that there is a scatter in the results. Main reasons behind this scatter are non-identical test conditions, possible defects occurred during specimen manufacturing, possible misalignment of the specimens in the test machine.

Therefore, more work should be done on material testing for obtaining more dependable results. One of the main points is preparing high quality specimens with better manufacturing conditions and better machining operations. Also, number of specimens should be increased for obtaining a better data distribution.

When the effect of post-curing is examined, it was found that post-curing does not have significant effect on the mechanical properties of composites. Because, post-curing is a process related with matrix material, and does not affect the properties of the fibers in the composite. Since the elastic modulus and tensile strength are fiber dominated properties, post-curing does not improve these properties significantly.

The elastic properties obtained from the mechanical tests are used in the finite element analysis of the UAV wing. The woven fabric is modeled as 2-D orthotropic layer in the analysis. In addition to mechanical testing, the elastic properties are also obtained with two other methods. One method is micromechanics of composites approach. In this approach, the properties are obtained based on the volume fractions of the constituents and their individual mechanical properties. The woven fabric is modeled as biaxial cross ply laminate in the analysis. Another method used for obtaining elastic properties is an approximate approach. This approach is simply based on the rule of mixtures. In this case, the woven fabric is modeled as 2-D orthotropic layer as well.

It can be concluded from the results of the full wing analysis that all three material definitions used give consistent and acceptable results. Especially, when the displacement results are observed, it is clear that all of them are nearly the same. This is true for the modal frequencies as

well, and this shows that the stiffness of the wing is approximated accurately by the different approaches. On the other hand, the stress values determined by the approximate methods deviated approximately 20% from the stress results obtained by using the material constants which are determined by the mechanical testing.

For simulating a load case of an actual flight condition, a spanwise distributed loading is applied over the front spar. The loading is calculated using a software of ESDU, which estimates the distribution of lift and moment coefficients over the wing. Using lift and moment equations, the wing loading for a level flight at stall speed is calculated, and that loading is distributed over the front spar. After the analysis, the results are compared with the results of tip loading case. It is found that, the assumption that ‘tip loading case simulates approximately 2.35 *g* flight condition’ is reasonable.

In addition to the full wing analysis, the front spar of the wing is analyzed separately with two different methods. The first method is the transformed section method, which is a simple method used for analyzing beams composed from different materials. The cross section is transformed into an equivalent cross section composed of only one material, and the beam is analyzed in the usual manner. Other method is, again, finite element analysis. Both methods are compared, and it is seen that the deflection results are close. On the other hand, the stress values are not too close as in the full wing analysis cases. This problem is examined and it is found that transformed section method estimates the stress results very close to the finite element results when the structure is meshed with solid elements, instead of shell elements. It is concluded that solid elements give more realistic results when compared to shell elements in this problem.

The results of the present study reveals that the methods used are appropriate for deflection and modal analysis. The methods can also be used effectively in aeroelastic analysis in which stiffness is the most significant parameter. In addition, for initial sizing and for deciding on

the composite layer configuration and fabric/resin selection, the stress analysis results of the three cases can also be used in the preliminary design phase. However, the complex structure of woven fabric geometry requires more detailed analyses in the micro level. For a detailed structural analysis, meso scale models should be used. In the meso scale models, the analysis begins with a detailed analysis of a representative unit cell taken within the lamina. Then, the analysis is expanded to the laminate, and the global elastic properties are obtained.

Finally, it can be concluded that the methods introduced in this study can be used as preliminary analysis tools in an aircraft design in the future projects. Based on the analysis results, initial sizing, configurations of the structural components and their positions can be decided.

This study can be extended with the following items suggested for the future work:

- i. For a detailed and more accurate material definition to be used in the finite element analysis, meso scale models can be studied and included in the analysis.
- ii. The finite element model can be improved with modeling all the details of the complex wing geometry, including the connection between the main and the outer wing.
- iii. Mechanical testing of the actual wing structure can be performed. The results in the linear region can be compared with the results of finite element analysis, and in the non-linear region where the deformation is high, the results can be compared with the non-linear finite element analysis.
- iv. Failure analysis can be performed, utilizing different failure theories.
- v. A comparative aeroelastic analysis can be performed based on the material properties obtained from coupon testing and other methods.

REFERENCES

- [1] Reddy, J. N., “*Mechanics of Laminated Composite Plates*”, CRC Press, 1997.
- [2] Mazumdar, S. K., “*Composites Manufacturing: Materials, Product, and Process Engineering*”, CRC Press, 2002.
- [3] Daniel, I. M. and Ishai, O., “*Engineering Mechanics of Composite Materials*”, Oxford University Press, 1994.
- [4] Jones, R. M., “*Mechanics of Composite Materials*”, Hemisphere Publishing Corporation, 1975.
- [5] Lubin, G., “*Handbook of Composites*”, Van Nostrand Reinhold Company Inc., 1982.
- [6] ASM International, “*Engineered Materials Handbook, Vol 1: Composites*”, ASM International, 1987.
- [7] Composites Horizons Inc. web site, “<http://www.chi-covina.com/>”, as accurate of February 27th, 2007.
- [8] US Department of Defense, “*Dictionary of Military and Associated Terms*”, Joint Publication 1-02.
- [9] Unmanned Vehicle Systems International web site, “<http://www.uvs-international.org/>”, as accurate of February 23rd, 2007.
- [10] ESDU 95010, “*Computer program for estimation of spanwise loading of wings with camber and twist in subsonic attached flow*”, IHS ESDU.
- [11] Armstrong, K. B. and Barret, R. T., “*Care and Repair of Advanced Composites*”, Society of Automotive Engineeris, Warrendale, PA, USA, 1997.
- [12] Data Sheet of “*Cold-curing epoxy system based on Araldite[®] LY 5052 / Aradur[®] 5052*”, Huntsman Advanced Materials, March 2004.
- [13] ASTM D 3039/D 3039M-00, “*Standard Test Method for Tensile Properties of Polymer Matrix Composite Materials*”, ASTM International, 2006.
- [14] Product catalog of “*Zwick/Roell Z010, Universal Static Testing Machine*”, Zwick Roell AG.
- [15] Naik, N. K., Shembekar, P. S., “*Elastic Behavior of Woven Fabric Composites: I - Lamina Analysis*”, Journal of Composite Materials, Vol. 26, No. 15, 1992, pp. 2196-2225.
- [16] Tanov, R., Tabiei, A., “*Computationally Efficient Micromechanical Models for Woven Fabric Composite Elastic Moduli*”, Journal of Applied Mechanics, Vol. 68, July 2001, pp. 553-560.
- [17] Cain, J. J., Post, N. L., Lesko, J. J., Case, S. W., Lin, Y.-N., Riffle, J. S., Hess, P. E. “*Post-Curing Effects on Marine VARTM FRP Composite Material Properties for Test and Implementation*”, Journal of Engineering Materials and Technology, Vol. 128, 2006, pp. 34-40.

- [18] Product data of “*Style 235, Style 20796 and Style G0801 fabrics*”, Hexcel Reinforcements, April 2007.
- [19] Lomov, S. V., Ivanov, D. S., Verpoest, I., Zako, M., Kurashiki, T., Nakai, H., Hirosawa, S., “*MESO-FE Modelling of Textile Composites: Road Map, Data Flow and Algorithms*”, 16th International Conference on Composite Materials, 2007.
- [20] Tsai, S. W., “*Theory of Composites Design*”, Think Composites, 1992.
- [21] Material Solutions on Polymer Composites web site, supported by ESR Technology “<http://www.admc.esrtechnology.com/Background/Laminate/#eprop-other>”, as accurate of July 13th, 2007.
- [22] Product data of “*Floormate 200*”, from Dow Styrofoam Solutions web site, <http://www.dow.com/styrofoam/europe/tr/proddata/pd03.htm>, as accurate of December 21st, 2006.
- [23] US Department of Agriculture, Forest Products Laboratory, “*Wood Handbook, Wood as an Engineering Material*”, General Technical Report, FPL-GTR-113, March 1999.
- [24] MSC Training and Support web site, “*How to model cloth composite plies, Solution#: 3098*”, (http://support.mscsoftware.com/kb/results_kb.cfm?S_ID=3098&requestTime-out=2000), as accurate of July 13th, 2007.
- [25] Gere, J. M., Timoshenko, S. P., “*Mechanics of Materials*”, PWS Publishing Company, 1997.

APPENDIX A

SPECIMEN DATA AND TENSILE TEST RESULTS

Table A.1: Average properties of specimens used in Tensile Test # 1, and test results.

SPECIMEN DATA			
Manufacturing date:	13 December 2005		
Testing date:	23 December 2005		
Specimen ID	Information		
3.1 – 3.6	3 ply Carbon (98) / Epoxy (5052)		
	Curing procedure:	1 day RT in vacuum	
	thickness / width / length [mm]	0.428 / 24.95 / 250	
	mass (w/o tabs) [g]	2.9	
	fiber volume fraction	0.515	
4.1 – 4.6	4 ply Kevlar (60) / Epoxy (5052)		
	Curing procedure:	1 day RT in vacuum	
	thickness / width / length [mm]	0.497 / 25.00 / 250	
	mass (w/o tabs) [g]	2.6	
	fiber volume fraction	0.497	
TEST RESULTS			
Specimen ID	\overline{E}_t [GPa]	$\overline{\sigma}_{max}$ [MPa]	% Elongation
3.1 – 3.6	40.3	439.10	0.95
4.1 – 4.6	22.9	310.53	1.60

Table A.2: Average properties of specimens used in Tensile Test # 2, and test results.

SPECIMEN DATA			
Manufacturing date:	Summer 2006		
Testing date:	02 October 2006		
Specimen ID	Information		
6.1.1 – 6.1.5	6 ply E-Glass (86) / Epoxy (5052)		
	Curing procedure:	1 day RT in vacuum	
	thickness / width / length [mm]	0.390 / 25.80 / 250	
	mass (w/o tabs) [g]	4.6	
	fiber volume fraction	0.500	
6.2.1 – 6.2.5	4 ply Kevlar (60) / Epoxy (5052)		
	Curing procedure:	1 day RT in vacuum	
	thickness / width / length [mm]	0.476 / 25.84 / 250	
	mass (w/o tabs) [g]	2.8	
	fiber volume fraction	0.465	
6.3.1 – 6.3.5	3 ply Carbon (98) / Epoxy (5052)		
	Curing procedure:	1 day RT in vacuum	
	thickness / width / length [mm]	0.378 / 26.03 / 250	
	mass (w/o tabs) [g]	3.0	
	fiber volume fraction	0.493	
TEST RESULTS			
Specimen ID	\bar{E}_t [GPa]	$\bar{\sigma}_{max}$ [MPa]	% Elongation
6.1.1 – 6.1.5	21.1	246.49	1.27
6.2.1 – 6.2.5	25.0	328.46	1.41
6.3.1 – 6.3.5	43.6	427.47	0.86

Table A.2: Average properties of specimens used in Tensile Test # 2, and test results (continued).

SPECIMEN DATA			
Manufacturing date:	12 July 2006		
Testing date:	02 October 2006		
Specimen ID	Information		
5.1.1 – 5.1.5	6 ply E-Glass (86) / Epoxy (5052)		
	Curing procedure:	1 day RT in vacuum 4 hr. in 100°C on 14 July 2006	
	thickness / width / length [mm]	0.492 / 25.73 / 250	
	mass (w/o tabs) [g]	4.6	
	fiber volume fraction	0.523	
7.1.1 – 7.1.5	6 ply E-Glass (86) / Epoxy (5052)		
	Curing procedure:	1 day RT in vacuum	
	thickness / width / length [mm]	0.504 / 25.80 / 250	
	mass (w/o tabs) [g]	4.6	
	fiber volume fraction	0.525	
5.2.1 – 5.2.5	4 ply Kevlar (60) / Epoxy (5052)		
	Curing procedure:	1 day RT in vacuum 4 hr. in 100°C on 14 July 2006	
	thickness / width / length [mm]	0.512 / 25.85 / 250	
	mass (w/o tabs) [g]	2.8	
	fiber volume fraction	0.486	
7.2.1 – 7.2.5	4 ply Kevlar (60) / Epoxy (5052)		
	Curing procedure:	1 day RT in vacuum	
	thickness / width / length [mm]	0.510 / 25.83 / 250	
	mass (w/o tabs) [g]	2.8	
	fiber volume fraction	0.485	
5.3.1 – 5.3.5	3 ply Carbon (98) / Epoxy (5052)		
	Curing procedure:	1 day RT in vacuum 4 hr. in 100°C on 14 July 2006	
	thickness / width / length [mm]	0.420 / 25.75 / 250	
	mass (w/o tabs) [g]	3.0	
	fiber volume fraction	0.518	
7.3.1 – 7.3.5	3 ply Carbon (98) / Epoxy (5052)		
	Curing procedure:	1 day RT in vacuum	
	thickness / width / length [mm]	0.390 / 25.89 / 250	
	mass (w/o tabs) [g]	3.0	
	fiber volume fraction	0.520	
TEST RESULTS			
Specimen ID	\bar{E}_t [GPa]	$\bar{\sigma}_{max}$ [MPa]	% Elongation
5.1.1 – 5.1.5	21.4	222.64	1.16
7.1.1 – 7.1.5	21.8	245.41	1.10
5.2.1 – 5.2.5	22.8	265.62	1.45
7.2.1 – 7.2.5	24.7	305.07	1.47
5.3.1 – 5.3.5	51.7	360.60	0.64
7.3.1 – 7.3.5	46.0	420.55	0.79

Table A.3: Average properties of specimens used in Tensile Test # 3, and test results.

SPECIMEN DATA			
Manufacturing date:	01 November 2006		
Testing date:	15 November 2006		
Specimen ID	Information		
8.1.1 – 8.1.5	6 ply E-Glass (86) / Epoxy (5052)		
	Curing procedure:	1 day RT in vacuum 4 hr. in 100°C on 03 November 2006	
	thickness / width / length [mm]	0.474 / 25.29 / 250	
	mass (w/o tabs) [g]	4.6	
	fiber volume fraction	0.506	
9.1.1 – 9.1.5	6 ply E-Glass (86) / Epoxy (5052)		
	Curing procedure:	1 day RT in vacuum	
	thickness / width / length [mm]	0.466 / 25.24 / 250	
	mass (w/o tabs) [g]	4.6	
	fiber volume fraction	0.504	
8.2.1 – 8.2.5	4 ply Kevlar (60) / Epoxy (5052)		
	Curing procedure:	x1 day RT in vacuum 4 hr. in 100°C on 03 November 2006	
	thickness / width / length [mm]	0.448 / 25.30 / 250	
	mass (w/o tabs) [g]	2.7	
	fiber volume fraction	0.472	
9.2.1 – 9.2.5	4 ply Kevlar (60) / Epoxy (5052)		
	Curing procedure:	1 day RT in vacuum	
	thickness / width / length [mm]	0.423 / 25.27 / 250	
	mass (w/o tabs) [g]	2.7	
	fiber volume fraction	0.472	
8.3.1 – 8.3.5	3 ply Carbon (98) / Epoxy (5052)		
	Curing procedure:	1 day RT in vacuum 4 hr. in 100°C on 03 November 2006	
	thickness / width / length [mm]	0.392 / 25.38 / 250	
	mass (w/o tabs) [g]	3.0	
	fiber volume fraction	0.505	
9.3.1 – 9.3.5	3 ply Carbon (98) / Epoxy (5052)		
	Curing procedure:	1 day RT in vacuum	
	thickness / width / length [mm]	0.384 / 25.37 / 250	
	mass (w/o tabs) [g]	3.0	
	fiber volume fraction	0.505	
TEST RESULTS			
Specimen ID	\bar{E}_t [GPa]	$\bar{\sigma}_{max}$ [MPa]	% Elongation
8.1.1 – 8.1.5	21.9	295.08	1.48
9.1.1 – 9.1.5	20.6	317.12	1.45
8.2.1 – 8.2.5	22.8	304.29	1.14
9.2.1 – 9.2.5	26.4	340.31	1.09
8.3.1 – 8.3.5	48.7	386.08	0.74
9.3.1 – 9.3.5	49.4	449.33	0.91

Table A.4: Average properties of specimens used in Tensile Test # 4, and test results.

SPECIMEN DATA			
Manufacturing date:	19 December 2006		
Testing date:	30 April 2007		
Specimen ID	Information		
10.1.1 – 10.1.5	6 ply E-Glass (86) / Epoxy (5052)		
	Curing procedure:	1 day RT in vacuum	
	thickness / width / length [mm]	0.500 / 25.27 / 250	
	mass (w/o tabs) [g]	4.5	
	fiber volume fraction	0.521	
11.1.1 – 11.1.5	6 ply E-Glass (86) / Epoxy (5052)		
	Curing procedure:	1 day RT in vacuum 8 hr. in 80°C on 20 December 2006	
	thickness / width / length [mm]	0.506 / 25.36 / 250	
	mass (w/o tabs) [g]	4.5	
	fiber volume fraction	0.523	
10.2.1 – 10.2.5	4 ply Kevlar (60) / Epoxy (5052)		
	Curing procedure:	1 day RT in vacuum	
	thickness / width / length [mm]	0.436 / 25.28 / 250	
	mass (w/o tabs) [g]	2.9	
	fiber volume fraction	0.453	
11.2.1 – 11.2.5	4 ply Kevlar (60) / Epoxy (5052)		
	Curing procedure:	1 day RT in vacuum 8 hr. in 80°C on 20 December 2006	
	thickness / width / length [mm]	0.428 / 25.22 / 250	
	mass (w/o tabs) [g]	2.9	
	fiber volume fraction	0.452	
10.3.1 – 10.3.5	3 ply Carbon (98) / Epoxy (5052)		
	Curing procedure:	1 day RT in vacuum	
	thickness / width / length [mm]	0.400 / 25.22 / 250	
	mass (w/o tabs) [g]	3.0	
	fiber volume fraction	0.496	
11.3.1 – 11.3.5	3 ply Carbon (98) / Epoxy (5052)		
	Curing procedure:	1 day RT in vacuum 8 hr. in 80°C on 20 December 2006	
	thickness / width / length [mm]	0.388 / 25.15 / 250	
	mass (w/o tabs) [g]	3.0	
	fiber volume fraction	0.493	
TEST RESULTS			
Specimen ID	\bar{E}_t [GPa]	$\bar{\sigma}_{max}$ [MPa]	% Elongation
10.1.1 – 10.1.5	28.0	270.69	1.41
11.1.1 – 11.1.5	22.4	278.18	1.37
10.2.1 – 10.2.5	26.2	351.32	1.62
11.2.1 – 11.2.5	28.7	333.28	1.35
10.3.1 – 10.3.5	52.4	423.73	0.72
11.3.1 – 11.3.5	49.5	449.04	0.79

Table A.4: Average properties of specimens used in Tensile Test # 4, and test results (continued).

SPECIMEN DATA			
Manufacturing date:	11 January 2007		
Testing date:	30 April 2007		
Specimen ID	Information		
12.1.1 – 12.1.5	6 ply E-Glass (86) / Epoxy (5052)		
	Curing procedure:	1 day RT in vacuum	
	thickness / width / length [mm]	0.536 / 25.44 / 250	
	mass (w/o tabs) [g]	5.0	
	fiber volume fraction	0.444	
13.1.1 – 13.1.5	6 ply E-Glass (86) / Epoxy (5052)		
	Curing procedure:	1 day RT in vacuum 8 hr. in 80°C on 15 January 2007	
	thickness / width / length [mm]	0.498 / 25.40 / 250	
	mass (w/o tabs) [g]	5.0	
	fiber volume fraction	0.444	
12.2.1 – 12.2.5	4 ply Kevlar (60) / Epoxy (5052)		
	Curing procedure:	1 day RT in vacuum	
	thickness / width / length [mm]	0.480 / 25.22 / 250	
	mass (w/o tabs) [g]	3.0	
	fiber volume fraction	0.433	
13.2.1 – 13.2.5	4 ply Kevlar (60) / Epoxy (5052)		
	Curing procedure:	1 day RT in vacuum 8 hr. in 80°C on 15 January 2007	
	thickness / width / length [mm]	0.472 / 25.26 / 250	
	mass (w/o tabs) [g]	3.0	
	fiber volume fraction	0.437	
12.3.1 – 12.3.5	3 ply Carbon (98) / Epoxy (5052)		
	Curing procedure:	1 day RT in vacuum	
	thickness / width / length [mm]	0.448 / 25.38 / 250	
	mass (w/o tabs) [g]	3.3	
	fiber volume fraction	0.443	
13.3.1 – 13.3.5	3 ply Carbon (98) / Epoxy (5052)		
	Curing procedure:	1 day RT in vacuum 8 hr. in 80°C on 15 January 2007	
	thickness / width / length [mm]	0.454 / 25.40 / 250	
	mass (w/o tabs) [g]	3.3	
	fiber volume fraction	0.443	
TEST RESULTS			
Specimen ID	\bar{E}_t [GPa]	$\bar{\sigma}_{max}$ [MPa]	% Elongation
12.1.1 – 12.1.5	22.8	274.84	1.65
13.1.1 – 13.1.5	18.9	293.29	1.59
12.2.1 – 12.2.5	27.1	325.31	1.45
13.2.1 – 13.2.5	23.2	322.27	1.58
12.3.1 – 12.3.5	41.6	465.50	0.82
13.3.1 – 13.3.5	39.0	387.75	0.72